Diallel analysis reveals *Mx1*-dependent and *Mx1*-independent effects on response to influenza A virus in mice

Paul L. Maurizio[*,†], **Martin T. Ferris**[†], **Gregory R. Keele**[*,†], **Darla R. Miller**[†], **Ginger D. Shaw**[†], **Alan C. Whitmore**[†], **Ande West**[†,‡], **Clayton R. Morrison**[†], **Kelsey E. Noll**[†,§], **Kenneth S. Plante**[†], **Adam S. Cockrell**[‡], **David W. Threadgill**[**], **Fernando Pardo-Manuel de Villena**[†,††], **Ralph S. Baric**[‡], **Mark T. Heise**[†,††] **and William Valdar**[†,††,1]

[*]Curriculum in Bioinformatics and Computational Biology, [†]Department of Genetics, [‡]Department of Epidemiology, and, [§]Department of Microbiology and Immunology, University of North Carolina, Chapel Hill, North Carolina, 27599-7435, [**]Institute of Genome Sciences and Society, Texas A&M University, College Station, Texas 77433-2470, [††]Lineberger Comprehensive Cancer Center, University of North Carolina, Chapel Hill, North Carolina, 27599-7265
ORCID IDs: 0000-0002-5859-6260 (P.L.M.), 0000-0003-1241-6268 (M.T.F.), 0000-0002-1843-7900 (G.R.K.), 0000-0002-0781-7254 (D.R.M.), 0000-0003-2590-4973 (G.D.S.), 0000-0002-3977-0083 (K.E.N.), 0000-0003-3538-1635 (D.W.T.), 0000-0002-5738-5795 (F.P.M.V.), 0000-0002-2419-0430 (W.V.)

1. ABSTRACT

1 Influenza A virus (IAV) is a respiratory pathogen that causes substantial morbidity and mortality during both seasonal and pandemic

2 outbreaks. Infection outcomes in unexposed populations are affected by host genetics, but this host genetic architecture is not well

3 understood. Here we obtain a broad view of how heritable factors affect a mouse model of response to IAV infection using an 8×8 diallel

4 of the eight inbred founder strains of the Collaborative Cross (CC). Expanding on a prior statistical framework for modeling treatment

5 response in diallels, we explore how a range of heritable effects modify acute host response to IAV through 4 days post-infection. Heritable

6 effects in aggregate explained about 57% of the variance in IAV-induced weight loss. Much of this was attributable to a pattern of additive

7 effects that became more prominent through day 4 post-infection and was consistent with previous reports of anti-influenza myxovirus

8 resistance 1 (*Mx1*) polymorphisms segregating between these strains; the additive effects largely recapitulated haplotype effects observed

9 at the *Mx1* locus in a previous study of the incipient CC (pre-CC), and are also replicated here in a CC recombinant intercross (CC-RIX)

10 population. Genetic dominance of protective *Mx1* haplotypes was observed to differ by subspecies origin: relative to the *domesticus* null

11 *Mx1* allele, *musculus* acts dominantly whereas *castaneus* acts additively. After controlling for *Mx1*, heritable effects, though less distinct,

12 accounted for about 34% of the phenotypic variance. Implications for future mapping studies are discussed.

13 Keywords: treatment response, multiparental population, causal effect, Bayesian model, multiple imputation

2. ARTICLE SUMMARY

15 Seasonal and pandemic influenza viruses comprise an important public health burden, but the architecture of host genetic resistance to

16 viruses is poorly understood. We conducted an influenza challenge in a diallel cross of eight inbred mouse strains. Roughly 60% of variation

17 in disease at 4 days post-infection was explained by genetic and non-genetic diallel effects, with about 34% of variation independent of the

18 host resistance factor, *Mx1*. The dominance of *Mx1* resistance was highly dependent on subspecies *Mx1* allelic origin, and similar *Mx1*

19 effect patterns were found in the related Collaborative Cross strains, motivating integrated infection studies in these populations.

---

[1]Corresponding author: Department of Genetics, University of North Carolina at Chapel Hill, 120 Mason Farm Road, Suite 5113, Genetic Medicine Building, Chapel Hill, NC 27599-7292, USA. Email: william.valdar@unc.edu

Manuscript compiled: Saturday 4th November, 2017

3. INTRODUCTION

Pathogenic response to viral infection varies dramatically between individuals infected with the same viral strain and dose, and much of this variation is heritable. The impact of host genetics is evident both on the primary exposure to a virus during early life (Strunk *et al.* 2013) and upon infection with newly emerging viral strains — the latter, where prior immune exposure to a variant viral strain is not cross-protective, being especially common for quickly evolving RNA viruses such as influenza A (IAV) (Morens *et al.* 2010). Pathogenesis induced by IAV, whether contracted during early childhood or later in life, is thus likely to have a significant heritable component. A greater understanding of this heritability should improve our ability not only to identify populations at risk of enhanced morbidity and mortality during an emerging pandemic but also to identify successful options for treatment.

The past several years have seen significant progress identifying and characterizing host genes that modulate susceptibility to IAV infection, via knockout mouse studies, in vitro screens, and studies of primary immunodeficiencies and allelic variants in humans (To *et al.* 2015). In humans, screening for inborn errors identified a major role for interferon regulatory factor 7 (*Irf7*) in modulating the the severity of primary IAV infection (Ciancanelli *et al.* 2015), and allelic variation in *Ifitm3*, which was identified in a high-throughput siRNA screen, was associated with differential severity of IAV infection outcomes during the 2009 H1N1 pandemic (Everitt *et al.* 2012).

Most of our insights into genes modulating host IAV resistance, however, have come from studies on mice. These include studies using knockout mice, which have identified host genetic factors critical to antiviral responses, including *Tlr3* (Hidaka *et al.* 2006) and *Isg15* (Lenschow *et al.* 2007), and studies that examine differences between laboratory inbred strains. Inbred strain studies were the first to identify the *Myxovirus resistance* (*Mx*) family of proteins as important for host antiviral response (Staeheli *et al.* 1988), and inbred studies have continued to demonstrate the relevance of genetic background to multiple aspects of IAV pathogenesis (Srivastava *et al.* 2009; Alberts *et al.* 2010; Leist *et al.* 2016; Samet and Tompkins 2017).

Yet despite the identification of clear phenotypic differences between inbred strains, there have been relatively few attempts to dissect the genetic basis of those differences using traditional quantitative trait locus (QTL) mapping approaches such as the use of F2s or backcrosses (although see Boivin *et al.* 2012). This may be in part because traditional QTL mapping approaches tend to rely on outbred animals — and when it comes to studying viral pathogenesis, outbreds are in many respects problematic. One important limitation is phenotyping. Studying the response to an infection is equivalent to studying the causal effect of an applied treatment: its strict definition relies on a comparison between otherwise identical individuals subject to infection vs. control. But such like-for-like comparisons are biologically and technically challenging to make in an outbred population, where every individual is genetically distinct, and this has undesirable consequences for downstream interpretation: namely, that when genetic determinants of severe IAV pathogenesis are confounded with those influencing baseline phenotypes, the roles of any detected QTL are ambiguous. A related disadvantage of outbreds from the perspective of genetics is the inability to obtain biological replicates. This makes it harder to distinguish which aspects of pathology are stable consequences of genetics versus products of stochastic variability. This is particularly important, since it also makes it almost impossible to follow-up on genuinely extreme responders for additional mechanistic and genetic analysis. Translating strain differences in IAV pathogenesis to meaningful QTL studies ideally requires an experimental paradigm that combines population-level genetic diversity with individual-level replicability.

An exciting opportunity is therefore presented by replicable genetic reference populations, in particular, those based on panels of recombinant inbred (RI) strains. Across a panel of RIs, genetic variation is often more or less evenly distributed, providing a basis for QTL mapping; within a RI strain, individuals are genetically identical, providing a basis for replication. The combination allows infection response to be rigorously defined and genomic regions affecting that response to be mapped. It also permits the creation of sophisticated

experiments that target a wider range of heritable mechanisms: crossing RIs with each other to form RI intercrosses (RIXs), or crossing them with outside strains, produces replicable systems capable of distinguishing, for example additive, dominance, and parent-of-origin effects, among others (Threadgill *et al.* 2002; Williams and Williams 2017).

Recombinant inbred (RI) genetic reference panels range from inbred lines derived from crosses between two mouse strains to more complex multi-parental crosses. The BxD RI panel, derived from two founder strains, has been used to study the impact of genetic variation on susceptibility to IAV infection and map QTL associated with these effects. Boon *et al.* (2009) studied H5N1 infection in females from 66 BXD strains, and Nedelko *et al.* (2012) studied H1N1 infection in 53 BXD strains, with both studies identifying QTL associated with susceptibility to infection. The Collaborative Cross (CC) RI panel is a multiparental population (MPP) descended from eight inbred founder strains (Threadgill *et al.* 2002; Churchill *et al.* 2004), with these founders including representatives from the three major domesticated house mouse subspecies (Yang *et al.* 2011). As such, the CC captures considerably more genetic diversity, and thanks to its breeding structure this diversity is also more uniformly distributed across the genome, with as many as eight distinct haplotypes segregating at any given locus within the population (Collaborative Cross Consortium 2012; Srivastava *et al.* 2017). The eight CC founder strains have distinct pathogenesis profiles in response to influenza virus (Leist *et al.* 2016), suggesting that the CC RI panel is capable of a broader phenotypic range than would be observed in less complex populations. Indeed, studies using an incompletely inbred, ancestor population of the CC (the pre-CC), demonstrated high levels of phenotypic variation across the population and successfully mapped several QTL associated with variation in susceptibility to IAV infection (Ferris *et al.* 2013; Bottomly *et al.* 2012). The CC therefore represents a promising resource for studying how genetically diverse populations respond to IAV infection.

Determining an optimal strategy for how the CC should be used to study the genetic architecture of IAV pathogenesis is nonetheless complicated because (1) the space of possible experimental designs is vast, and (2) information about what types of heritable effects are likely to be present is extremely limited. Regarding (1), with more than 70 CC strains currently available, including all reciprocal F1 hybrids (so called CC-RIXs), there are more than 4900 potential replicable configurations; since only a subset of these configurations can be explored within any realistic experiment, any chosen experimental design necessarily targets some types of heritable effects to the exclusion of others. Regarding (2), to date, most in vivo studies of IAV pathogenesis have been confined to candidate genes or additive interactions at single loci; studies investigating the broader question of what types of heritability are at play during IAV infection are largely absent.

In order to rationally design studies of heritable effects in complex populations such as the CC it is therefore helpful to have advance knowledge of which types of heritable effects might be present. One source of such information is phenotype data collected on the multiparental founders and their F1 hybrid offspring, a combination that can be more formally described as an (inbred) diallel. Diallels have long history in quantitative genetics, having been used originally in plant breeding studies to judge the relative merits of different strain combinations and subsequently for gaining insight into the heritable architecture of a broad range of phenotypes (*e.g.*, refs in Christie and Shattuck 1992; Lenarcic *et al.* 2012; Okoro and Mbajiorgu 2017), including host-pathogen interactions in, *e.g.*, crickets (Rantala and Roff 2006), flies (Wayne *et al.* 2011), and insects (Pereira *et al.* 2015) (see Methods and Discussion for connections to other diallel literature).

Here we use a diallel of the CC founders and their reciprocal F1 hybrids (hereafter, a CC founder diallel) to give an overall predictive picture of the range and relative influence of different types heritable effects on IAV pathogenesis likely to be present in CC founder-derived MPPs, a group that includes not only replicable MPPs such as the CC and the CC-RIX but also irreplicable ones such as the Diversity Outbred population (Churchill *et al.* 2012). We take advantage of the diallel design's replicability to measure IAV-induced pathogenesis in a precise way, as the response to an applied treatment defined in terms of post-infection weight-loss differences (deltas) between matched sets of mock and infected individuals. Adapting a recently developed statistical framework for analyzing treatment-response diallels (Crowley *et al.* 2014), we use those deltas to model how pathogenic response to IAV is modulated by parentage, sex and their interaction,

framed in terms of additive genetics, dominance, epistasis, parent-of-origin, and sex-specific versions thereof.

After observing that, following IAV infection, diallel individuals show a broad, continuous distribution of day 4 post-infection weight loss, we find, through statistical modeling, that the IAV-induced weight loss includes substantial contributions of host additive, epistatic, and sex-specific effects, with much of the heritable variation closely tracking the genotype state implied by the three distinct functional alleles of the previously identified susceptibility locus *Mx1*. Confirming previous findings, the functional CAST/EiJ *Mx1* allele, in contrast with functional NZO/HlLtJ and PWK/PhJ *Mx1* alleles, provides intermediate levels of protection against H1N1 influenza strains. Unexpectedly, and confirmed through additional modeling, we found that different classes of functional *Mx1* alleles exhibit distinct functional patterns, additive or dominant, when combined with null *Mx1* alleles. Further, illustrating our general rationale, we show that the major strain-specific *Mx1* effect patterns are consistent across two CC founder-derived MPPs: the pre-CC, as determined from reanalysis of a previously published dataset (Ferris *et al.* 2013), and a previously unpublished 117-line CC-RIX, in which we conduct a limited analysis focused on the *Mx1* locus.
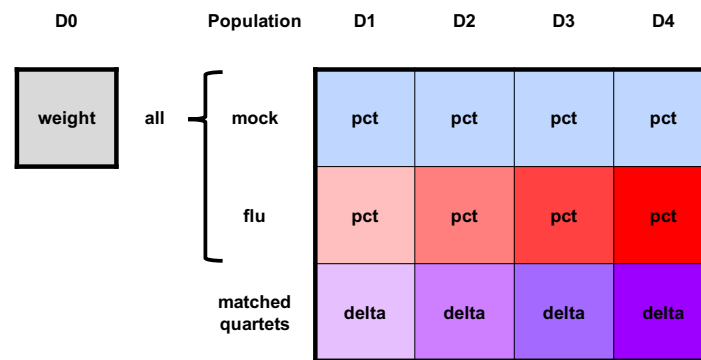

Figure 1 Phenotype and treatment response classes for analysis of influenza A virus infection in the diallel. Each filled square represents a weight or weight change phenotype that is modeled independently. The gray square represents the starting body weight in all animals, prior to treatment, at day 0 (D0) (analyzed with Model 1 in **Table 2**). Light blue squares represent animals that were mock-treated and red squares represent animals infected with IAV, with daily weights for each taken from D1 through D4 post-infection (and these analyzed with Model 2 in **Table 2**). Purple squares represent infection response, the primary quantity of interest, estimated using match quartets of 1 mock to 3 infected mice (analyzed with Models 3 and 4 in **Table 2**). Labels within each square indicate phenotypes analyzed, where weight = pre-infection body weight, pct = post-infection percent change in starting D0 weight (post), and delta = infection response, as described in the **Statistical Methods** section. The coloring increases in saturation from D1 through D4 for the influenza and matched quartet groups to indicate an overall increasing amount of post-infection weight loss over time.

4. EXPERIMENTAL MATERIALS AND METHODS

A. CC founder diallel mice

The inbred and F1 mice used within this study were bred in-house at the University of North Carolina at Chapel Hill (UNC-CH). This colony was directly descended from the subset of animals used to generate the initial CC funnels (Collaborative Cross Consortium 2012), and included mice from the following eight strains at the Jackson Laboratory: A/J ("AJ", #000646); C57BL/6J ("B6", #000664);

111 129S1/SvImJ ("129", #002448) NOD/ShiLtJ ("NOD", #001976); NZO/HlLtJ ("NZO", #002105); CAST/EiJ ("CAST", #000928); PWK/PhJ

112 ("PWK", #003715); and WSB/EiJ ("WSB", #001145). Mice from the UNC-CH colony were then used to generate all 62 possible inbred and

113 (reciprocal) F1 combinations between these 8 strains, excluding NZO×CAST and NZO×PWK matings which are non-productive (Chesler

114 *et al.* 2008) (**Figure 2**A). This yielded a total of 124 distinct combinations of sex and parentage (hereafter, described as "diallel categories").

115 Lung tissues were collected from a subset of each of the founder inbred strains in this study, at D2 and D4 post-infection, and were used for

116 a separate comparative RNA-seq analysis by Xiong *et al.* (2014).

B. Mouse infections in the diallel

118 Mice were weaned at approximately 21 days old and housed 4 per cage, within each diallel category, under standard conditions (12 h

119 light/dark; food and water ad libitum Of the 4 mice in a cage, 1 was randomly assigned to mock and 3 to influenza infection, as there is no

120 evidence that mice can transmit influenza virus. Each cage was then assigned to a harvest timepoint – Day 2 post-infection (D2 p.i., n=533

121 mice), or D4 p.i. (n=510 mice).

122 At 8-12 weeks of age, based on their assignments, mice were anesthetized with isoflurane and inoculated intranasally with 500

123 plaque-forming units (PFU) of mouse-adapted influenza A virus (H1N1 A/Puerto Rico/8/1934; short name PR8) or with the diluent,

124 phosphobuffered saline (PBS) alone as a mock control. For each inbred line and F1 cross, about 6 mice (range: 5-9) of each sex were infected

125 with IAV PR8, and about two mice (range: 2-3) of each sex were mock-infected, giving a total of 1,043 mice across 54 experimental batches.

126 Treatment assignment was random: same-sex siblings from the same cage (and therefore batch) were randomly assigned at weaning to

127 mock or infected groups prior to being moved to new cages. Body mass was recorded daily. All animal experiments were carried out in

128 compliance with the Guide for the Care and Use of Laboratory Animals (Institute of Laboratory Animal Resources, National Research

129 Council, 1996, https://www.ncbi.nlm.nih.gov/books/NBK232589/). Animal protocols were approved by the Institutional Animal Care and Use
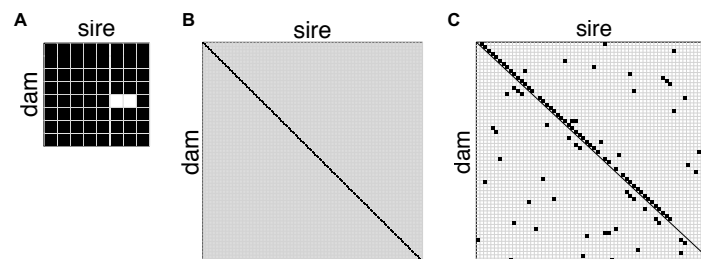
130 Committee of UNC-CH.

Figure 2 Diagram of breeding strategy for diallel, pre-CC, and CC-RIX. (A) The diallel cross produces inbred (n=8) and F1 (n=54 lines) genotypes from an 8×8 cross of inbred strains. (B) The pre-CC is comprised of incompletely inbred (n=155 lines) genotypes from 155 inbreeding funnels. (C) The CC-RIX produces F1 hybrid lines (n=105 lines) from a sparse, round robin-like cross of 65 inbred CC strains.

C. Mouse infections in the pre-CC and CC-RIX

132 In order to verify strain-specific haplotype effects measured in the diallel for host resistance locus, *Mx1*, we sought out CC-related IAV

133 infection data sets for which we could isolate *Mx1* locus-specific effects.

134 **C.1. Existing data from pre-CC study**. In the QTL mapping study of host response to IAV infection of Ferris *et al.* (2013), 155 female

135 pre-CC mice from as many pre-CC lines were infected with IAV (PR8) at 8-12 weeks of age and assayed for post-infection weight loss via

136 daily weights, with phenotypes collected including starting weight (D0) and weight at D4 p.i. (**Figure 2B**). This study did not include

137 mock-infected mice.

138 ***C.2. CC-RIX study***. As part of a larger as yet unpublished study of genetic factors affecting host response to IAV, 1,402 female mice were

139 bred from 105 F1 crosses of CC strains (*i.e.*, 105 CC-RIX lines) as described in Supplemental Material (**Figure 2C**, **Figure S2**). These mice

140 were infected at 8-12 weeks of age with 5,000 PFU IAV (A/California/04/2009; short name CA04), a human 2009 pandemic H1N1 isolate

141 (Itoh *et al.* 2009), and phenotypes were collected, including starting weight (D0) and weight at D7 p.i. CC-RIX were bred under similar

142 conditions to diallel mice. This experiment, whose broader analysis is still ongoing, included both flu-infected and mock-treated mice.

143 However, since the design did not match these to the same exacting degree as the diallel, with mock controls missing entirely for some

144 batch/line combinations, in the current study we consider data from the infected mice only. CC animals used to generate CC-RIX lines

145 were purchased from the Systems Genetics Core at UNC-Chapel Hill; information about CC strains available for distribution is found at

146 http://csbio.unc.edu/CCstatus/index.py?run=AvailableLines (Morgan and Welsh 2015).

5. STATISTICAL MODELS AND METHODS

148 Our statistical analysis of heritable effects in the diallel (hereafter, diallel effects) relies heavily on the BayesDiallel model and approach

149 described by Lenarcic *et al.* (2012) and Crowley *et al.* (2014). BayesDiallel was originally proposed in Lenarcic *et al.* (2012) for diallel analysis

150 of routine, single-outcome phenotypes, describing how the mean value of those phenotypes was shifted by changes in parentage and sex.

151 Although in some ways the method was built upon a canon of existing diallel literature (*e.g.*, refs in Christie and Shattuck 1992), including

152 more recent work that used random effects (Zhu and Weir 1996; Tsaih *et al.* 2005) and Bayesian hierarchical modeling (Greenberg *et al.*

153 2010), in other ways it represents a new parameterization, and a generalization of many earlier methods (see Lenarcic *et al.* 2012 for explicit

154 connections to those methods). In Crowley *et al.* (2014), we extended BayesDiallel to treatment response phenotypes, in particular, to when

155 the modeled outcome is the phenotypic difference between placebo and treated matched pairs; the model in this case describes a causal

156 effect modification, or, in a slight abuse of terminology, a gene-by-treatment (G×T) effect. Herein, that treatment response approach is

157 extended further: to our more complex matching regime of quartets rather than pairs, and with a different imputation procedure to deal

158 with quartets that are incomplete.

159 This section begins by reviewing the BayesDiallel model for single-outcome phenotypes. This is used not only to analyze our primary

160 baseline phenotype, body weight at day 0 (D0 weight), but is also foundational for our subsequent analyses. Then we introduce our

161 definition of infection response based on matched quartets, which gives rise to treatment responses defined for each of four time-points

162 (D1, D2, D3, and D4 p.i.), and describe how they are modeled using BayesDiallel. The analysis is then modified further to estimate the

163 impact of haplotype state at the susceptibility locus *Mx1*, and we describe how the interaction of haplotype pairs of this locus is examined

164 by estimating relative degrees of haplotype additivity and dominance. Last we describe an illustrative comparative analysis of the effect of

165 the *Mx1* locus on IAV response in pre-CC and CC-RIX mice.

A. Diallel model for single outcome phenotypes

167 Diallel effects for single outcome phenotypes, that is, phenotypes measured as a single value per mouse, were modeled using the "fulls"

168 model of BayesDiallel (Lenarcic *et al.* 2012; Crowley *et al.* 2014). BayesDiallel is a Bayesian linear mixed model that decomposes phenotypic

169 variation into separate heritable components corresponding to additive genetics, dominance/inbred effects, parent-of-origin ("maternal"),

epistasis, and all sex-specific versions thereof. It models the phenotype value y_i of mouse i as

$$y_i = \mu + \mathbf{c}_i^{\mathsf{T}} \boldsymbol{\alpha} + \sum_{r=1}^{R} u_i^{(r)} + \mathbf{d}_i^{\mathsf{T}} \boldsymbol{\beta} + \varepsilon_i \,, \tag{1}$$

where μ is the intercept, and ε_i is the residual error, normally distributed as $\varepsilon_i \sim \mathrm{N}(0, \sigma^2)$, with variance σ^2. The $\mathbf{c}_i^{\mathsf{T}} \boldsymbol{\alpha}$ term represents the contribution of an arbitrary set of user-specified fixed effect covariates, with predictors encoded in vector $\mathbf{c}_i$ and fixed effects $\boldsymbol{\alpha}$; the $\sum_{r=1}^{R} u_i^{(r)}$ term represents the contribution of an arbitrary set of R user-defined random effect covariates, which for single outcome phenotypes in this study always includes an effect of experimental batch; and the $\mathbf{d}_i^{\mathsf{T}} \boldsymbol{\beta}$ term represents the contribution of heritable components of the diallel, written as a linear combination of the diallel effects vector $\boldsymbol{\beta}$ and diallel category vector $\mathbf{d}_i$. Here $\mathbf{d}_i$ is shorthand for $\mathbf{d}_{\{jks\}[i]}$, where $\{jks\}[i]$ denotes i's diallel category, that is, its unique combination of mother strain j, father strain k and sex s. The diallel category vector $\mathbf{d}_{\{jks\}}$ is defined with the diallel effects $\boldsymbol{\beta}$ so as to give following linear combination:

$$\mathbf{d}_{\{jks\}}^{\mathsf{T}} \boldsymbol{\beta} = \underbrace{a_j + a_k}_{\text{additive}} + \underbrace{m_j - m_k}_{\text{maternal}} + \underbrace{I_{\{j=k\}} \left(\beta_{\text{inbred}} + b_j \right)}_{\text{inbred penalty}}$$

$$+ \underbrace{I_{\{j \neq k\}} \left(v_{jk} + S_{\{j<k\}} \cdot w_{jk} \right)}_{\text{epistasis}}$$

$$+ S_{\{s=\text{female}\}} \cdot \left[\underbrace{\phi} + \underbrace{\phi_j^a + \phi_k^a}_{\text{sex}\times\text{additive}} + \underbrace{\phi_j^m - \phi_k^m}_{\text{sex}\times\text{maternal}} \right. \tag{2}$$

$$\left. + \underbrace{I_{\{j=k\}} \left(\phi_{\text{inbred}} + \phi_j^b \right)}_{\text{sex}\times\text{inbred penalty}} + \underbrace{I_{\{j \neq k\}} \left(\phi_{jk}^v + S_{\{j<k\}} \cdot \phi_{jk}^w \right)}_{\text{sex}\times\text{epistasis}} \right] \,,$$

where a_j is the additive effect of strain j (*e.g.*, the additive effect parameter a_{AJ} is the expected increase in phenotype on adding one haploid genome of strain AJ), m_j is an additional increase in phenotype induced by strain j being the mother (parent-of-origin effect), indicator $I_{\{X\}}$ is 1 if X is true and 0 otherwise, β_{inbred} is the overall effect of being inbred, b_j is the additional effect of being inbred for strain j, v_{jk} is the additional effect of the combining strains j with k regardless of which is the mother (symmetric epistasis), indicator $S_{\{X\}}$ is $\frac{1}{2}$ if X is true and $-\frac{1}{2}$ otherwise, w_{jk} is a deviation from v_{jk} induced by parent-of-origin (asymmetric epistasis); ϕ is the effect of being female rather than male, and ϕ_j^a is the sex-specific deviation from additive effect a_j, with other superscripted ϕ terms (*e.g.*, ϕ^m, etc.) defined analogously. Each set of related variables, *e.g.*, the additive effects $a_1, \ldots, a_J$ for J parents, is modeled as a group via a constrained normal distribution, that is, $a_1, a_2, \ldots, a_J \sim$ marginally $\mathrm{N}(0, \tau_a^2)$, but subject to $\sum_j a_j = 0$, after Crowley *et al.* (2014). The variance of each group, *e.g.*, τ_a^2, was modeled with a weak inverse gamma prior, $\tau_a^{-2} \sim \chi^2(\mathrm{d.f.} = 0.2, \mathrm{mean} = 0.2)$, with this prior also used for the residual variance σ^2. The prior for fixed effects, *e.g.*, μ, is set to a vague normal distribution, $\mu \sim \mathrm{N}(0, 10^3)$. A summary of the diallel effects parameters is given in **Table 1**. Model fitting proceeded using Markov Chain Monte Carlo (MCMC) via Gibbs sampling (algorithm in Lenarcic *et al.* 2012), with results based on samples from 12.5×10^6 MCMC iterations (5 chains of length 2500, after 500 iterations burnin). See also later section **Reporting BayesDiallel results**.

■ Table 1 Model parameters, random and fixed (overall), from Eqn 1, Eqn 2, and Eqn 5.

Parameter	Color	Description	Type	Levels
μ (or θ)		overall mean (or overall infection response)	fixed	1
α		D0 body weight	fixed	1
$u^{(\text{batch})}$		experimental batch	random	44 or 52 [a]
$u^{(Mx1\ \text{diplo})}$		*Mx1* diplotype	random	6
a_j		strain-specific additive	random	8
m_j		strain-specific maternal (parent-of-origin)	random	8
β_{inbred}		overall inbred penalty	fixed	1
b_j		strain-specific inbred penalty	random	8
v_{jk}		strain pair-specific symmetric epistasis	random	28
w_{jk}		strain pair-specific asymmetric epistasis (parent-of-origin)	random	28
ϕ		overall female	fixed	1
ϕ_j^a		sex-by-strain-specific additive	random	8
ϕ_j^m		sex-by-strain-specific maternal (parent-of-origin)	random	8
ϕ_{inbred}		overall female inbred	fixed	1
ϕ_j^b		sex-by-strain-specific inbred penalty	random	8
ϕ_{jk}^v		sex-by-strain pair-specific symmetric epistasis	random	28
ϕ_{jk}^w		sex-by-strain pair-specific asymmetric epistasis (parent-of-origin)	random	28

[a] Random effect levels for $u^{(\text{batch})}$ differ according to the number of experimental batchs within each phenotype being modeled: 52 levels for D0, D1pct, D2pct, D1delta, D2delta, and 44 levels for D3pct, D4pct, D3delta, and D4delta. In the text, h is used to indicate the level of batch for a given individual or quartet.

B. Modeling infection response as mock-corrected percent change in body weight post-infection

A standard measure used to assess pathogenesis in IAV-infected mice is weight loss. Weight loss correlates with several host and viral factors, including viral load, immune response phenotypes and lung histopathology (Ferris *et al.* 2013; Leist *et al.* 2016); as such, it provides a simple, non-invasive measure of infection pathology that can be assessed for a large number of mice. We measured the percentage change in body weight relative to D0

$$\text{pct}_i^{\text{day[group]}} = 100 \times \text{weight}_i^{\text{day[group]}} / \text{weight}_i^{\text{D0[group]}}, \tag{3}$$

for mouse i on day $\in \{\text{D1, D2, D3, D4}\}$ in group $\in \{\text{flu, mock}\}$, where, *e.g.*, $\text{weight}_i^{\text{D4[flu]}}$ and $\text{weight}_i^{\text{D0[flu]}}$ are the body weight for IAV-infected mouse i at D4 and at D0, respectively. These measures, which we describe as single outcome phenotypes, were analyzed using BayesDiallel as above (**Table** 2), but they were not the main focus of our study. Our main focus was a derived measure, IAV infection response, defined next.

In defining IAV infection response we note that from a causal inference perspective (described more fully in **Appendix A**), weight loss in an IAV-infected mouse (*e.g.*, $\text{pct}_i^{\text{D4[flu]}}$) reflects two confounded processes: weight loss due to IAV-induced pathogenesis and weight loss due to other aspects of the experimental procedure. To obtain an unconfounded estimate of weight loss due to IAV-induced pathogenesis alone, we defined IAV infection response as the difference between weight loss in mice subject to infection by IAV and those subject to mock. Specifically, since in our experimental design we match one mock mouse to three infected — this reflecting our expectation that phenotypes from infected mice will be more variable and will thus need more replicates for comparable precision — infection response

206 was defined in terms of "matched quartets", $q = 1, \ldots, Q$, where each matched quartet q comprised four mice of the same diallel category

207 from the same experimental batch, with the first three mice, $q[1]$, $q[2]$ and $q[3]$, being IAV-infected and the last mouse, $q[4]$, receiving mock

208 treatment. Infection response at a given day for quartet q was thus defined as a "delta",

$$\text{delta}_q^{\text{day}} = \frac{1}{3} \sum_{f=1}^{3} \text{pct}_{q[f]}^{\text{day [flu]}} - \text{pct}_{q[4]}^{\text{day [mock]}} , \tag{4}$$

209 following the more general definition in Eq 11 in **Appendix A**.

210 Diallel effects on infection response were then modeled using BayesDiallel in manner analogous to the single outcome case in Eq 1, as

$$\text{delta}_q^{\text{day}} = \theta + \mathbf{c}_q^{\text{T}} \boldsymbol{\alpha} + \sum_{r=1}^{R} u_q^{(r)} + \mathbf{d}_q^{\text{T}} \boldsymbol{\beta} + \varepsilon_q , \tag{5}$$

211 where now the unit of observation is the matched quartet q, rather than the individual i, and where, for example, $\mathbf{d}_q$ is shorthand for

212 $\mathbf{d}_{\{jk,s\}[q]}$, the diallel category appropriate for q. The shift to modeling treatment response does, however, change how the parameters

213 are interpreted. The intercept in the above formula, relabeled at θ, now acquires a special meaning, representing an overall causal effect

214 due to infection, and the diallel effects in $\boldsymbol{\beta}$ now describe how that causal effect is modified by parentage, sex and their interaction;

215 for example, the additive effect parameter a_{AJ} is the expected increase in infection response on adding one haploid genome of strain

216 AJ. Regarding covariates, as for the single outcome phenotypes, this model included a random effect of batch, and, to reduce potential

217 dependence between the deltas and baseline body weight, we also included a fixed effect covariate for the quartet mean D0 weight (ie,

218 $\text{D0}_q = \sum_{f=1}^{4} \text{weight}_{q[f]}^{\text{D0}} / 4$) in $\mathbf{c}_q$ (**Table 2**).

■ **Table 2 Models used for each analysis in this study.**

Model No.	Model [a]		Phenotype(s)	Unit	Variance Parameters
1	$y_i = \mu + u_i^{\text{(batch)}} +$	$\mathbf{d}_i^{\text{T}} \boldsymbol{\beta} + \varepsilon_i$	pre [b]	individuals	12 [c]
2	$y_i = \mu + u_i^{\text{(batch)}} + c_i^{\text{(D0)}} \alpha +$	$\mathbf{d}_i^{\text{T}} \boldsymbol{\beta} + \varepsilon_i$	post [d]	individuals	12 [c]
3	$\text{delta}_q = \theta + u_q^{\text{(batch)}} + c_q^{\text{(D0)}} \alpha +$	$\mathbf{d}_q^{\text{T}} \boldsymbol{\beta} + \varepsilon_q$	delta [e]	quartets	12 [c]
4	$\text{delta}_q = \theta + u_q^{\text{(batch)}} + c_q^{\text{(D0)}} \alpha + u_q^{\text{(Mx1 diplo)}} +$	$\mathbf{d}_q^{\text{T}} \boldsymbol{\beta} + \varepsilon_q$	delta [e]	quartets	13 [f]

[a] See study design in **Figure 1** for overview of analyses. See **Table 1** and Statistical Methods for parameter and phenotype definitions.
[b] D0 [all].
[c] This count includes τ_{batch}^2, $\{\tau_a^2, \tau_m^2, \tau_b^2, \tau_v^2, \tau_w^2\}$, $\{\tau_{\phi a}^2, \tau_{\phi m}^2, \tau_{\phi b}^2, \tau_{\phi v}^2, \tau_{\phi w}^2\}$, and σ^2.
[d] D1pct, D2pct, D3pct, D4pct [mock] and D1pct, D2pct, D3pct, D4pct [flu]
[e] D1delta, D2delta, D3delta, D4delta
[f] This count includes $\tau_{\text{Mx1 diplo}}^2$ and parameters in [c].

219 Although our experimental design stipulated even multiples of 4 mice per diallel category, practical constraints on animal breeding and

220 availability meant that in some cases this number was 3 or 5, such that some quartets had either missing infecteds or surplus mocks. To

221 ensure the definition of delta in Eq 4 remained consistent, and in particular that deltas from different quartets had comparable precision, the

222 diallel analysis was performed on $M = 1,000$ imputed versions of the data, with each imputed dataset being composed of exact quartets in

223 which missing phenotypes had been filled using stochastic regression imputation and surplus mocks had been (randomly) deleted (details

224 in **Appendix B**). On each imputed dataset we collected 125 MCMC samples from 12,500 total time steps (*i.e.*, by recording values at every

225 100th timestep); results were based on the aggregate of these samples from the M imputed datasets (*i.e.*, on 125,000 MCMC samples in

226 total).

C. Reporting BayesDiallel results: HPD, MIP, VarP and TreVarP

Point and interval estimates of individual diallel effects, *e.g.*, additive effect a_{AJ}, are reported as posterior means and 95% highest posterior density (HPD) intervals. The overall contribution of a particular inheritance group is reported in two ways: as a Variance Projection (VarP), *e.g.*, VarP[a] for the contribution of additive effects to a phenotype or Treatment Response Variance Projections (TreVarPs), *e.g.*, TreVarP[a] for the contribution of additive effects to an infection response; and as a model inclusion probability (MIP), *e.g.*, MIP[a] for the probability of additive effects being included in the model.

The VarP is a heritability-like measure that predicts how much of the total phenotypic sum of squares would be explained by each component in a new, completely balanced diallel. Unlike traditional heritability, it is calculated based on the effects, β, rather than the variance components, $\tau_a^2, \ldots, \tau_w^2, \sigma^2$, and as such benefits not only from greater interpretability but also from the stability and accuracy provided by hierarchical shrinkage (as detailed in Crowley *et al.* 2014). Since the VarP is a function of the posterior predictive distribution and calculated at each iteration of the MCMC chain, reported via Bayesian posterior summaries, specifically, the posterior mean and the α-level equiprobable central posterior quantile (posterior interval). The VarPs for infection response phenotypes are, following Crowley *et al.* (2014), given the special name of TreVarPs, to acknowledge their more delicate interpretation.

The MIP reflects a different type of inference: rather than being a function of the parameters estimated in the full, sexed BayesDiallel model of Eq 1 and Eq 2, it describes the results of model selection, that is, an assessment of which diallel categories could be excluded without a substantial loss in fit. As in Crowley *et al.* (2014), we use the exclusionary Gibbs group sampler of Lenarcic *et al.* (2012). Each diallel category is set to have a prior inclusion probability of 0.5, reflecting a prior opinion that inclusion and exclusion are equally likely. This prior is then updated by the phenotype data and the model selection procedure to give a (posterior) MIP. MIPs are interpreted following the conventions in Crowley *et al.* (2014): MIPs in the range (0.25,0.75) indicate that the data does not provide sufficient evidence to make an informed decision about exclusion or inclusion; MIPs within (0.05,0.25] or [0.75,0.95) represent positive evidence for exclusion or inclusion respectively; (0.01,0.05] or [0.95,0.99) represent strong evidence; and [0,0.01] or [0.99,1] represent strong to decisive evidence. These conventions are based on those proposed by Kass and Raftery (1995) for Bayes factors, which are connected to MIPs by the relation

$$\text{Bayes Factor} = \frac{\text{MIP}}{1 - \text{MIP}} \times \frac{1 - \text{MIP}_0}{\text{MIP}_0} \, ,$$

where MIP_0 is the prior inclusion probability, and where the above simplifies to $\text{MIP}/(1 - \text{MIP})$ in our case of $\text{MIP}_0 = 0.5$.

D. Estimating *Mx1* effects in the diallel

The critical host resistance factor (*Mx1*) has been shown to drive IAV-resistance in the CC founder strains and has been mapped in the pre-CC (Ferris *et al.* 2013). *Mx1* was previously described as having three major, naturally occurring functional classes of resistance to influenza H1N1 arising from the subspecies *Mus musculus domesticus* (hereafter, *dom*; members include AJ, B6, 129, NOD and WSB), *M. m. castaneous* (*cast*; CAST) and *M. m. musculus* (*mus*; PWK and NZO), of which *dom* is considered to be null whereas *mus* and *cast* are protective. (Note that *dom Mx1* in the CC founder strains is comprised of two unique null alleles, and that the subspecific *Mx1* alleles observed in the CC may not be representative of the those segregating in the wild.) To estimate the contribution of *Mx1* haplotypes as discernible in the diallel, and thereby also estimate the extent of heritable effects that remain after *Mx1* is controlled for, we define the following haplotype combinations (diplotypes) as six levels of the random effect, $u^{(Mx1 \text{ diplo})}$: {*dom* × *dom*}, {*dom* × *cast*}, {*cast* × *cast*}, {*cast* × *mus*}, {*mus* × *dom*}, and {*mus* × *mus*}; we then repeat our diallel analysis with this effect included (Model 4 in **Table 2**).

260 **D.1. Estimating a dominance index for Mx1 alleles.** Dominance is typically defined in the context of bialleles. Since in this population,

261 *Mx1* has a multiallelic series, we define dominance between allele pairs. Following Kacser and Burns (1981), which is built on the work of

262 (Wright 1934), we define the "dominance index" for a wild-type (wt) against a mutant (mut) allele as

$$\mathcal{D}^{(\text{wt; mut})} = \frac{u^{(\text{wt wt})} - u^{(\text{wt mut})}}{u^{(\text{wt wt})} - u^{(\text{mut mut})}},\tag{6}$$

263 where values for $\mathcal{D}$ are close to -0.5 when the effect of the wild-type is overdominant to the mutant (the effect of the mutant is underrecessive),

264 0 when the effect of the wild-type is completely dominant to the mutant (the effect of the mutant is recessive), close to 0.5 when the

265 effect of the wild-type is additive (not dominant, or incompletely dominant) to the mutant, close to 1 when the effect of the wild-type is

266 recessive (the effect of the mutant is dominant), and close to 1.5 when the effect is underrecessive (the effect of the mutant is overdominant).

267 Overdominance is given by values of $\mathcal{D}$ that are much less than 0 and underdominance by values that are much greater than 1. This

268 definition is used to define dominance indices $u^{(cast; dom)}$ and $u^{(mus; dom)}$, describing the degree of dominance of the protective alleles *cast*

269 and *mus* respectively against the null allele *dom*. To assess the degree to which *cast* and *mus* differ in their relation to *dom*, we further define

270 a "dominance difference index",

$$\mathcal{DD}^{(mus-cast; dom)} = \mathcal{D}^{(mus; dom)} - \mathcal{D}^{(cast; dom)},\tag{7}$$

271 where negative values indicate that *mus* has more of a dominance-based relationship to *dom* than does *cast*, positive values indicate the

272 converse, and zero indicates that the relationships of *cast* and *mus* to *dom* show dominance equally.

273 When the BayesDiallel model includes *Mx1* effects, the aforementioned dominance index and dominance difference index are both

274 functionals of the posterior; posterior samples of these indices were therefore obtained by simply applying Eq 6 and Eq 7 to the sampled

275 *Mx1* effects at each timestep of the MCMC chain.

276 The Kacser and Burns (1981) dominance index is a simple re-parameterization of the degree of dominance parameter, a_{CR}, defined by

277 Comstock and Robinson (1948) and used by Gardner and Lonnquist (1959). In the Comstock and Robinson model, the mean centered

278 phenotypes are coded, translating our model above, as: $u^{(\text{wt; wt})} = w$, $u^{(\text{wt; mut})} = aw$, and $u^{(\text{mut; mut})} = -w$. This gives the relation

279 $\mathcal{D}^{(\text{wt; mut})} = (1 - a_{\text{CR}})/2$ or equivalently, $a_{\text{CR}} = 1 - 2\mathcal{D}^{(\text{wt; mut})}$.

280 **E. Estimating haplotype effects at the *Mx1* locus in the pre-CC and CC-RIX**

281 The additive effect parameters estimated in the diallel do not precisely distinguish the effects at the *Mx1* locus because they are confounded

282 with any potential effects genome-wide that follow the same pattern of strain classification. An unconfounded estimate of haplotype

283 effects at *Mx1* requires a population in which the remainder of the genome is randomized, *e.g.*, by recombination. To this end, we make

284 use of two related data sets on IAV-induced weight loss in two CC-derived MPPs: IAV (PR8) infection in the pre-CC and IAV (CA04)

285 infection in a set of CC-RIX lines. These two studies, described in more detail below, were in other respects less rigorous than our diallel:

286 the experimental measurement of the infection response was based on infected mice only with no mocks in the pre-CC, and although

287 mocks were collected in the CC-RIX, their relative sparsity (200-300 mocks to >1400 infecteds) complicates analysis based on matching

288 alternate treatment groups; the experimental batching was subject to a less exacting degree of randomization across genetically distinct

289 categories; the available combinations of *Mx1* diplotypes are limited mostly to homozygotes in the pre-CC, and incompletely and unevenly

290 sampled in the CC-RIX; the *Mx1* diplotype state for each line is known only probabilistically, having been inferred by hidden Markov

291 models (HMMs) applied to genotyping data. Nonetheless, if effects at the *Mx1* locus were largely independent of those elsewhere in the

292 genome, we might expect that *Mx1* effects in the pre-CC and CC-RIX would be broadly consistent with those in the diallel.

Estimation of haplotype effects at the *Mx1* locus was performed using the Diploffect model (Zhang *et al.* 2014), a Bayesian hierarchical model that estimates effects of diplotype substutions at a specified QTL when the diplotype states themselves are known only probabilistically. The effects estimated by Diploffect are analogous to those estimated by BayesDiallel: phenotype y_i of mouse i is modeled as

$$y_i = \mu + \mathbf{c}_i^{\mathrm{T}}\boldsymbol{\alpha} + \sum_{r=1}^{R} u_i^{(r)} + \mathrm{dip}_i^{\mathrm{T}}\boldsymbol{\beta} + \varepsilon_i \,, \tag{8}$$

where dip_i is a vector representing the diplotype state of mouse i at the QTL and is shorthand for $\mathrm{dip}_{\{jk\}[i]}$, where $\{jk\}[i]$ denotes i's diplotype state composed of haplotypes from CC founder strains j and k, $\boldsymbol{\beta}$ are the corresponding effects, and all other variables are as in Eq 1. The diplotype vector $\mathrm{dip}_{\{jk\}}$ is defined with $\boldsymbol{\beta}$ so as to give the linear predictor

$$\mathrm{dip}_{\{jk\}}^{\mathrm{T}}\boldsymbol{\beta} = a_j + a_k + I_{\{j\neq k\}}\gamma_{jk} \,, \tag{9}$$

where a_j and a_k are additive (haplotype) effects modeled as $a_j \sim \mathrm{N}(0, \tau_{\mathrm{add}}^2)$, broadly equivalent to the additive effects in BayesDiallel's Eq 2, and $\gamma_{jk} \sim \mathrm{N}(0, \tau_{\mathrm{dom}}^2)$ are dominance deviations, which are the converse to BayesDiallel's inbred parameters. Dominance deviations are expected to be poorly informed when heterozygotes are sparsely represented, as in the CC-RIX and in particular the largely inbred pre-CC, but are nonetheless included to stabilize inference of additive effects. For numerical stability, phenotypes were first centered and scaled to unit variance, and variance parameters (σ^2 or τ_{effect}^2, where effect is add, dom or $r \in R$) were given mildly informative priors of the form $\tau_{\mathrm{effect}}^{-2} \sim \mathrm{Ga}(1,1)$. Estimation proceeded by importance sampling (the DF.IS and DF.IS.kinship methods in Zhang *et al.* 2014) using integrated nested Laplace approximations (INLA; Martins *et al.* 2013), with 100 importance samples taken, and parameter estimates for additive effects are reported as posterior means, posterior medians and HPD intervals.

E.1. Pre-CC study. In the study of Ferris *et al.* (2013), IAV infection response was measured on 155 mice from as many pre-CC lines as weight loss following infection with IAV (PR8 variant, as for the diallel). QTL mapping of D4 p.i. weight loss, equivalent to $\mathrm{pct}_i^{\mathrm{D4}}$ in the diallel study, identified a QTL, *HrI1*, containing the *Mx1* gene, with peak marker JAX00072951 (chr16:98,148,641; Mouse Diversity Array of Yang *et al.* 2009). We estimated haplotype effects at this peak marker using Diploffect (Zhang *et al.* 2014), applied to the phenotype and the original HMM probabilities of Ferris *et al.* (2013), with the model including a fixed effect covariate for D0 weight.

E.2. CC-RIX study. For the CC-RIX study of infection response to IAV (CA04 strain), we calculated weight loss values for all 1,402 infected mice at D7 p.i. (analogous to a $\mathrm{pct}_i^{\mathrm{D7}}$ measure), and for all 105 CC-RIX lines obtained diplotype probabilities at marker UNC27478095 (16:97,591,482; MegaMUGA array, described in Morgan *et al.* 2016) from the Inbred Strain Variant database (ISVdb; Oreper *et al.* 2017). Haplotype effects were then estimated by Diploffect applied to debatched CC-RIX line means as follows. First, we fit linear mixed model (by REML using R package lme4 of Bates *et al.* 2015) to the individual-level phenotypes (n=1,402) with fixed effects of D0 weight and lab (2 levels), and random effects of mating (107 levels: 105 RIXs + 2 additional levels distinguishing minor breeding differences, when CC010 and CC042 strains were re-derived from breeder females into a new facility) and infection date (59 levels). The residuals of this model were then averaged over the n_i mice of each CC-RIX line i, and used as the response y_i in Eq 8 with precision-weighting $\varepsilon_i \sim \mathrm{N}(0, \sigma^2/n_i)$ and a between-line polygenic random effect $\mathbf{u} \sim \mathrm{N}(\mathbf{0}, \mathbf{G}\tau_G^2)$, where 105×105 genetic relationship matrix $\mathbf{G}$ was calculated between all CC-RIX pairs based on the founder haplotype probabilities (dosages) at each locus, according to the method described in Gatti *et al.* (2014).

F. Availability of Data and Software

Analyses were conducted in the statistical programming language R (R Core Team 2017). In addition to R packages cited above, we used the packages BayesDiallel (Lenarcic *et al.* 2012) and Diploffect.INLA (Zhang *et al.* 2014). The data, analysis software, and scripts are available on flu-diallel repository on GitHub, at https://github.com/mauriziopaul/flu-diallel. A static version is posted as a public, open access Zenodo repository, at http://dx.doi.org/10.5281/zenodo.293015. Phenotype data from the diallel and CC-RIX animals used in this study will be available on the Mouse Phenome Database (Grubb *et al.* 2014), at https://phenome.jax.org with persistent identifier RRID:SCR_003212.

File S1 contains an account of the supplemental files which can be used to reproduce our analysis. File S2 contains the software packages used for this analysis. File S3 contains the diallel data file, and File S4, S5, and S6 contain the data analysis files required for analyzing the diallel, pre-CC, and CC-RIX, respectively. After unzipping, the files FluDiData.csv, Flu-pre-CC-data.csv, and Flu-CC-RIX-data.csv contain raw phenotypes, cross (or line, strain), and mouse ID information from the three mouse populations used in this study. The script files MIMQ*.sh are used in bash to call R scripts to run the BayesDiallel analysis on diallel phenotypes. The script files main_analysis*.R are used with Diploffect to run Diploffect analysis on the pre-CC and CC-RIX phenotypes. Additional *.RData, *.pl, *.alleles, and *.csv files are uploaded which contain settings, genotypes, and founder haplotype probabilities used by the scripts.
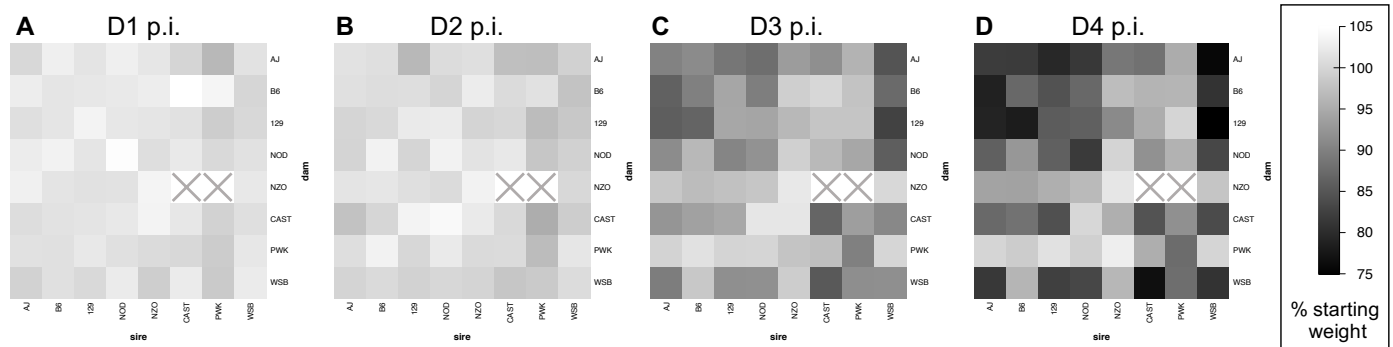
6. RESULTS

Figure 3 Influenza-induced weight loss in an 8×8 diallel cross of mice, through four days post-infection. Mean weight change, as % D0 weight, is shown at (A) day 1, (B) day 2, (C) day 3, and (D) day 4 post-infection with 500pfu IAV (PR8) in male and female inbreds and F1 hybrids of CC founder strains (n=774 for D1 and D2, n=382 for D3 and n=381 for D4). Results from mock-infected mice not shown. Squares with a grey "X" indicate matings that do not produce offspring.

Mice from the eight inbred founder strains of the CC were used to generate a near-complete 8×8 diallel. This study used offspring (n=1,043) of both sexes (519 females, 524 males) representing 62 of the 64 crosses (**Figure S1**), including all inbred combinations (n=129) and all F1 hybrids (n=914) except NZO×CAST and NZO×PWK. Within each diallel category, defined as the combination of sex and (reciprocal) parentage, and in each experimental batch, mice were randomly assigned at weaning to infection or mock groups in a ratio of 3:1; complete sets of 3 infected with 1 mock were described as matched quartets. Mice in the infected group were inoculated with IAV PR8 and in the mock group with PBS. For each mouse, body weight was measured prior to infection (D0 or baseline weight), and at days 1-4 post-infection (D1, D2, D3, D4). D0 weight is reported in grams whereas post-infection weight is hereafter reported as a percentage of D0 weight, *e.g.*, D4pct. Not all mice survived the protocol: one infected mouse died after D3 weights were taken and one mouse died from anesthesia on D0.
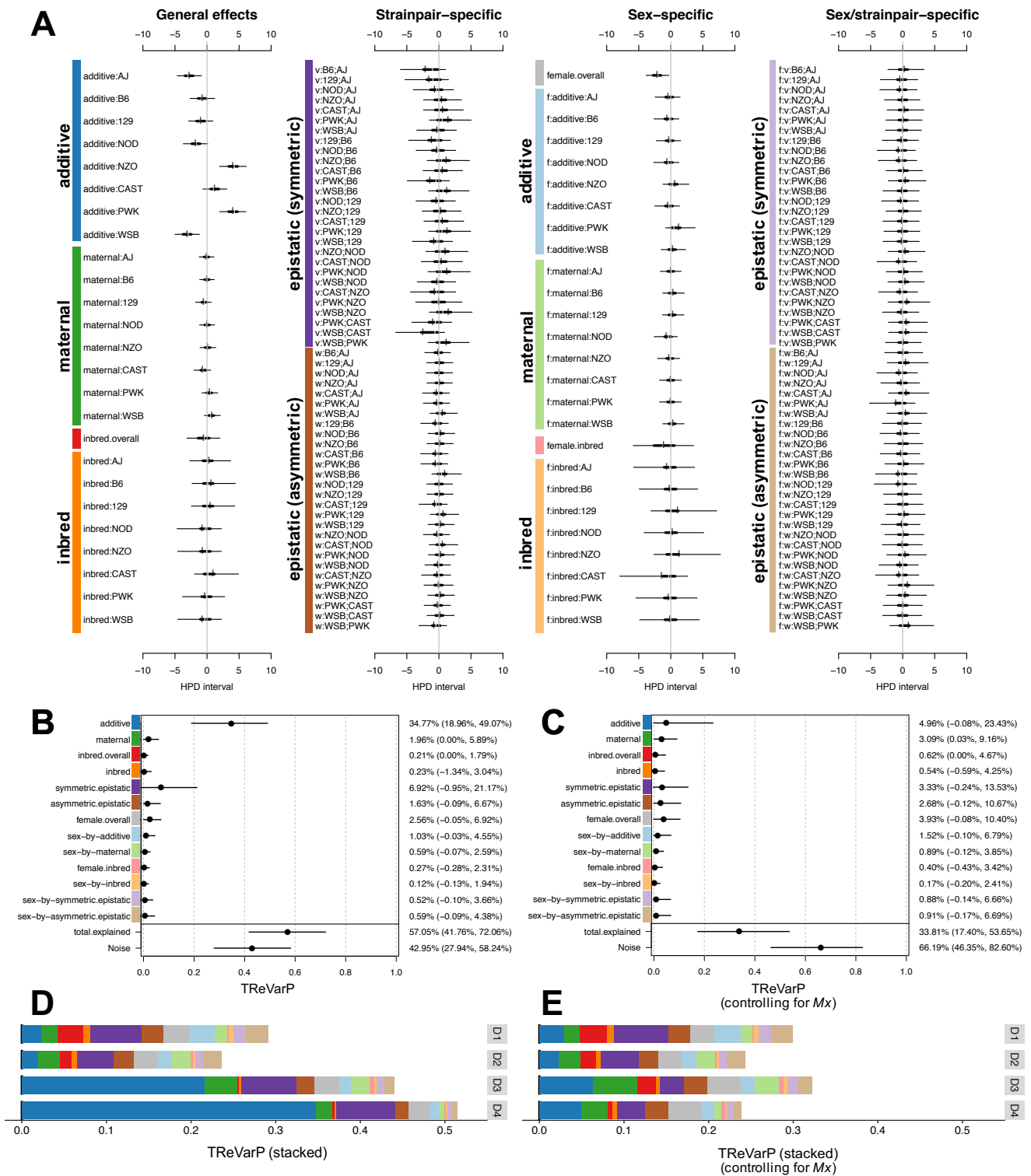
Figure 4 Diallel effects on host weight IAV-infection response, before and after accounting for *Mx1* haplotypes. A) Effect estimates for additive, maternal, inbred, and epistatic effects, including sex-specific effects, are presented as highest posterior density (HPD) intervals across 163 individual effects categories for IAV-induced weight change at D4 p.i. (phenotype D4delta). HPDs are given for each parameter, including 95% (thin line) and 50% (thick line) intervals, and median (white break) and mean (black vertical line). Parameters are labeled according to the methods. Symmetric epistatic, asymmetric epistatic, and sex-specific parameters are indicated by "v:", "w:", and "f:", respectively. The overall treatment effect, θ, (not shown) is -8.85% (-9.92%, -7.78%). B-C) Treatment Response Variance projections (TReVarPs), a generalization of heritability for diallel effects classes, at D4 are shown for three fixed (overall) effects, five random effects classes and five corresponding sex-specific random effects classes (posterior median and 95% quantile-based confidence intervals) before (B) and (C) after accounting for diplotypes of the host influenza resistance allele, *Mx1*. D-E) TReVarPs before and after *Mx1* for all four post-infection timepoints.

A. F1 hybrids of the CC founders show a wide range of phenotypic outcomes

The CC founders include five strains we have previously characterized as susceptible to IAV-induced pathology (AJ, B6, 129, NOD, and WSB), two strains as resistant (NZO and PWK), and one (CAST) that exhibits a distinct intermediate weight loss phenotype (Ferris *et al.* 2013). Results for the inbred founders measured in our diallel replicate those earlier findings, and the post-infection weight loss among the infected F1 hybrids spanned the range of phenotypes observed in the founders (**Figure S3**), consistent with the notion of IAV-induced weight loss being a complex trait with contributions from multiple loci.

B. Diallel effects on baseline mouse weight strongly replicate previous CC founder diallel studies

The effects of parentage and sex on D0 weight were estimated using BayesDiallel. Described further in **Methods**, BayesDiallel decomposes the heritable effects observable in the diallel into 160 parameters (diallel effects) grouped into 13 distinct heritability classes. In sketch form, it models the average phenotype of mice of sex *s* bred from mother of strain *j* and father of strain *k* as

$$\text{ave.phenotype}_{jks} = \underset{\text{\& covariates}}{\text{overall mean}} + \underbrace{a_j + a_k + \text{inbred}_j + \text{other}_{jks}}_{\text{diallel effects}},$$

where covariates always includes experimental batch, a_j and a_k are the additive effects of the two parents, inbred_j is an additional effect included only when $j = k$), and other_{jks} models the effects of further nuances of sex and parentage as deviations from this base model (listed in **Methods** and **Table** 1).

Diallel effects estimated for D0 weight are reported in **Figure S6A** as 95% HPD intervals for each parameter, and two summary measures, VarPs and MIPs, for each of the 13 heritability classes are given in **Figure S6B,C**. Briefly, VarPs (**Figure S6C**) report the contribution of the effect group as the proportion of the total phenotypic variance, whereas MIPs (**Figure S6B**) assess the strength of support for whether an effect group should be included at all, with probabilities near 1 providing stronger support for inclusion, probabilities near 0 supporting exclusion, and probabilities near 0.5 reflecting a lack of information either way.

The pattern of effects for D0 weight was strikingly similar to that seen for baseline body weight in two previous diallels of the CC founders (Lenarcic *et al.* 2012; Crowley *et al.* 2014), despite those earlier studies being independent experiments with no particular attempt made to align experimental protocols, and included substantial additive effects, strain-specific parent-of-origin effects, signals of epistasis, and sex-specific versions thereof. For example, we largely replicated the pattern of inbred, additive, and maternal effects observed in both Lenarcic *et al.* (2012) and Crowley *et al.* (2014), and also found a higher-order sex-specific PWK×CAST symmetric epistatic effect in Lenarcic *et al.* (2012). We also observed some new epistatic and sex-specific epistatic effects largely due to increased power from a larger sample size.

C. Diallel effects on IAV infection response

Infection response was defined as the percentage change in body weight induced by IAV infection, with more negative values indicating more severe pathogenesis. This was calculated at each timepoint, D1, D2, D3, and D4 p.i., as the difference between matched infected and mock mice, yielding a single infection response number (a "delta", *e.g.*, D4delta) for each matched quartet (3 infected mice and 1 mock). The effects of parentage and sex on infection response were then analyzed for each timepoint separately using BayesDiallel as above, with an additional covariate of D0 weight (see **Methods** for details). Although results are provided in Supplemental Materials for all timepoints, we will focus on those for D4 p.i. since this showed the greatest difference between infected and mock.

C.1. IAV infection causes weight loss through day 4 post-infection, with greater susceptibility in females. IAV infection in the diallel induced an overall mean change in body weight (*i.e.*, overall infection response θ in **Eq** 5 and **Table** 1) of -0.13% (95% HPD interval: -0.48,

0.22; MIP=1) on D1 p.i., -0.83% (-1.33%,-0.32%; MIP=1) on D2 p.i., -5.60% (-6.47%, -4.73%; MIP=1) on D3, and -8.85% (-9.92%, -7.78%; MIP=1) on D4 (**Table** S3; see also progression in **Figure** **3**). Consistent with previous mouse studies of sex effects on infection (Robinson *et al.* 2011; Lorenzo *et al.* 2011), females given the same dose of virus as male mice had increased weight loss: a negative effect of female sex was estimated at all four time points p.i., gradually increasing in magnitude from -0.89% (-1.45%, -0.36%) at D1 p.i. to -2.11% (-3.87%, -0.30%) at D4 p.i. (**Figure** **4**), suggesting that enhanced susceptibility in females may occur at least as early as D1 p.i. Although all mice received the same dose of virus regardless of starting body weight, heavier mice experienced a transient increase in percent weight loss at D2 p.i. compared with lighter mice: the D0 weight effect (α in **Eq** 5) on the infection response at D2 p.i. was -0.31% (-0.52%, -0.09%), such that for every 10 grams of starting weight beyond 0 grams, an additional $\approx 3.1\%$ weight was lost on D2; however, this effect disappeared by D3 p.i. No other significant effects of starting weight on IAV-induced weight loss were detected at other time points, indicating that heavier mice were infected at least as effectively as lighter mice, and that starting body weight does not in general confound our exploration of strain and cross-specific effects.

C.2. Diallel effects on infection response reflect mostly additive genetics, consistent with differences in *Mx1* haplotype. Infection response in our diallel was strongly driven by additive effects. On D3 p.i., enhanced susceptibility to weight loss in infected animals was affected most by contributions from strain AJ, -2.17% (-3.72%, -0.61%), and enhanced resistance from contributions of NZO, 2.54% (0.72%, 4.27%), and PWK, 1.70% (0.12%, 3.23%), strains. On D4 p.i., enhanced suscepitibility was greatest from AJ, -2.77% (-4.66%, -0.86%) and WSB, -3.09% (-5.01%, -1.18%), with enhanced resistance greatest from NZO, 4.07% (1.95%, 6.12%), and PWK, 4.06% (1.97%, 6.08%) (**Figure** **4A**). In terms of its additive effect, CAST was more resistant than the *Mx1*-null strains (AJ, B6, 129, NOD, and WSB) but about half as resistant as the *Mx1*-functional strains (NZO and PWK), consistent with it conferring intermediate protection in the heterozygote state.

To summarize these effects: for each dose of AJ or WSB genomes inherited from a parent, about 2%-3% of additional starting body weight is lost post-infection, indicating enhanced susceptibility compared with the overall mean weight loss; for each NZO and PWK genome inherited, about 4% more of starting body weight is retained post-infection, compared with the mean treatment effect, indicating enhanced resistance.

Diallel effects explained over half of the total variance of infection response at D4, with a treatment response VarP for all effect groups collectively of 57% (TReVarP[all]=0.571; 0.418, 0.721). The variance explained by additive effects only, which is related to the narrow-sense heritability, was estimated as 34.8% (TReVarP[a]=0.348; 0.190, 0.491), and also detected were potential additional contributions of epistasis (TReVarP[v]=0.069; -0.001, 0.212) and maternal effects (TReVarP[m]=0.020; 0.000, 0.059) (**Figure** **4B,D**, **Table** S1).

C.3. Evidence for additive, inbred, epistatic and parent-of-origin effects mounts as disease progresses. The relevance of diallel effects to infection response became more marked with time (**Table** S3, **Figure** **S7-S10**). At D1 and D2 p.i., model inclusion probabilities gave strong support only to an overall infection response, with no evidence of this effect being modified by sex or parentage (**Figure** **S7-S8**). At D3 p.i., however, we found positive to strong evidence of additive (MIP[a]=0.978), inbred (MIP[b]=0.958), and asymmetric epistatic (MIP[w]=0.820; *i.e.*, parent-of-origin epistatic) effects (**Figure** **S9**). By D4 p.i., support for additive (MIP[a]=0.998) and inbred (MIP[b]=0.999) effects had become decisive (see **Methods** for MIP interpretation), and there was strong support for both symmetric epistatic (MIP[v]=0.960) and asymmetric epistatic (MIP[w]=0.966) effects (**Figure** **S10**, **Table** S3).

D. Modeling effects consistent with *Mx1* haplotype

To help distinguish diallel effects that are consistent with the subspecies haplotype of the resistance factor *Mx1* (hereafter, *Mx1* effects), we incorporated the *Mx1* subtype explicitly into the model as a genotype covariate with three alleles, one for each subspecies branch: *dom* (AJ,

415 B6, 129, NOD, WSB), *cast* (CAST), and *mus* (NZO, PWK).

416 **D.1. Mx1 *effects are increasingly evident with disease progression; explain ~40% of the diallel effects at D4 p.i.*** In keeping with the

417 increased support seen for diallel effects over time, evidence for a non-zero *Mx1* effect increases from positive evidence of exclusion

418 on D1 (MIP=0.035) to no evidence for inclusion or exclusion on D2 (MIP=0.552), to decisive evidence for inclusion on D3 (MIP=1.000)

419 and D4 (MIP=1.000) (**Figure S11-S14**); a comparable level of support for inclusion in the model was seen only for effects of overall

420 treatment and batch. After controlling for *Mx1*, the variance explained by diallel effects at D4 was substantially reduced, from 57% to 33.8%

421 (TReVarP[all|*Mx1*]=0.338; 0.174,0.537) (**Figure 4C,E**, **Table S2**). This was consistent with *Mx1* accounting for about 40% of the variance

422 explained by the diallel, including most of the additive effects (mathematically the *Mx1* term models effects that compete with a subset of
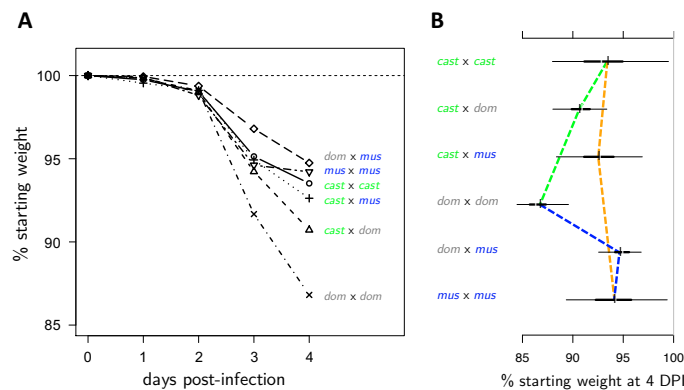
423 the additive and dominance diallel effects).

Figure 5 Time course of subspecies-specific *Mx1* haplotype effects on IAV-induced weight change in the diallel. A) Predictive means of *Mx1* diplotype effects across four days post-infection, modeled simultaneously with other diallel effects and covariates. B) HPD intervals of *Mx1* diplotype effects on weight change on day 4 post-infection. Increased resistance is indicated by values further to the right. Dashed lines highlight the mode of interaction between *Mx1* haplotypes: green (- - -) shows the additive effect of crossing *cast* with *dom*, blue (- - -) the dominant effect of crossing *mus* with *dom*, and orange (- - -) the neglible effect of *cast* crossed with *mus*.

424 **D.2. *Evidence for distinct additive and non-additive effects of Mx1 functional groups*** After controlling for other diallel effects, the

425 predicted weight loss over the course of 4 days varies in a manner consistent with *Mx1* allele combination (**Figure 5A**). We observed that,

426 as expected, *dom* × *dom* crosses were predicted to have much more overall post IAV-infection weight loss at D3 and D4 compared with all

427 other crosses. Notably, the most protected group appeared to be the *dom* × *mus* haplotype, at both D3 and D4 post-infection, although the

428 HPD intervals overlap with other *Mx1*-functional groups. The rank order of effects changes from D3 to D4 due to the dramatic slowing of

429 weight loss in the *mus* × *mus* crosses from D3 to D4 compared with D2 to D3.

430   Although we did not observe any strain- or pairwise-specific non-additive effects in the diallel prior to inclusion of the *Mx1* random

431 effect, we did observe a pattern of dominance in crosses between *mus* and *dom*, even as there was a pattern of additivity in the crosses

432 between *cast* and *dom* (**Figure 5B**). Whereas it might be expected that host alleles from *Mx1*-null strains should act in a recessive manner,

433 this appears not to be the case for this phenotype and time point in crosses of *cast* with *dom*, such that the functional *Mx1* allele from CAST

434 appears to operate in an additive manner. This further supports the previous observation that the CAST *Mx1* alleles differ from the *mus*

435 *Mx1* alleles in their protective host response to IAV (Ferris *et al.* 2013).

436 **D.3. Dominance and additivity of Mx1 *alleles against the functional null: mus is dominant, cast acts additively.*** To better characterize

437 how the *Mx1* effects on infection response exhibit aspects of genetic dominance vs. genetic additivity, we estimated for each functional *Mx1*

438 allele a "dominance index", after Kacser and Burns (1981). This measures the distance between the expected phenotype of a homozygous

439 functional allele, in our case *mus* or *cast*, and the heterozygote formed with a null allele, in our case *dom*. On this scale, 0 denotes the

440 functional allele being dominant to the null, 1 denotes it being recessive and 0.5 indicates pure additivity (see x-axis scale in **Figure 6A, B**,
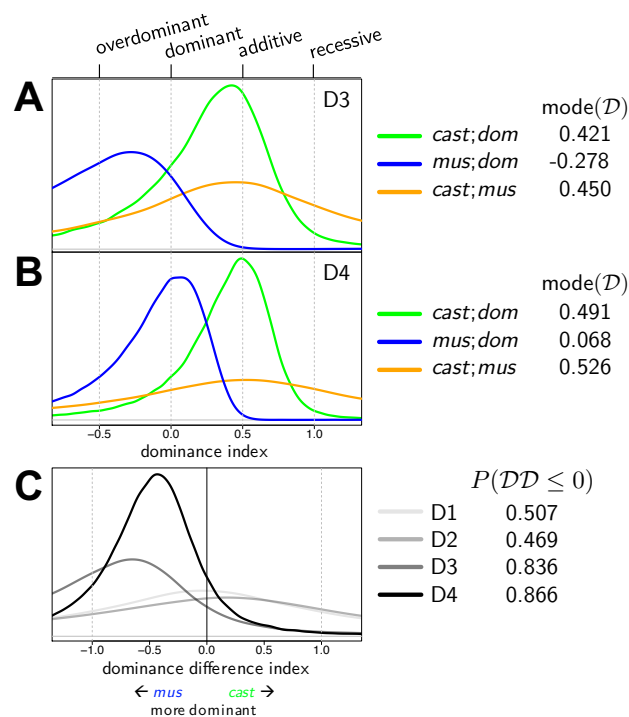
441 and more details in **Methods**).

Figure 6 Posterior density of the dominance index on (A) D3 and (B) D4. C) Posterior density of the dominance difference index, *i.e.*, the difference between the dominance indices of *cast* and *mus*, across all 4 days.

442   The dominance indices of the two functional *Mx1* alleles, *mus* and *cast*, were sharply different (**Figure 6A,B; Table** S8). We found that *mus*

443 against *dom* was -0.278 (=posterior mode of $\mathcal{D}^{(mus;\,dom)}$; 80% HPD interval -2.547, 0.329) at D3 and 0.068 at D4 (-0.568, 0.380), a clear signal of

444 *mus* exerting classical dominance over the functional null. In contrast, the dominance index of *cast* against *dom* was 0.421 (-0.534 to 0.907)

445 and 0.491 (-0.028,0.836) for D3 and D4, consistent with *cast* and the functional null being codominant (*i.e.*, having an additive relationship).

446 The difference of the two dominance indices, whose posterior distribution is shown in **Figure 6** for each timepoint, quantifies the distinction

447 between *mus* and *cast* more directly, putting the probability that *mus* is more dominant than *cast* (*i.e.*, $P[\mathcal{D}^{(mus;\,dom)} > \mathcal{D}^{(cast;\,dom)}]$) at 83.6%
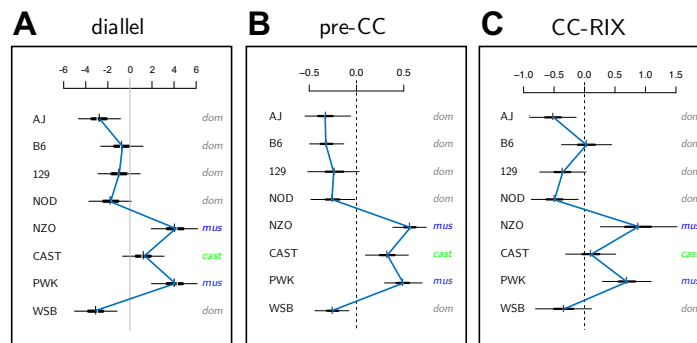
448 for D3 and 86.6% for D4.

Figure 7 Additive CC-strain haplotype effects on IAV-induced weight loss across three CC-related populations. A) Additive effects from the CC founder diallel of mice infected with IAV (PR8) or mock virus (n_{flu}=393, n_{mock}=131) at day 4 p.i. (from **Figure 1**). B) Additive strain haplotype effects at the *Mx1* locus for female pre-CC mice (n=155) infected with IAV (PR8) at day 4 p.i. C) Additive strain haplotype effects at *Mx1* for female CC-RIX mice (n=1,402) infected with IAV (CA04) at day 7 p.i. Estimates are shown as HPD intervals as described in **Figure 1**, with blue lines connecting posterior means. Parameter scales are given as additional IAV-induced weight loss per dose of strain in % of (A) D0, and (B, C) normalized effect size.

E. *Mx1* effects show consistent pattern in related multiparent populations, pre-CC and CC-RIX.

We examined effects associated with the *Mx1* locus in two related recombinant CC populations, the pre-CC of Ferris *et al.* (2013) and a set of CC-RIX lines first described here, and observed that the pattern of locus-specific strain haplotype effects was strikingly similar to that observed in our diallel **Figure 7**). This suggests that the pattern of genome-wide additive effects in the diallel is largely driven by the effect of *Mx1* haplotypes in the founder strains. This similarity in pattern is consistent, even though the virus isolate and the peak weight loss timepoint differed in the CC-RIX population (CA04 human pandemic strain, D7 p.i.) compared with the diallel and pre-CC (PR8 mouse-adapted strain, D4 p.i.) (**Table** S4). In all three populations, NZO and PWK alleles provide the most resistance to IAV-induced weight loss, and CAST alleles are slightly less protective. In the pre-CC, effects of AJ, B6, 129, NOD, and WSB haplotypes are all approximately the same, and clearly separated from the additive effects of strains with functional *Mx1*. In the diallel and in the CC-RIX (at *Mx1*), however, AJ and WSB haplotypes are on average more susceptible than the B6 haplotype, and there is less separation between additive effects of CAST and those from from *Mx1*-null strains. The proportion of variance in weight loss explained by *Mx1* was estimated as 0.5 (95 % HPD interval: 0.43, 0.54) and 0.54 (0.42, 0.63) for pre-CC and CC-RIX mice, respectively (**Figure S16** and **Figure S17**). Note that an in-depth analysis of dominance indices for the *Mx1* locus was not possible in these populations owing to the relatively sparse coverage of heterozygote diplotype states in the pre-CC and homozygous functional diplotype states in the CC.

7. DISCUSSION

We describe a general approach for investigating heritable effects on host susceptibility to virus-induced disease — in our case pathogenesis induced by IAV — using a diallel cross of the eight CC founder strains. The results from this diallel are informative not only in more clearly defining genetic architecture of the host influenza response, but also prospectively: they anticipate sources of heritable variation likely to be present in the CC, the DO and other derived experimental populations, and therefore provide a ready basis for the rational design of future studies. As an illustration of this, we demonstrate concordant effects of viral resistance locus *Mx1* across the CC founder diallel, pre-CC and a set of CC-RIX lines.

With regard specifically to IAV pathogenesis, our study sought to better understand host genetic effects on this outcome in terms of their (1) time-dependence, (2) consistency across related populations, and (3) conditionality; for example, dependence on interactions between alleles at the same locus (dominance, at *Mx1*) or at different loci (epistasis). Regarding time-dependence (1), we found that, whereas the effect of being female rather than male is evident from day 1, the effects of genetics appear later, becoming evident only on day 3 and then increasing through day 4 post-infection. Regarding consistency (2), we found that the effects of the *Mx1* alleles seen previously in the CC founders remain stable across inbred, F1, and recombinant populations. Regarding conditionality (3), we found something unexpected: evidence that the two *Mx1* functional classes, *casteneus* (CAST) and *musculus* (NZO and PWK), which were previously characterized as being functional alleles, in fact behave differently when present in the heterozygous state with susceptible *Mx1* alleles from *domesticus* (AJ, B6, 129, NOD, WSB). Specifically, the protection conferred by the presence of a *musculus Mx1* allele is the same regardless of whether it is in the homozygote state or paired as a heterozygote with the null *domesticus* allele; the *musculus* allele is therefore dominant to *domesticus*. But for the CAST allele, when paired in the same way with *domesticus*, its protection is weakened, to an extent consistent with CAST and *domesticus* being codominant, that is, having an additive relationship.

A. The level of resistance to IAV among different inbred mice is conditional on IAV subtype and strain

Differences in *Mx1* function have been identified between a variety of inbred mouse strains, including the CC founders (Ferris *et al.* 2013; Xiong *et al.* 2014; Leist *et al.* 2016). Our results were largely consistent with those studies.

Notably, in their examination of the CC founders with H3N2 infection, Leist *et al.* (2016) identified AJ and WSB strains as being most susceptible, and NZO and PWK as being most resistant, which agrees with our diallel additive effects. However, in contrast with our results showing partial protection against H1N1 IAV with CAST *Mx1*, which is consistent with our prior findings in the pre-CC (Ferris *et al.* 2013), they found CAST mice, grouping with AJ and WSB, to be highly susceptible. This difference could arise for at least two reasons. First, across the influenza field, even in identical RI panels (Boon *et al.* 2009; Nedelko *et al.* 2012), host genetic effects appear to be IAV subtype-specific. Second, the effectiveness of *Mx1*'s antiviral activities can vary depending on IAV subtypes (Riegger *et al.* 2015; Dittmann *et al.* 2008; Zimmermann *et al.* 2011; Mänz *et al.* 2013; Verhelst *et al.* 2012). Differentiating these two possibilities, however, is beyond the scope of this work.

Although the molecular differences in CAST *Mx1* that produce a deficient response in comparison with *mus Mx1* have not been defined, some work has been done in inbred mice to better understand CAST/EiJ-(strain)-specific antiviral responses. In order to interpret what they saw as a unique antiviral deficiency of CAST mice, transcriptomic experiments by Leist *et al.* (2016) suggested enhanced susceptibility is due to leucocyte recruitment deficiency (relative to NZO and PWK) in the lung. In the CC founder study of Xiong *et al.* (2014), several transcriptomic differences separated the CAST response to PR8 from the that of the other strains, including differential splicing of *Irak1* and lack of *Ifng* expression at D4 p.i., which was consistent with *Ifng* deficiency observed by Earl *et al.* (2012) leading to lethal monkeypox infection of CAST mice. Because these studies were completed in inbred CAST mice, the role of CAST *Mx1* is confounded with the genome-wide differences between CAST and the other CC founders.

Thus, there are several challenges to understanding the unique IAV resistance profile of CAST *Mx1* based on existing studies: (1) studies in inbred lines are unable to probe the overall or *Mx1*-specific dominance architecture due to a lack of heterozygosity; and (2) studies in non-recombinant lines that identify a unique phenotype in CAST compared with other founders are unable to separate the effect of CAST *Mx1* from effects arising from the rest of the CAST genome. Our study in part circumvents these shortcomings by: (1) additionally examining F1 hybrids, and (2) exploring the emerging phenotypes from an ongoing IAV infection screen using CC-RIX, themselves F1s of RI strains.

B. Complex additive effects patterns mask strong signals of dominance

In our initial analysis, we found that most of the phenotypic variation explained in infection response is driven by additive genetics with no particular signal of dominance. However, when we explicitly modeled *Mx1* status, using a term that competes with a subset of the additive and dominance diallel effects, we found that the *Mx1* functional classes act in a manner consistent with a strong dominance pattern for *musculus Mx1* (**Figure 5**). It seems striking that such a pattern of dominance could be underlying an apparently heavily additive effect signal.

Identifying dominance requires a good basis for comparing inbreds with hybrids. However, since the diallel is mainly composed of F1 hybrids with relatively few (8 vs 54) inbreds, this basis for comparison is often weak. The BayesDiallel model handles this by considering the hybrid state as the baseline and treats the inbred state as the exception (a deviation) relevant to a minority of categories, as discussed further in Lenarcic *et al.* (2012). Inferred dominance effects are therefore vague because the data that informs it is sparse, and low estimates of dominance variance comes from absence of information rather than from information about the absence of an effect. Nonetheless, greater precision was available when considering dominance of substrain-specific *Mx1* because dominance information was pooled across multiple strains and strainpairs.

The fact that the proportion of estimated additive vs. non-additive variance is influenced by model parameterization motivates careful consideration of both study design and analysis. As Huang and Mackay (2016) have recently described, model parameterizations can have critical effects on the detection of non-additivity, with the same data strongly supporting evidence for mostly additive or mostly non-additive effects, depending on the model. Related issues have been described at the locus level by Sabourin *et al.* (2015), who showed that when applying penalized regression to multi-SNP fine-mapping in GWAS, genotype parameterization interacts with how priors/penalties are assigned and can make biallelic dominance hard to identify in some cases. Yet even when dominance is not of interest per se, failure to accommodate it can disrupt estimation of additivity: in the pre-CC QTL mapping study of Phillippi *et al.* (2014), dominance signals arising from residual heterozygosity disrupted detection of an additive QTL for basal levels of CD23 (encoded by *Fcerii*); this was resolved by treating heterozygote diplotypes, whose occurence was too sparse to be modeled, as inherently noisier via downweighting.

C. Antiviral genes are expected to be dominant, but CAST *Mx1* exhibits additivity

The degree of genetic dominance of host resistance factors to viral infection in humans and mice has not been thoroughly explored. In general, in the context of biochemical and immunological studies one might expect, just as with *musculus Mx1* combined with *domesticus Mx1*, that genes encoding strong-acting antivirals when combined with a null mutant would be mostly dominant. In quantitative genetics, however, it is more often expected that genetic contributions will be mostly additive. In this study, at the *Mx1* locus, we observe both.

In genetic crosses of functional and null mice, major host determinants of pathogenesis are might normally be expected to be classified as either recessive or dominant: recessive when null results in loss-of-susceptibility for a host factor required for disease susceptibility; dominant when null results in loss-of-function for a host gene required for virus resistance. The recessive case is especially true of passive immunity gained by knockout of host genes critical to viral entry and life cycle, and has been demonstrated in a variety of studies on crop resistance (Fraser 1990; Kang *et al.* 2005; Truniger and Aranda 2009; Hashimoto *et al.* 2016), and explored in studies of the effects of CCR5 deficiency (CCR5-delta32 deletion) in resistance to HIV infection and pathogenesis in humans (Samson *et al.* 1996; Liu *et al.* 1996; Hütter *et al.* 2009), however the degree of protection in the CCR5-delta32 heterozygous individuals is not fully understood (Marmor *et al.* 2001; Trecarichi *et al.* 2006). The dominant case could be considered for a viral sensor, where a single inherited functional copy still provides sufficient sensitivity for viral detection and control, resembling that of an individual inheriting two copies, one from each parent. This type of dominance is best explained by the model proposed by Kacser and Burns (1981), a metabolic-enzymatic model for the architecture of

dominance at specific loci, and has been explored further in studies of viral resistance in plants, such as in Fraser and Loon (1986) and Fraser (1992). The Kascer-Burns model also provides a mechanism that could in some cases give rise to additivity.

Kacser and Burns (1981) predicted that, biochemically, for most enzymes, if there is a 50% reduction in enzyme activity in the heterozygote of a null × functional cross, then in most cases the resulting phenotype will resemble that in the homozygous functional individual and the null allele would likely be characterized as operating in a "recessive" manner. According to their model, the phenotype (or "flux") resulting from a given enzymatic pathway with multiple enzymes joined by "kinetic linking" is a summation of the change in flux due to each specific enzyme activity ("selectivity coefficient"). This means that even a dramatic change in activity for any one enzyme in a physiological system results in barely discernible changes in the system overall, as long as some functional enzyme from the locus of interest is produced.

However, the authors also describe two cases where systemic flux can be partially reduced in the heterozygote: (1) in pathways where there are exceptionally few enzymes involved in the system (this case is unlikely for an IFN-responsive antiviral pathway such as *Mx1*); and (2) in pathways where the selectivity coefficient (functional activity) of the enzyme is very low, a case termed heterozygote "indeterminacy," which we henceforth equate to additivity. As further explored by Keightley (1996), dominance may be incomplete when less active allelic members of a series are involved in a cross with null mutants, resulting in a more additive relationship; this seems most likely to explain our observation of CAST *Mx1* effects, and the lower antiviral activity of CAST *Mx1* observed in Nürnberger *et al.* (2016), discussed below, appears to support this.

D. Recent work exploring CAST *Mx1* antiviral deficiency

Important insights into why CAST *Mx1* might be additive come from recent functional studies. Nürnberger *et al.* (2016) engineered B6 mice expressing either the CAST-derived or A2G-derived MX1 proteins. A2G encodes an MX1 protein sequence similar to the NZO and PWK *musculus* class described in this study. CAST MX1 differs from A2G and *musculus*, with corresponding amino acid changes G83R and A222V in the G domain, which is important for enzymatic and antiviral function. Nürnberger *et al.* (2016) clearly show that CAST provides intermediate protection from IAV, in their case using H7N7 (SC35M) and H5N1 (R65) viruses, and suggest that sequence changes in the CAST *Mx1* allele result in reduced enzyme stability, metabolic instability, and possibly in altered dimerization of MX1 monomers and/or changes in MX1 GTPase antiviral activity. It is unknown whether the differences they observed would lead to changes in the dominance of CAST and A2G *Mx1*, although we might expect this to be the case given our mouse infection results. We have verified that the same variants, G83R and A222V, differentiate CAST coding sequence from NZO and PWK, as in Srivastava *et al.* (2009) and using http://isvdb.unc.edu (Oreper *et al.* 2017), and that these are the only nonsynonymous variants on coding transcripts of *Mx1* that differentiate CAST from NZO and PWK. Although we see substantial protection from weight loss in CAST mice, we see a deficiency in the anti-viral effects (as measured by RNA-seq viral reads in infected lungs) of CAST *Mx1* on D2 and D4 post-infection (data not shown, via RNA-seq reads from Xiong *et al.* 2014, and transcript analysis in Ferris *et al.* 2013). Our work motivates further functional studies of the MX1 protein using *Mx1* transgenic mice.

E. *Mx1*-independent effects and their follow-up: new studies should leverage CAST *Mx1* additivity

A substantial proportion of heritable variance in the diallel was *Mx1*-independent (VarP[all|*Mx1*]=33.81, **Table S2**). This was broadly driven additive genetics and both symmetric and asymmetric epistasis (*i.e.*, differing by parent-of-origin) (**Figure 4C**, **Figure 4E**). Relatedly, in our analysis of the *Mx1* locus in the CC-RIX, we estimated *Mx1*-independent effects attributable to overall genome-similarity to account for 21% of phenotypic variance. Both observations suggest the presence of additional QTL that could be drawn out given a suitable follow-up design.

Consider the design of a second CC-RIX. Here our knowledge of differences in *Mx1* dominance becomes a valuable guide: prioritizing CC F1s with one copy of *musculus Mx1* would reduce power because it would cause *Mx1*-independent drivers to be masked; however, prioritizing CC F1s with one or fewer copies of *castaneous Mx1* would leave the *Mx1*-independent effects exposed and QTL underlying them more easily detected.

The inclusion of mice with a single functional *Mx1* in a mapping population provides a basis for mapping loci that modify the effect of *Mx1*, as well as mapping *Mx1*-independent loci controlling disease. Shin *et al.* (2015) showed that even the protectiveness of *Mx1* from the A2G inbred strain is conditional and depends on host genetic background. Thus, CC-RIX designs that incorporate heterozygous classes of *domesticus Mx1* crossed with either CAST *Mx1* or *musculus Mx1* can be of substantial benefit for mapping novel loci affecting infection outcomes, and at least 40% of the F1 crosses in our CC-RIX study incorporate lines which have one single copy (CAST or *musculus*) of *Mx1*.

F. Diallels as pilot data more generally

Diallels have a long history in quantitative genetics (Schmidt 1919; and refs in, eg, Christie and Shattuck 1992; Verhoeven *et al.* 2006; Lenarcic *et al.* 2012), and have most commonly been used as a way to assess the relative potency of different genomes with respect to a studied trait, yielding, for example, estimates of generalized combining ability (GCA) for each strain and estimates of specific combining ability (SCA) for each F1. More ambitiously, they have been used to obtain an overall picture of a trait's genetic architecture. In many respects, this picture is clearly incomplete: even within the limited genetic space spanned by the founders, the diallel shows only the effects of swapping intact haploid genomes, with no ability to see the effects of recombination. But in other respects it is comprehensive: in considering every F1 combination, one can observe evidence for types of effects — dominance, epistasis, parent-of-origin, epistasis by parent-of-origin, all sex-specific versions thereof — that would be hard or impossible to identify in other settings, *e.g.*, outbreeding populations derived from the same set of founders.

A number of studies have sought to combine the features of a diallel with those of such derived outbred crosses to obtain picture of genetic architecture that is in some way informed by both. These include studies that map QTL across multiple biparental (*e.g.*, F2) crosses derived from a diallel or diallel-like population (*e.g.*, Rebai and Goffinet 1993; Xu 1998; Rebaï and Goffinet 2000; Liu and Zeng 2000; Ogut *et al.* 2015), and at least one theoretical study, that of Verhoeven *et al.* (2006), examining the extent to which such information can be analyzed jointly and reconciled with data from the original diallel itself.

The goals of our study were more prospective: we use the diallel to prioritize follow-up designs in target populations that segregate genetic material from the same set of founders; the diallel provides evidence of heritable features that would be expected to exist in the CC, and that could be examined in more detail in a suitably designed CC-based experiment. A comprehensive view of IAV resistance architecture, even within the genetic space of the CC-founder genomes, would be achievable only asymptotically through countless, diverse studies; in this, the diallel can be seen as a compass, identifying promising initial directions.

G. Potential for joint analysis

Despite our diallel focus, since we do examine data from two other closely related populations it is nonetheless interesting to consider the potential value of analyzing all three populations jointly. In theory, a joint analysis could, in bringing greater numbers, sharpen estimates of key parameters representing effects that are shared across the studies while also serving to more precisely characterize key differences between them — the idea being that such formal consideration of similarities and differences would lead to a more nuanced picture of the examined trait's genetic architecture, in particular the relationship between QTL and overall effects (see for example related discussions in Holland 2007).

616 A related hope would be that the effects estimated in the diallel could increase power to map QTL in the pre-CC and CC-RIX, for

617 example, by serving as priors in a Bayesian model of the QTL allelic series (such as that proposed by Jannink and Wu 2003).

618 Our preference against a joint analysis in this case centers on the fact that the three studies differ not only in their genetic configuration,

619 which if alone might make such an analysis justified, but also in other important respects that would make formally-estimated between-

620 study discrepancies hard to interpret and potentially misleading.

621 First, the studies differed in their phenotype definitions. Infection response in the diallel was defined rigorously, in terms of mock

622 and infected mice, but in the pre-CC and CC-RIX its definition was looser, lacking mock controls; although the effects for *Mx1* across

623 populations turned out to be consistent, any discrepancies identified in a joint model would have been hard to attribute to differences in

624 genetics vs. differences in protocol.

625 Second, the studies differed in the IAV variant used. In the pre-CC and diallel we used PR8 but for the newer CC-RIX experiment we

626 switched to CA04. Our reason for this change is that CA04, a mouse-adapted virus from a 2009 H1N1 clinical isolate, infects mice with a

627 lower rate of mortality, making it a better candidate for QTL-mapping studies of IAV pathogenesis, and, being a human virus, CA04 is

628 more amenable to translational studies.

629 Nonetheless, absent these conflationary factors, a joint analysis could be valuable, and we expect that joint analyses of heritable effects

630 across populations are likely to be particularly apt when comparable experiments are repeated across subsets of the CC-founder diallel, the

631 DO, the CC, and CC-RIX, or more generally across different components of a multiparent super-population.

H. Summary

633 Our study demonstrates the use of diallel crosses for identifying different types of heritable effects that can affect host responses to IAV

634 infection. As such, we find reproducible effects of *Mx1* alleles across first order crosses and recombined populations (despite inexact

635 coordination between protocols), confirming our previous findings that the CAST *Mx1* allele exhibits an intermediate resistance phenotype

636 against H1N1 strains of influenza virus (Ferris *et al.* 2013), and also identifying novel attributes of the CAST and *musculus Mx1* alleles with

637 respect to additivity and dominance. Despite a body of literature on the effects of null mutations in *Mx1*, the importance of allelic variation

638 at this antiviral gene is just beginning to be understood. A GWAS study published in 2011 found that *Mx1* allelic variation likely plays a

639 role in viral disease manifestation in humans, specifically with regards to West Nile virus infection (Bigham *et al.* 2011), highlighting a need

640 for further study of the role of natural allelic variation in *Mx1* on virus infections in future research.

8. FUNDING INFORMATION

9. ACKNOWLEDGMENTS

651 the referees and editors who contributed to this manuscript by providing the authors with detailed questions and comments.

10. APPENDIX A: DEFINING A POTENTIAL OUTCOMES MODEL OF TREATMENT RESPONSE WITH QUARTETS

656 In the potential outcomes framework of Neyman (1923) and Rubin (1974) the causal effect of an applied treatment on a measured outcome

657 in an individual i is defined as the difference between the outcome under treatment and the outcome that would have been observed if i

658 were instead to have received the control. In our case, for some outcome measure y, we defined the causal effect as the infection response

$$\Delta_i = y_i^{\text{flu}} - y_i^{\text{mock}},$$

659 where y_i^{flu} and y_i^{mock} are "potential outcomes", one of which is observed (the factual) and other of which is unobserved (the counterfactual).

660 Since it is impossible to observe both simultaneously, the causal effect Δ_i can never be measured directly (Holland 1986). It can however be

661 estimated as

$$\widehat{\Delta}_i = y_i^{\text{flu}} - y_{i'}^{\text{mock}},$$

662 with the accuracy of this estimate depending on how closely i' matches i. Our desire for lack of bias in this measure motivates our treatment

663 assignment being randomly ascribed within a group of matched individuals.

664 In the treatment-response diallel, we are primarily interested not in infection response for a particular mouse but rather the expectation

665 of this quantity for mice within a given diallel category, or more generally within a group of matched individuals q,

$$\Delta_q = \text{E}(y_q^{\text{flu}} - y_q^{\text{mock}}) = \text{E}(y_q^{\text{flu}}) - \text{E}(y_q^{\text{mock}}), \tag{10}$$

666 where in our case q is defined as mice specific to a given diallel category and experimental batch. In practice it is natural to estimate this

667 quantity as

$$\widehat{\Delta}_q = \frac{1}{n_{\text{flu}}} \sum_{i \in q[\text{flu}]} y_i^{\text{flu}} - \frac{1}{n_{\text{mock}}} \sum_{i' \in q[\text{mock}]} y_{i'}^{\text{mock}}, \tag{11}$$

668 where $q[\text{flu}]$ and $q[\text{mock}]$ are, respectively, the set of mice in group q assigned to flu and mock treatment groups. The variance of this

669 estimate is

$$\text{Var}(\widehat{\Delta}_q) = \frac{\text{Var}(y_q^{\text{flu}})}{n_{\text{flu}}} + \frac{\text{Var}(y_q^{\text{mock}})}{n_{\text{mock}}}, \tag{12}$$

670 and if it is considered likely, as in this study, that the infected phenotypes will be more variable than the mock, $\text{Var}(y^{\text{flu}}) > \text{Var}(y^{\text{mock}})$,

671 then it is most efficient experimentally to devote more individuals to the the infected arm than the mock arm, *i.e.*, $n_{\text{flu}} > n_{\text{mock}}$.

672 In our experimental design, we have flu:mock in the ratio 3:1 for each group q. It is therefore natural to define the unit of observation q

673 as a quartet, that is, Eq 11 with $n_{\text{flu}} = 3$ and $n_{\text{mock}} = 1$. This means that each diallel category can be represented by multiple quartets,

674 corresponding to multiple observations of $\widehat{\Delta}_q$, denoted in the **Methods** as delta$_q$.

675 We now note several assumptions and connections. Eq 10 equates unit-level with marginal causal effects and thereby assumes no

676 interference between units, specifically, that mice in the same quartet do not affect each other's outcomes; this is approximately true based

677 on the well-established evidence that mice do not transmit H1N1 influenza virus (Lowen *et al.* 2006; Edenborough *et al.* 2012), a finding we

678   have also verified by weight loss profiles and RNA-seq of CC founder strains co-housed with H1N1(PR8)-infected mice (Xiong *et al.* 2014).

679   Last, the definition of $\hat{\Delta}_q$ in Eq 11 is analogous to an inverse probability weighted causal effect estimate.

11. APPENDIX B: STOCHASTIC REGRESSION IMPUTATION OF MISSING QUARTET PARTNERS

681   The equation for the variance of $\hat{\Delta}_q$, namely Eq 12, implies that modeling the residual in Eq 5 as homoskedastic would require n_{flu} and

682   n_{mock} to be constant throughout — in other words, in order to ensure comparable precision of infection responses, all quartets should be

683   complete. However, in the diallel experiment some combinations of batch and diallel category had one or more flu mice missing. In these

684   cases, quartets were defined to have missing values that would be filled in by imputation. The imputation scheme used here corresponds to

685   stochastic regression imputation (*e.g.*, Gelman and Hill 2006) whereby the incomplete dataset is repeatedly augmented to a completed data

686   set using sampled variates from a prediction model, each completed dataset is subject to the BayesDiallel analysis described in **Methods**,

687   and then results across the completed datasets are aggregated.

688   Each imputation required two steps: since the target phenotype of a missing mouse, namely its p.i. weight loss, was considered

689   potentially dependent on its day 0 weight, we first imputed missing values for D0 and then imputed missing p.i. weight loss conditional

690   on D0. In addition, at each day p.i., there was one batch/diallel category combination with 1 mock and 4 infecteds; for this case only, in

691   each round of imputation, we created a completed quartet by randomly deleting one of the four infecteds.

692   The two-step stochastic regression imputation was performed as follows. Define the observed diallel data for D0 and $\text{pct}^{\text{day[flu]}}$ as

693   D0_{obs} and $\text{pct}^{\text{day[flu]}}_{\text{obs}}$ respectively, and lett $\overset{\text{sim}}{\sim}$ represent regression with BayesDiallel followed by stochastic regression imputation, that is,

694   sampling from the posterior predictive. For each $t = 1, \ldots, 1000$ round of imputation, we first impute missing D0 values as

$$\text{D0}^{(t)}_{\text{mis}} \overset{\text{sim}}{\sim} \text{BayesDiallel}\left(\text{D0}_{\text{obs}}\right), \tag{13}$$

695   where BayesDiallel is fitted as Model 1 in **Table 2**. These imputed values are then combined with observed D0 values to give the completed

696   set,

$$\text{D0}^{(t)}_{\text{complete}} = \left\{\text{D0}^{(t)}_{\text{mis}}, \text{D0}_{\text{obs}}\right\}, \tag{14}$$

697   which are then used to impute p.i. weight loss at all timepoints (D1 to D4) for the missing mice as

$$\text{pct}^{\text{day[flu]},(t)}_{\text{mis}} \overset{\text{sim}}{\sim} \text{BayesDiallel}\left(\text{pct}^{\text{day[flu]}}_{\text{obs}}, \text{D0}^{(t)}_{\text{complete}}\right), \tag{15}$$

698   leading in each case to the completed flu p.i. weight loss data,

$$\text{pct}^{\text{day[flu]},(t)}_{\text{complete}} = \left\{\text{pct}^{\text{day[flu]},(t)}_{\text{mis}}, \text{pct}^{\text{day[flu]}}_{\text{obs}}\right\}, \tag{16}$$

699   and subsequent calculation of quartet-based infection response values as

$$\text{delta}^{\text{day},(t)} = \text{Quartets}\left\{\text{pct}^{\text{day[flu]},(t)}_{\text{complete}}, \text{pct}^{\text{day[mock]}}\right\}. \tag{17}$$

700   Each of the 1000 infection response data sets is analyzed separately using BayesDiallel (Model 3 in **Table 2**). The MCMC chains from each

701   replicate are aggregated and thinned (sampled across even intervals) and the aggregate results are reported, according to the procedure

702   outlined in **Algorithm 1** in the Supplement.

The number of animals imputed were 33 at D1, 33 at D2, 15 at D3, and 16 at D4, in each case corresponding to a small proportion (2.8%-3.1%) of the total data set. Phenotypes were not imputed non-productive diallel genotypes (which contain no mock or infected mice at all), *i.e. jk* ∈ {NZO×CAST, NZO×PWK} (Chesler *et al.* 2008).

LITERATURE CITED

Alberts, R., B. Srivastava, H. Wu, N. Viegas, R. Geffers, F. Klawonn, N. Novoselova, T. Zaverucha do Valle, J.-J. Panthier, and K. Schughart, 2010 Gene expression changes in the host response between resistant and susceptible inbred mouse strains after influenza A infection. Microbes and Infection **12**: 309–318.

Bates, D., M. Mächler, B. Bolker, and S. Walker, 2015 Fitting linear mixed-effects models using lme4. Journal of Statistical Software **67**: 1–48.

Bigham, A. W., K. J. Buckingham, S. Husain, M. J. Emond, K. M. Bofferding, H. Gildersleeve, A. Rutherford, N. M. Astakhova, A. A. Perelygin, M. P. Busch, K. O. Murray, J. J. Sejvar, S. Green, J. Kriesel, M. A. Brinton, and M. Bamshad, 2011 Host Genetic Risk Factors for West Nile Virus Infection and Disease Progression. PLoS ONE **6**: e24745.

Boivin, G. A., J. Pothlichet, E. Skamene, E. G. Brown, J. C. Loredo-Osti, R. Sladek, and S. M. Vidal, 2012 Mapping of clinical and expression quantitative trait loci in a sex-dependent effect of host susceptibility to mouse-adapted influenza H3N2/HK/1/68. Journal of Immunology **188**: 3949–60.

Boon, A. C. M., J. DeBeauchamp, A. Hollmann, J. Luke, M. Kotb, S. Rowe, D. Finkelstein, G. Neale, L. Lu, R. W. Williams, and R. J. Webby, 2009 Host genetic variation affects resistance to infection with a highly pathogenic H5N1 influenza A virus in mice. Journal of Virology **83**: 10417–10426.

Bottomly, D., M. T. Ferris, L. D. Aicher, E. Rosenzweig, A. Whitmore, D. L. Aylor, B. L. Haagmans, L. E. Gralinski, B. G. Bradel-Tretheway, J. T. Bryan, D. W. Threadgill, F. P.-M. de Villena, R. S. Baric, M. G. Katze, M. Heise, and S. K. McWeeney, 2012 Expression quantitative trait Loci for extreme host response to influenza a in pre-collaborative cross mice. G3 (Bethesda, Md.) **2**: 213–21.

Chesler, E. J., D. R. Miller, L. R. Branstetter, L. D. Galloway, B. L. Jackson, V. M. Philip, B. H. Voy, C. T. Culiat, D. W. Threadgill, R. W. Williams, G. A. Churchill, D. K. Johnson, and K. F. Manly, 2008 The Collaborative Cross at Oak Ridge National Laboratory: developing a powerful resource for systems genetics. Mammalian Genome **19**: 382–389.

Christie, B. R. and V. I. Shattuck, 1992 The diallel cross: design, analysis, and use for plant breeders. Plant Breeding Reviews **9**: 9–36.

Churchill, G. A., D. C. Airey, H. Allayee, J. M. Angel, A. D. Attie, J. Beatty, W. D. Beavis, J. K. Belknap, B. Bennett, W. Berrettini, A. Bleich, M. Bogue, K. W. Broman, K. J. Buck, E. Buckler, M. Burmeister, E. J. Chesler, J. M. Cheverud, S. Clapcote, M. N. Cook, R. D. Cox, J. C. Crabbe, W. E. Crusio, A. Darvasi, C. F. Deschepper, R. W. Doerge, C. R. Farber, J. Forejt, D. Gaile, S. J. Garlow, H. Geiger, H. Gershenfeld, T. Gordon, J. Gu, W. Gu, G. de Haan, N. L. Hayes, C. Heller, H. Himmelbauer, R. Hitzemann, K. Hunter, H.-C. Hsu, F. A. Iraqi, B. Ivandic, H. J. Jacob, R. C. Jansen, K. J. Jepsen, D. K. Johnson, T. E. Johnson, G. Kempermann, C. Kendziorski, M. Kotb, R. F. Kooy, B. Llamas, F. Lammert, J.-M. Lassalle, P. R. Lowenstein, L. Lu, A. Lusis, K. F. Manly, R. Marcucio, D. Matthews, J. F. Medrano, D. R. Miller, G. Mittleman, B. A. Mock, J. S. Mogil, X. Montagutelli, G. Morahan, D. G. Morris, R. Mott, J. H. Nadeau, H. Nagase, R. S. Nowakowski, B. F. O'Hara, A. V. Osadchuk, G. P. Page, B. Paigen, K. Paigen, A. A. Palmer, H.-J. Pan, L. Peltonen-Palotie, J. Peirce, D. Pomp, M. Pravenec, D. R. Prows, Z. Qi, R. H. Reeves, J. Roder, G. D. Rosen, E. E. Schadt, L. C. Schalkwyk, Z. Seltzer, K. Shimomura, S. Shou, M. J. Sillanpää, L. D. Siracusa, H.-W. Snoeck, J. L. Spearow, K. Svenson, L. M. Tarantino, D. Threadgill, L. A. Toth, W. Valdar, F. Pardo-Manuel de Villena, C. Warden, S. Whatley, R. W. Williams, T. Wiltshire, N. Yi, D. Zhang, M. Zhang, and F. Zou, 2004 The Collaborative Cross, a community resource for the genetic analysis of complex traits. Nature Genetics **36**: 1133–1137.

Churchill, G. A., D. M. Gatti, S. C. Munger, and K. L. Svenson, 2012 The Diversity Outbred mouse population. Mammalian Genome **23**: 713–718.

Ciancanelli, M. J., S. X. L. Huang, P. Luthra, H. Garner, Y. Itan, S. Volpi, F. G. Lafaille, C. Trouillet, M. Schmolke, R. A. Albrecht, E. Israelsson, H. K. Lim, M. Casadio, T. Hermesh, L. Lorenzo, L. W. Leung, V. Pedergnana, B. Boisson, S. Okada, C. Picard, B. Ringuier, F. Troussier, D. Chaussabel, L. Abel, I. Pellier, L. D. Notarangelo, A. García-Sastre, C. F. Basler, F. Geissmann, S.-Y. Zhang, H.-W. Snoeck, and J.-L. Casanova, 2015 Life-threatening influenza and impaired interferon amplification in human IRF7 deficiency. Science (New York, N.Y.) **348**: 448–53.

Collaborative Cross Consortium, 2012 The genome architecture of the Collaborative Cross mouse genetic reference population. Genetics **190**: 389–401.

Comstock, R. and H. Robinson, 1948 The Components of Genetic Variance in Populations of Biparental Progenies and Their Use in Estimating the Average Degree of Dominance. Biometrics **4**: 254–266.

Crowley, J. J., Y. Kim, A. B. Lenarcic, C. R. Quackenbush, C. J. Barrick, D. E. Adkins, G. S. Shaw, D. R. Miller, F. P.-M. de Villena, P. F. Sullivan, and W. Valdar, 2014 Genetics of adverse reactions to haloperidol in a mouse diallel: a drug-placebo experiment and Bayesian causal analysis. Genetics **196**: 321–47.

Dittmann, J., S. Stertz, D. Grimm, J. Steel, A. García-Sastre, O. Haller, and G. Kochs, 2008 Influenza A Virus Strains Differ in Sensitivity to the Antiviral Action of Mx-GTPase. Journal of Virology **82**: 3624–3631.

Earl, P. L., J. L. Americo, and B. Moss, 2012 Lethal monkeypox virus infection of CAST/EiJ mice is associated with a deficient gamma interferon response. Journal of Virology **86**: 9105–9112.

Edenborough, K. M., B. P. Gilbertson, and L. E. Brown, 2012 A Mouse Model for the Study of Contact-Dependent Transmission of Influenza A Virus and the Factors That Govern Transmissibility. Journal of Virology **86**: 12544–12551.

Everitt, A. R., S. Clare, T. Pertel, S. P. John, R. S. Wash, S. E. Smith, C. R. Chin, E. M. Feeley, J. S. Sims, D. J. Adams, H. M. Wise, L. Kane, D. Goulding, P. Digard, V. Anttila, J. K. Baillie, T. S. Walsh, D. A. Hume, A. Palotie, Y. Xue, V. Colonna, C. Tyler-Smith, J. Dunning, S. B. Gordon, K. Everingham, H. Dawson, D. Hope, P. Ramsay, T. S. Walsh (Local Lead Investigator), A. Campbell, S. Kerr, D. Harrison, K. Rowan, J. Addison, N. Donald, S. Galt, D. Noble, J. Taylor, N. Webster (Local Lead Investigator), I. Taylor (Local Lead Investigator), J. Aldridge (Local Lead Investigator), R. Dornan, C. Richard, D. Gilmour, R. Simmons (Local Lead Investigator), R. White (Local Lead Investigator), C. Jardine, D. Williams (Local Lead Investigator), M. Booth (Local Lead Investigator), T. Quasim, V. Watson, P. Henry, F. Munro, L. Bell, J. Ruddy (Local Lead Investigator), S. Cole (Local Lead Investigator), J. Southward, P. Allcoat, S. Gray, M. McDougall (Local Lead Investigator), J. Matheson, J. Whiteside (Local Lead Investigator), D. Alcorn, K. Rooney (Local Lead Investigator), R. Sundaram, G. Imrie (Local Lead Investigator), J. Bruce, K. McGuigan, S. Moultrie (Local Lead Investigator), C. Cairns (Local Lead Investigator), J. Grant, M. Hughes, C. Murdoch (Local Lead Investigator), A. Davidson (Local Lead Investigator), G. Harris, R. Paterson, C. Wallis (Local Lead Investigator), S. Binning (Local Lead Investigator), M. Pollock, J. Antonelli, A. Duncan, J. Gibson, C. McCulloch, L. Murphy, C. Haley, G. Faulkner, T. Freeman, D. A. Hume, J. K. Baillie (Principal Investigator), D. Chaussabel, W. E. Adamson, W. F. Carman, C. Thompson, M. C. Zambon, P. Aylin, D. Ashby, W. S. Barclay, S. J. Brett, W. O. Cookson, L. N. Drumright, J. Dunning, R. A. Elderfield, L. Garcia-Alvarez, B. G. Gazzard, M. J. Griffiths, M. S. Habibi, T. T. Hansel, J. A. Herberg, A. H. Holmes, T. Hussell, S. L. Johnston, O. M. Kon, M. Levin, M. F. Moffatt, S. Nadel, P. J. Openshaw, J. O. Warner, S. J. Aston, S. B. Gordon, A. Hay, J. McCauley, A. O'Garra, J. Banchereau, A. Hayward, P. Kellam, J. K. Baillie, D. A. Hume, P. Simmonds, P. S. McNamara, M. G. Semple, R. L. Smyth, J. S. Nguyen-Van-Tam, L.-P. Ho, A. J. McMichael, P. Kellam, R. L. Smyth, P. J. Openshaw, G. Dougan, A. L. Brass, and P. Kellam, 2012 IFITM3 restricts the morbidity and mortality associated with influenza. Nature **484**: 519–523.

777   Ferris, M. T., D. L. Aylor, D. Bottomly, A. C. Whitmore, L. D. Aicher, T. A. Bell, B. Bradel-Tretheway, J. T. Bryan, R. J. Buus, L. E. Gralinski,

778   B. L. Haagmans, L. McMillan, D. R. Miller, E. Rosenzweig, W. Valdar, J. Wang, G. A. Churchill, D. W. Threadgill, S. K. McWeeney, M. G.

779   Katze, F. Pardo-Manuel de Villena, R. S. Baric, and M. T. Heise, 2013 Modeling host genetic regulation of influenza pathogenesis in the

780   collaborative cross. PLoS Pathogens **9**: e1003196.

781   Fraser, R., 1990 The Genetics Of Resistance To Plant Viruses. Annual Review of Phytopathology **28**: 179–200.

782   Fraser, R. S. S., 1992 The genetics of plant-virus interactions: implications for plant breeding. Euphytica **63**: 175–185.

783   Fraser, R. S. S. and L. C. V. Loon, 1986 Genes for resistance to plant viruses. Critical Reviews in Plant Sciences **3**: 257–294.

784   Gardner, C. and J. Lonnquist, 1959 Linkage and the Degree of Dominance of Genes Controlling Quantitative Characters in Maize. Agronomy

785   Journal **51**: 524–528.

786   Gatti, D. M., K. L. Svenson, A. Shabalin, L.-Y. Wu, W. Valdar, P. Simecek, N. Goodwin, R. Cheng, D. Pomp, A. Palmer, E. J. Chesler, K. W.

787   Broman, and G. a. Churchill, 2014 Quantitative Trait Locus Mapping Methods for Diversity Outbred Mice. G3: Genes | Genomes | Genetics

788   **4**: 1623–1633.

789   Gelman, A. and J. Hill, 2006 Missing Data Imputation. In *Data analysis using regression and multilevel/hierarchical models*, chapter 25, pp.

790   529–543, Cambridge University Press.

791   Greenberg, A. J., S. R. Hackett, L. G. Harshman, and A. G. Clark, 2010 A hierarchical Bayesian model for a novel sparse partial diallel

792   crossing design. Genetics **185**: 361–373.

793   Grubb, S. C., C. J. Bult, and M. A. Bogue, 2014 Mouse Phenome Database. Nucleic Acids Research **42**: D825–D834.

794   Hashimoto, M., Y. Neriya, Y. Yamaji, and S. Namba, 2016 Recessive Resistance to Plant Viruses: Potential Resistance Genes Beyond

795   Translation Initiation Factors. Frontiers in Microbiology **7**: 1695.

796   Hidaka, F., S. Matsuo, T. Muta, K. Takeshige, T. Mizukami, and H. Nunoi, 2006 A missense mutation of the Toll-like receptor 3 gene in a

797   patient with influenza-associated encephalopathy. Clinical Immunology **119**: 188–194.

798   Holland, J. B., 2007 Genetic architecture of complex traits in plants. Current Opinion in Plant Biology **10**: 156–161.

799   Holland, P. W., 1986 Statistics and Causal Inference. Journal of the American Statistical Association **81**: 945–960.

800   Huang, W. and T. F. C. Mackay, 2016 The Genetic Architecture of Quantitative Traits Cannot Be Inferred from Variance Component Analysis.

801   PLOS Genetics **12**: e1006421.

802   Hütter, G., D. Nowak, M. Mossner, S. Ganepola, A. Müßig, K. Allers, T. Schneider, J. Hofmann, C. Kücherer, O. Blau, *et al.*, 2009 Long-term

803   control of hiv by ccr5 delta32/delta32 stem-cell transplantation. New England Journal of Medicine **360**: 692–698.

804   Itoh, Y., K. Shinya, M. Kiso, T. Watanabe, Y. Sakoda, M. Hatta, Y. Muramoto, D. Tamura, Y. Sakai-Tagawa, T. Noda, S. Sakabe, M. Imai,

805   Y. Hatta, S. Watanabe, C. Li, S. Yamada, K. Fujii, S. Murakami, H. Imai, S. Kakugawa, M. Ito, R. Takano, K. Iwatsuki-Horimoto,

806   M. Shimojima, T. Horimoto, H. Goto, K. Takahashi, A. Makino, H. Ishigaki, M. Nakayama, M. Okamatsu, K. Takahashi, D. Warshauer,

807   P. A. Shult, R. Saito, H. Suzuki, Y. Furuta, M. Yamashita, K. Mitamura, K. Nakano, M. Nakamura, R. Brockman-Schneider, H. Mitamura,

808   M. Yamazaki, N. Sugaya, M. Suresh, M. Ozawa, G. Neumann, J. Gern, H. Kida, K. Ogasawara, and Y. Kawaoka, 2009 In vitro and in vivo

809   characterization of new swine-origin H1N1 influenza viruses. Nature **460**: 1021–1025.

810   Jannink, J.-L. and X.-L. Wu, 2003 Estimating allelic number and identity in state of QTLs in interconnected families. Genetical Research **81**:

811   S0016672303006153.

812   Kacser, H. and J. A. Burns, 1981 The molecular basis of dominance. Genetics **97**: 639–66.

813   Kang, B.-C., I. Yeam, and M. M. Jahn, 2005 Genetics of plant virus resistance. Annual Review of Phytopathology **43**: 581–621.

814   Kass, R. E. and A. E. Raftery, 1995 Bayes Factors. Journal of the American Statistical Association **90**: 773–795.

815 Keightley, P. D., 1996 A Metabolic Basis for Dominance and Recessivity. Genetics **143**: 621–625.

816 Leist, S. R., C. Pilzner, J. M. A. van den Brand, L. Dengler, R. Geffers, T. Kuiken, R. Balling, H. Kollmus, and K. Schughart, 2016 Influenza
817   H3N2 infection of the collaborative cross founder strains reveals highly divergent host responses and identifies a unique phenotype in
818   CAST/EiJ mice. BMC Genomics **17**: 143.

819 Lenarcic, A. B., K. L. Svenson, G. A. Churchill, and W. Valdar, 2012 A general Bayesian approach to analyzing diallel crosses of inbred
820   strains. Genetics **190**: 413–35.

821 Lenschow, D. J., C. Lai, N. Frias-Staheli, N. V. Giannakopoulos, A. Lutz, T. Wolff, A. Osiak, B. Levine, R. E. Schmidt, A. Garcia-Sastre, D. A.
822   Leib, A. Pekosz, K.-P. Knobeloch, I. Horak, and H. W. Virgin, 2007 From the cover: IFN-stimulated gene 15 functions as a critical antiviral
823   molecule against influenza, herpes, and Sindbis viruses. Proceedings of the National Academy of Sciences **104**: 1371–1376.

824 Liu, R., W. A. Paxton, S. Choe, D. Ceradini, S. R. Martin, R. Horuk, M. E. MacDonald, H. Stuhlmann, R. A. Koup, and N. R. Landau, 1996
825   Homozygous defect in hiv-1 coreceptor accounts for resistance of some multiply-exposed individuals to hiv-1 infection. Cell **86**: 367–377.

826 Liu, Y. and Z. B. Zeng, 2000 A general mixture model approach for mapping quantitative trait loci from diverse cross designs involving
827   multiple inbred lines. Genetical Research **75**: 345–55.

828 Lorenzo, M. E., A. Hodgson, D. P. Robinson, J. B. Kaplan, A. Pekosz, and S. L. Klein, 2011 Antibody responses and cross protection against
829   lethal influenza A viruses differ between the sexes in C57BL/6 mice. Vaccine **29**: 9246–9255.

830 Lowen, A. C., S. Mubareka, T. M. Tumpey, A. Garcia-Sastre, and P. Palese, 2006 The guinea pig as a transmission model for human influenza
831   viruses. Proceedings of the National Academy of Sciences **103**: 9988–9992.

832 Mänz, B., D. Dornfeld, V. Götz, R. Zell, P. Zimmermann, O. Haller, G. Kochs, and M. Schwemmle, 2013 Pandemic Influenza A Viruses
833   Escape from Restriction by Human MxA through Adaptive Mutations in the Nucleoprotein. PLoS Pathogens **9**: e1003279.

834 Marmor, M., H. W. Sheppard, D. Donnell, S. Bozeman, and C. Celum, 2001 Homozygous and heterozygous ccr5-[delta] 32 genotypes are
835   associated with resistance to hiv infection. JAIDS Journal of Acquired Immune Deficiency Syndromes **27**: 472–481.

836 Martins, T. G., D. Simpson, F. Lindgren, and H. Rue, 2013 Bayesian computing with INLA: New features. Computational Statistics & Data
837   Analysis **67**: 68–83.

838 Morens, D. M., J. K. Taubenberger, and A. S. Fauci, 2010 The 2009 H1N1 Pandemic Influenza Virus: What Next? mBio **1**: 00211–10.

839 Morgan, A. P., C.-P. Fu, C.-Y. Kao, C. E. Welsh, J. P. Didion, L. Yadgary, L. Hyacinth, M. T. Ferris, T. A. Bell, D. R. Miller, P. Giusti-Rodriguez,
840   R. J. Nonneman, K. D. Cook, J. K. Whitmire, L. E. Gralinski, M. Keller, A. D. Attie, G. A. Churchill, P. Petkov, P. F. Sullivan, J. R.
841   Brennan, L. McMillan, and F. Pardo-Manuel de Villena, 2016 The Mouse Universal Genotyping Array: From Substrains to Subspecies. G3
842   (Bethesda) **6**: 263–279.

843 Morgan, A. P. and C. E. Welsh, 2015 Informatics resources for the Collaborative Cross and related mouse populations. Mammalian Genome
844   **26**: 521–539.

845 Nedelko, T., H. Kollmus, F. Klawonn, S. Spijker, L. Lu, M. Heßman, R. Alberts, R. W. Williams, and K. Schughart, 2012 Distinct gene loci
846   control the host response to influenza H1N1 virus infection in a time-dependent manner. BMC Genomics **13**: 411.

847 Neyman, J., 1923 On the application of probability theory to agricultural experiments: principles (in Polish with German summary).
848   Roczniki Nauk Rolniczch (Annals of Agricultural Sciences) **10**: 1–51.

849 Nürnberger, C., V. Zimmermann, M. Gerhardt, and P. Staeheli, 2016 Influenza Virus Susceptibility of Wild-Derived CAST/EiJ Mice Results
850   from Two Amino Acid Changes in the MX1 Restriction Factor. Journal of Virology **90**: 10682–10692.

851 Ogut, F., Y. Bian, P. J. Bradbury, and J. B. Holland, 2015 Joint-multiple family linkage analysis predicts within-family variation better than
852   single-family analysis of the maize nested association mapping population. Heredity **114**: 552–563.

853 Okoro, V. and C. Mbajiorgu, 2017 Diallel cross in swine production: A review. Indian Journal of Animal Research **51**: 212–218.

854 Oreper, D. G., Y. Cai, L. M. Tarantino, F. Pardo-Manuel de Villena, and W. Valdar, 2017 Inbred Strain Variant Database (ISVdb): A Repository
855 For Probabilistically Informed Sequence Differences Among The Collaborative Cross Strains And Their Founders. G3 (Bethesda) **7**:
856 1623–1630.

857 Pereira, R., E. A. Souza, Q. L. Barcelos, A. F. B. Abreu, and S. S. Librelon, 2015 Aggressiveness of Pseudocercospora griseola strains in
858 common bean genotypes and implications for genetic improvement. Genetics and molecular research : GMR **14**: 5044–5053.

859 Phillippi, J., Y. Xie, D. Miller, T. Bell, Z. Zhang, A. Lenarcic, D. Aylor, S. Krovi, D. Threadgill, F. Pardo-Manuel De Villena, W. Wang,
860 W. Valdar, and J. Frelinger, 2014 Using the emerging Collaborative Cross to probe the immune system. Genes and Immunity **15**: 38–46.

861 R Core Team, 2017 *R: A Language and Environment for Statistical Computing*. R Foundation for Statistical Computing, Vienna, Austria.

862 Rantala, M. J. and D. A. Roff, 2006 Analysis of the importance of genotypic variation, metabolic rate, morphology, sex and development
863 time on immune function in the cricket, Gryllus firmus. Journal of Evolutionary Biology **19**: 834–843.

864 Rebai, A. and B. Goffinet, 1993 Power of tests for QTL detection using replicated progenies derived from a diallel cross. Theoretical and
865 Applied Genetics **86**: 1014–1022.

866 Rebaï, A. and B. Goffinet, 2000 More about quantitative trait locus mapping with diallel designs. Genetical research **75**: 243–7.

867 Riegger, D., R. Hai, D. Dornfeld, B. Mänz, V. Leyva-Grado, M. T. Sánchez-Aparicio, R. A. Albrecht, P. Palese, O. Haller, M. Schwemmle,
868 A. García-Sastre, G. Kochs, and M. Schmolke, 2015 The Nucleoprotein of Newly Emerged H7N9 Influenza A Virus Harbors a Unique
869 Motif Conferring Resistance to Antiviral Human MxA. Journal of Virology **89**: 2241–2252.

870 Robinson, D. P., M. E. Lorenzo, W. Jian, and S. L. Klein, 2011 Elevated 17β-estradiol protects females from influenza A virus pathogenesis
871 by suppressing inflammatory responses. PLoS Pathogens **7**.

872 Rubin, D. B., 1974 Estimating causal effects of treatments in randomized and nonrandomized studies. Journal of Educational Psychology
873 **66**: 688–701.

874 Sabourin, J., A. B. Nobel, and W. Valdar, 2015 Fine-mapping additive and dominant SNP effects using group-LASSO and fractional
875 resample model averaging. Genetic Epidemiology **39**: 77–88.

876 Samet, S. J. and S. M. Tompkins, 2017 Focus: Comparative medicine: Influenza pathogenesis in genetically defined resistant and susceptible
877 murine strains. The Yale Journal of Biology and Medicine **90**: 471.

878 Samson, M., F. Libert, B. J. Doranz, J. Rucker, C. Liesnard, C.-M. Farber, S. Saragosti, C. Lapouméroulie, J. Cognaux, C. Forceille, *et al.*, 1996
879 Resistance to hiv-1 infection in caucasian individuals bearing mutant alleles of the ccr-5 chemokine receptor gene. nature **382**: 722–725.

880 Schmidt, J., 1919 La valeur de l'individu à titre de génratéur appréciée suivant la méthode du croisement dialléle. Comptes rendus des
881 travaux du laboratoire Carlsberg **14**: 1–33.

882 Shin, D.-L., B. Hatesuer, S. Bergmann, T. Nedelko, and K. Schughart, 2015 Protection from Severe Influenza Virus Infections in Mice
883 Carrying the Mx1 Influenza Virus Resistance Gene Strongly Depends on Genetic Background. Journal of Virology **89**: 9998–10009.

884 Srivastava, A., A. P. Morgan, M. L. Najarian, V. K. Sarsani, J. S. Sigmon, J. R. Shorter, A. Kashfeen, R. C. McMullan, L. H. Williams,
885 P. Giusti-Rodríguez, M. T. Ferris, P. Sullivan, P. Hock, D. R. Miller, T. A. Bell, L. McMillan, G. A. Churchill, and F. P. M. De Villena, 2017
886 Genomes of the mouse collaborative cross. Genetics **206**: 537–556.

887 Srivastava, B., P. Błazejewska, M. Hessmann, D. Bruder, R. Geffers, S. Mauel, A. D. Gruber, K. Schughart, P. Blazejewska, M. Hessmann,
888 D. Bruder, R. Geffers, S. Mauel, A. D. Gruber, and K. Schughart, 2009 Host genetic background strongly influences the response to
889 influenza A virus infections. PLoS One **4**: e4857.

890 Staeheli, P., R. Grob, E. Meier, J. G. Sutcliffe, and O. Haller, 1988 Influenza virus-susceptible mice carry Mx genes with a large deletion or a

nonsense mutation. Molecular and cellular biology **8**: 4518–4523.

Strunk, T., S. E. Jamieson, and D. Burgner, 2013 Genetic and epigenetic susceptibility to early life infection. Current Opinion in Infectious Diseases **26**: 241–7.

Threadgill, D. W., K. W. Hunter, and R. W. Williams, 2002 Genetic dissection of complex and quantitative traits : from fantasy to reality via a community effort. Mammalian Genome **13**: 175–178.

To, K. K.-W., J. Zhou, J. F.-W. Chan, and K.-Y. Yuen, 2015 Host genes and influenza pathogenesis in humans: an emerging paradigm. Current Opinion in Virology **14**: 7–15.

Trecarichi, E. M., M. Tumbarello, K. de Gaetano Donati, E. Tamburrini, R. Cauda, C. Brahe, and F. D. Tiziano, 2006 Partial protective effect of ccr5-delta 32 heterozygosity in a cohort of heterosexual italian hiv-1 exposed uninfected individuals. AIDS research and therapy **3**: 22.

Truniger, V. and M. Aranda, 2009 Recessive Resistance to Plant Viruses. In *Advances in virus research*, edited by G. Loebenstein and J. P. Carr, volume 75, chapter 4, pp. 119–231, Academic Press/Elsevier, London, UK, first edition.

Tsaih, S.-W., L. Lu, D. C. Airey, R. W. Williams, and G. a. Churchill, 2005 Quantitative trait mapping in a diallel cross of recombinant inbred lines. Mammalian Genome **16**: 344–355.

Verhelst, J., E. Parthoens, B. Schepens, W. Fiers, and X. Saelens, 2012 Interferon-inducible protein Mx1 inhibits influenza virus by interfering with functional viral ribonucleoprotein complex assembly. Journal of Virology **86**: 13445–55.

Verhoeven, K. J. F., J.-L. Jannink, and L. M. McIntyre, 2006 Using mating designs to uncover QTL and the genetic architecture of complex traits. Heredity **96**: 139–149.

Wayne, M. L., J. Pienaar, M. Telonis-Scott, L. S. Sylvestre, S. V. Nuzhdin, and L. M. Mcintyre, 2011 Expression of defense genes in drosophila evolves under a different selective regime from expression of other genes. Evolution **65**: 1068–1078.

Williams, R. W. and E. G. Williams, 2017 Resources for Systems Genetics. Methods Mol Biol **1488**: 3–29.

Wright, S., 1934 Physiological and Evolutionary Theories of Dominance. The American Naturalist **68**: 24–53.

Xiong, H., J. Morrison, M. T. Ferris, L. E. Gralinski, A. C. Whitmore, R. Green, M. J. Thomas, J. Tisoncik-Go, G. P. Schroth, F. F. Pardo-Manuel de Villena, R. S. Baric, M. T. Heise, X. Peng, and M. G. Katze, 2014 Genomic profiling of Collaborative Cross founder mice infected with respiratory viruses reveals novel transcripts and infection-related strain-specific gene and isoform expression. G3 (Bethesda, Md.) **4**: 1429–44.

Xu, S., 1998 Mapping quantitative trait loci using multiple families of line crosses. Genetics **148**: 517–24.

Yang, H., Y. Ding, L. Hutchins, J. Szatkiewicz, T. Bell, B. Paigen, J. Graber, F. Pardo-Manuel De Villena, and G. Churchill, 2009 A customized and versatile high-density genotyping array for the mouse. Nature Methods **6**: 663–666.

Yang, H., J. Wang, J. Didion, R. Buus, T. Bell, C. Welsh, F. Bonhomme, A. Yu, M. Nachman, J. Pialek, and Others, 2011 Subspecific origin and haplotype diversity in the laboratory mouse. Nature Genetics **43**: 648–655.

Zhang, Z., W. Wang, and W. Valdar, 2014 Bayesian Modeling of Haplotype Effects in Multiparent Populations. Genetics **198**: 139–156.

Zhu, J. and B. Weir, 1996 Mixed model approaches for diallel analysis based on a bio-model. Genetics Research **68**: 233–240.

Zimmermann, P., B. Manz, O. Haller, M. Schwemmle, and G. Kochs, 2011 The Viral Nucleoprotein Determines Mx Sensitivity of Influenza A Viruses. Journal of Virology **85**: 8133–8140.

12. DATA UPLOAD DETAILS

Data and analysis files in this supplement include:

- File_S1_Readme.pdf - read me file providing overview of data upload.
- File_S2_Packages.tar.gz - packages used for analysis.
- File_S3_FluDiData.csv - diallel data file.
- File_S4_diallel.tar.gz - diallel analysis files.
- File_S5_preCC.tar.gz - pre-CC data and analysis files.
- File_S6_CC-RIX.tar.gz - CC-RIX data and analysis files.

After unzipping supplemental files S2, S4, S5, and S6 in a common folder, the directory structure will be as follows:

```
├── CC-RIX
...
├── diallel
├── packages
└── preCC
    └── preCCflu_happy_cache
        ├── additive
        |   └── chr16
        ├── full
        |   └── chr16
        └── genotype
            └── chr16
```

A. Diallel Analysis

The files that are needed to reproduce the diallel analysis are given in the "diallel" folder, which includes the raw phenotype file, `FluDiData.csv`, and the following settings files, `CategoriesToImputeD4.csv`, and `settings.config.D4`. Additional *.R, *.sh, and *.pl scripts necessary to run the analysis are included.

To run the analysis for D4 treatment response on a macOS machine with both R and Perl installed, first install prerequisites, as necessary, and then install BayesDiallel, BayesSpike, and treatmentResponseDiallel. On a bash shell, from the "diallel" directory, use the following command (example using D4):

```
bash MIMQ_Run_D4.sh &
```

When the jobs on all cores are complete, then run:

```
bash MIMQ_PostRun_D4.sh &
```

Again, when the jobs on all cores are complete, run the following to clean up temporary files:

```
bash MIMQ_cleanup.sh &
```

B. pre-CC Analysis

The files that are needed to reproduce the pre-CC analysis are given in the "preCC" folder. The raw phenotype file is `Flu-preCC-data.csv`, and the analysis script is `main_analysis_preCC.R`. To run the analysis, install the required prerequisites, and then INLA and Diploffect; proceed to run the analysis script from R.

C. CC-RIX Analysis

The files that are needed to reproduce the CC-RIX analysis are given in the "CC-RIX" folder. The raw phenotype file is `Flu-CC-RIX-data.csv`, and the analysis script is `main_analysis_CC_RIX.R`. To run the analysis, install the required prerequisites, and then INLA and Diploffect; proceed to run the analysis script from R.

D. Packages

The specific versions of the main analysis software packages used in this paper are provided in the "packages" folder. The packages, data and code required to reproduce the analysis in this manuscript are available as a data repository at http://dx.doi.org/10.5281/zenodo.293015, which is a static version of the GitHub repository maintained here: https://github.com/mauriziopaul/flu-diallel. The BayesDiallel and Diploffect software packages have been previously published (Lenarcic et al., 2012, *Genetics*; Zhang et al., 2014, *Genetics*), and are available at the Valdar lab website software page (http://valdarlab.unc.edu/software.html). The R package that facilitates the treatment response analysis in this paper is provided in the file `treatmentResponseDiallel_0.0.0.9000.tar.gz`, and is available at the following GitHub site: https://github.com/mauriziopaul/treatmentResponseDiallel. It can be installed according to instructions on the website. It can also be installed using the command 'R CMD INSTALL treatmentResponseDiallel_0.0.0.9000.tar.gz' in a terminal. The following prerequisite packages for treatmentResponseDiallel can be installed in a similar fashion: `configfile_0.11.tar.gz` and `cmdline_1.1.tar.gz`.

E. File Types

- *.R - These are R scripts used for analysis of the respective populations.
- *.pl - This is a Perl script used in the diallel analysis.
- *.sh - These are bash scripts used for the diallel analysis.
- *.RData - These files in the happy_format and happy_cache directories contain data that can be loaded in R that is necessary for the Diploffect models to run.
- *.csv - These are comma-separated files containing raw data and/or analysis settings.
- *.alleles - This file can be used to generate a full model in the happy cache.

984 **13. SUPPLEMENTAL FIGURES AND TABLES**

A

B
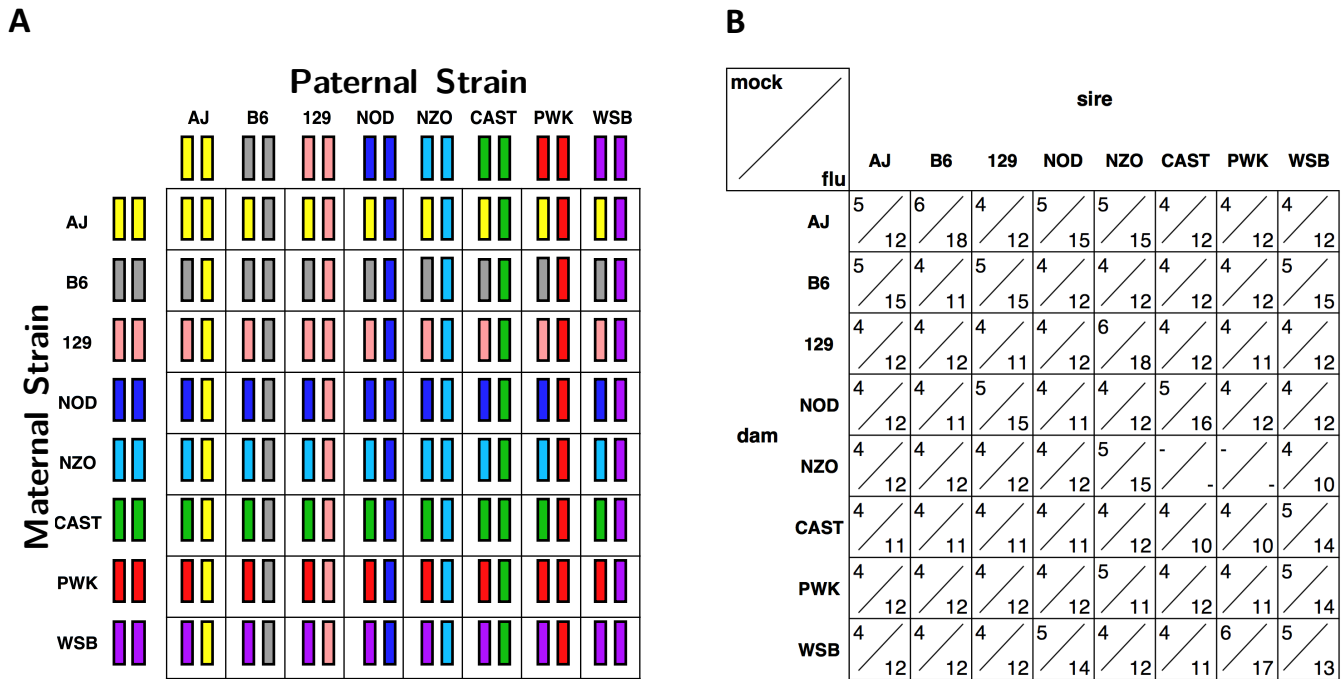
Figure S1 Diallel crossing design for the influenza diallel experiment. (A) Eight inbred *Mus musculus* strains were crossed in both directions to generate animals used in this experiment. All of the animals were followed from D0 through D2. Approximately half of the animals were followed through D4, and the remaining half of the mice were sacrificed on D2 (for analysis not included in this manuscript). (B) Of the 1,043 mice in this experiment, 268 received mock treatment, and 775 received influenza (flu) inoculation, or approximately 1 mock for every 2.9 infected mice within each category. There were one hundred twenty-nine inbred mice and 914 heterozygous (hybrid F1) mice used in this study. Crosses that were not observed (marked with a "-") include NZO×CAST and NZO×PWK, for which viable offspring cannot be produced.
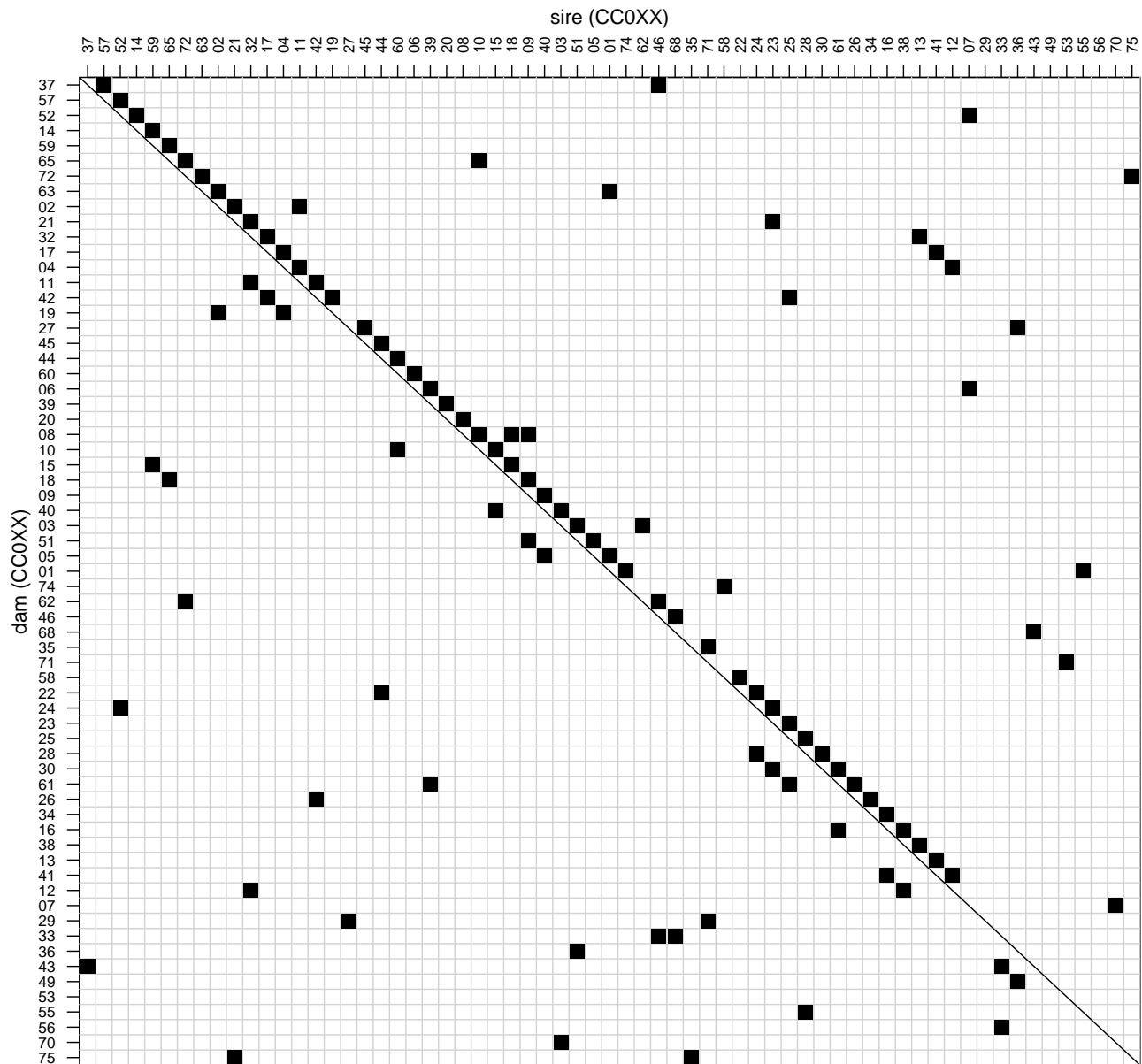
Figure S2 CC-RIX crossing design for the influenza infection experiment. As part of a larger CC-RIX QTL mapping experiment, 65 Collaborative Cross (CC) RI strains were crossed, approximately once as dam and once as sire in a round robin breeding scheme, to generate female animals in 105 CC-RIX lines, aged 8-12 weeks, that were sacrificed on day 7 (D7) post-infection, and used in this experiment. Weights for all of the animals were measured from D0 through D7. There were 1,402 heterozygous (hybrid F1) mice used in this study.
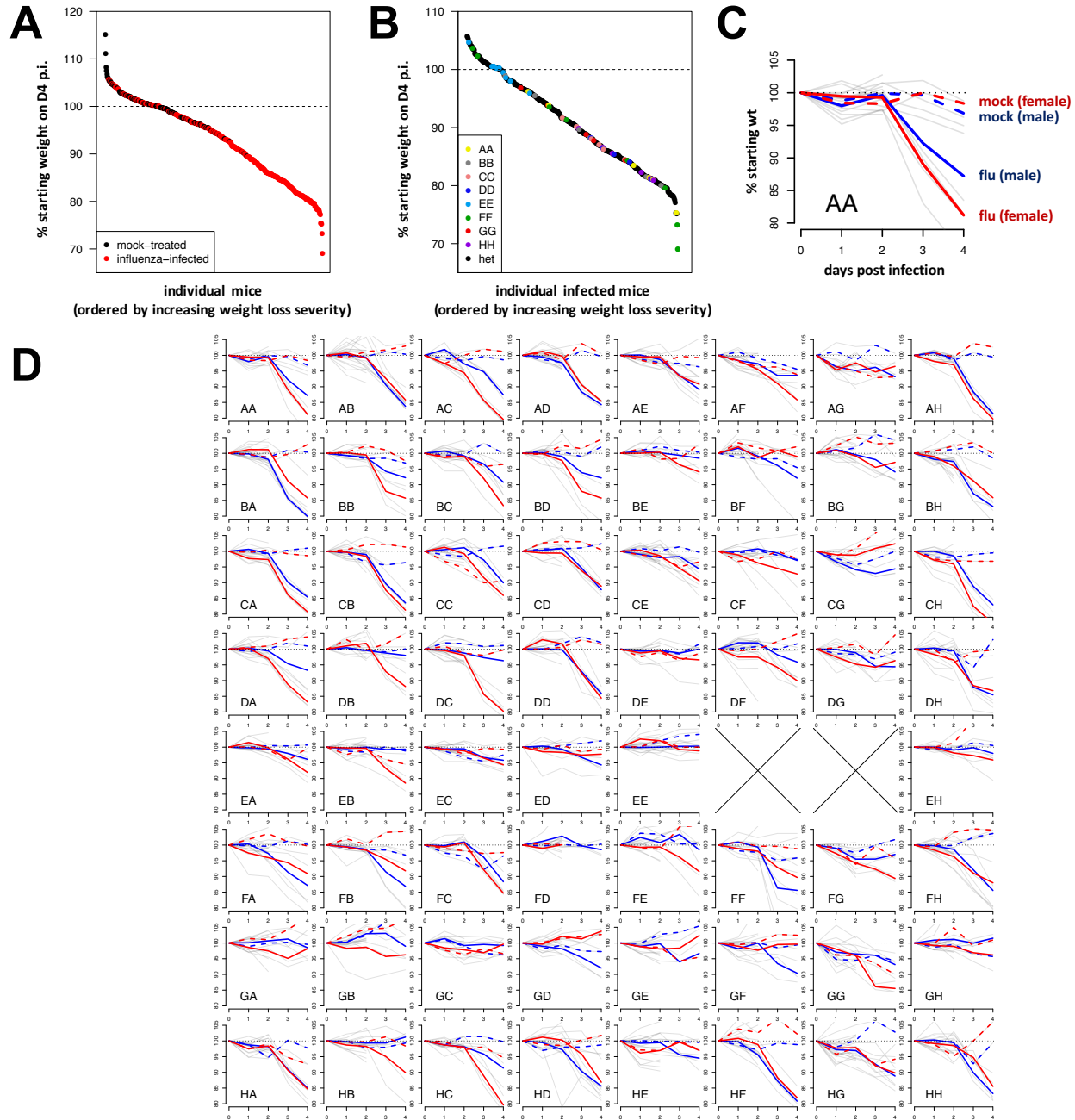
Figure S3 The raw distribution and timecourse of mock- and flu-induced weight change in the diallel. (A) Rank-ordered distribution of individual mock- and flu-induced percent weight change of inbred and F1 animals at D4 p.i. (B) Rank-ordered distribution of inbred and F1 flu-infected percent weight change at D4 p.i. (C) An example of raw weight change curves for AA (AJ×AJ) male and female mice. (D) The panel of raw weights for the 62 possible diallel categories. In (C) and (D), y-axes indicate percent of D0 weight, and x-axes indicate day(s) post-infection, while grey lines indicate individual weight change trajectories; colored lines indicate mean male (blue) and mean female (red) weight trajectories, and among these means, colored line styles indicate mock (dashed) and influenza (solid) treatment means within each group. In (D), the large X's in EF and EG indicate non-productive F1 matings. Inbred mouse lines AJ, B6, 129, NOD, NZO, CAST, PWK, and WSB are indicated by letters A through H, respectively, with the first letter indicating maternal parentage and the second letter indicating paternal parentage.
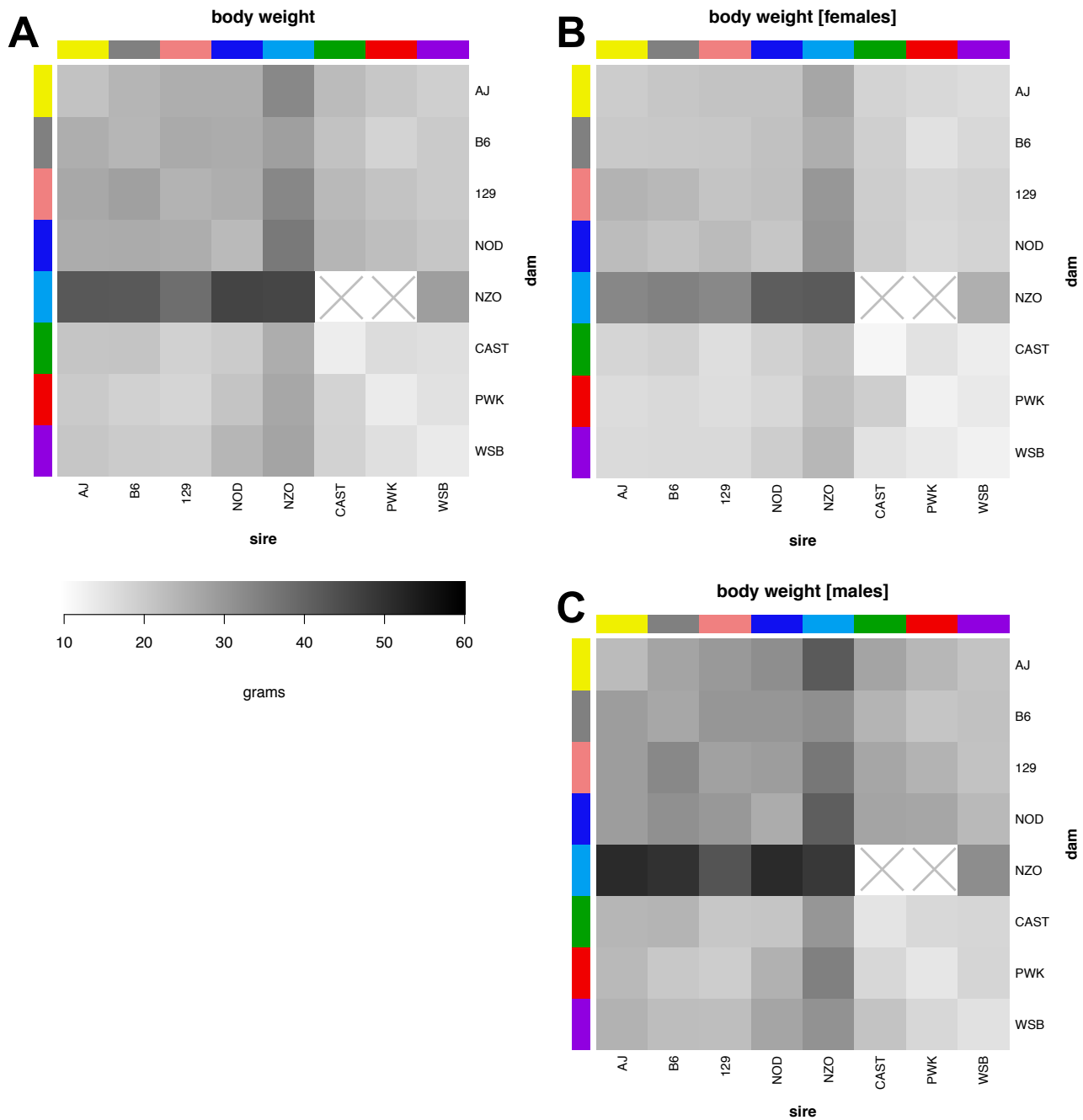
Figure S4 Body mass in a diallel cross of inbred mice. (A) Baseline body weight (in grams) for (B) male and (C) female 8-12 week old mice (n=1,043), presented as mean values across 62 inbred and F1 diallel categories.
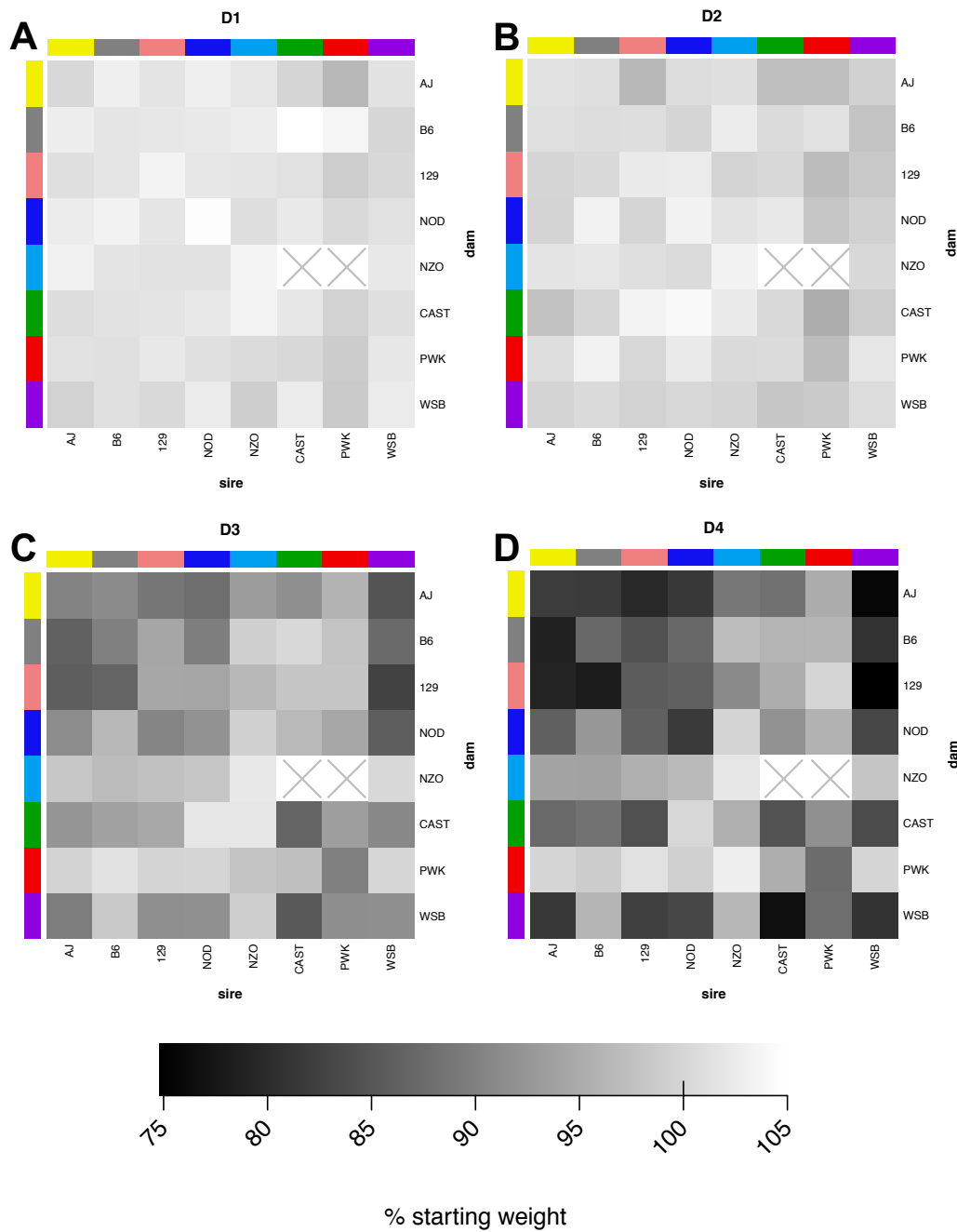
Figure S5 Weight loss in influenza-infected mice from a diallel cross of inbred mice. (A) Change in body weight on (A) day 1 (D1), (B) D2, (C) D3, and (D) D4 post-infection, presented as mean values of percent starting weight across 62 inbred and F1 diallel categories.
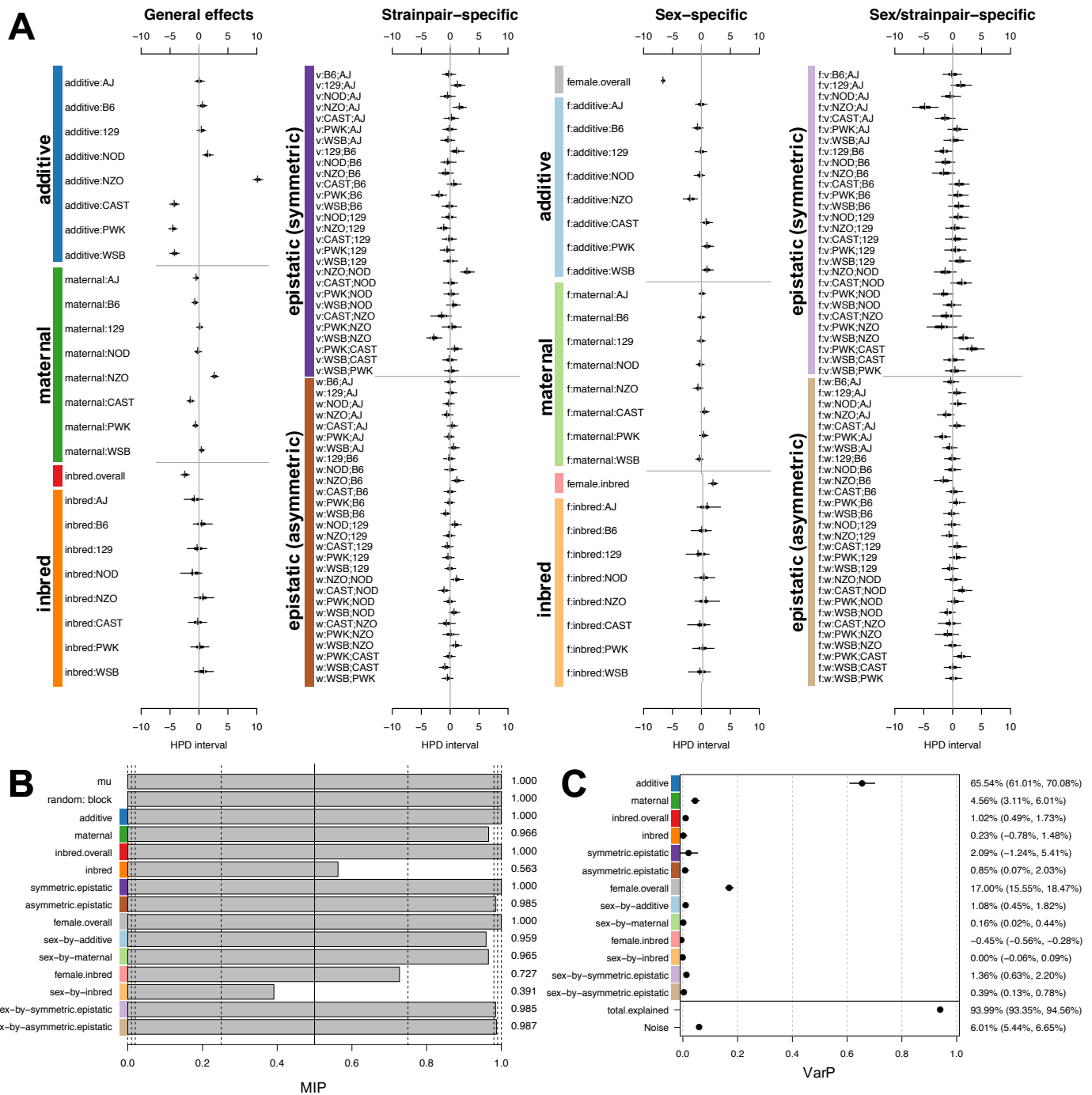
Figure S6 Diallel effects on D0 body weight in a diallel cross of inbred mice. (A) Effect estimates for additive, maternal, inbred, and epistatic effects, including sex-specific effects, are presented as highest posterior density intervals (in grams) for adult baseline body weight in 8-12 week old mice (n=1,043). Parameters are labeled according to the methods, and intervals are presented as in Figure 4A. Symmetric epistatic, asymmetric epistatic, and sex-specific parameters are indicated by "v:", "w:", and "f:", respectively. The overall mean, μ, (not shown) is 23.97 (23.56, 24.41) grams. (B) Posterior mean model inclusion probabilities (MIPs) are given for effect parameter classes. (C) Variance projection (VarPs), a generalization of heritability to the diallel effects classes, are shown for three overall effects, five random effects classes, and five corresponding sex-specific random effects classes (with posterior median and 95% HPDs).

Figure S7 Diallel effects on host infection response (weight change) at D1 post-infection, using multiple imputation matched quartets. Effect estimates for additive, maternal, inbred, and epistatic effects, including sex-specific effects, are presented as highest posterior density intervals (in percent starting weight) in 8-12 week old mice (n=1,042). Parameters are labeled according to the methods, and intervals are presented as in Figure 4A. Symmetric epistatic, asymmetric epistatic, and sex-specific parameters are indicated by "v:", "w:", and "f:", respectively. The overall treatment effect θ is -0.131% (-0.484%,0.223%). (B) Model inclusion probabilities (MIPs) are given (posterior mean $\pm$ 1 s.d.) for effect parameter classes. (C) Treatment response variance projections (TReVarPs), a generalization of heritability to the diallel effects classes, are shown for three overall effects, five random effects classes, and five corresponding sex-specific random effects classes (with posterior median and 95% HPDs).

Figure S8 Diallel effects on host infection response (weight change) at D2 post-infection, using multiple imputation matched quartets. Effect estimates for additive, maternal, inbred, and epistatic effects, including sex-specific effects, are presented as highest posterior density intervals (in percent starting weight) in 8-12 week old mice (n=1,042). Parameters are labeled according to the methods, and intervals are presented as in Figure 4A. Symmetric epistatic, asymmetric epistatic, and sex-specific parameters are indicated by "v:", "w:", and "f:", respectively. The overall treatment effect θ is -0.833% (-1.328%,-0.318%). (B) Model inclusion probabilities (MIPs) are given (posterior mean $\pm$ 1 s.d.) for effect parameter classes. (C) Treatment response variance projections (TReVarPs), a generalization of heritability to the diallel effects classes, are shown for three overall effects, five random effects classes, and five corresponding sex-specific random effects classes (with posterior median and 95% HPDs).
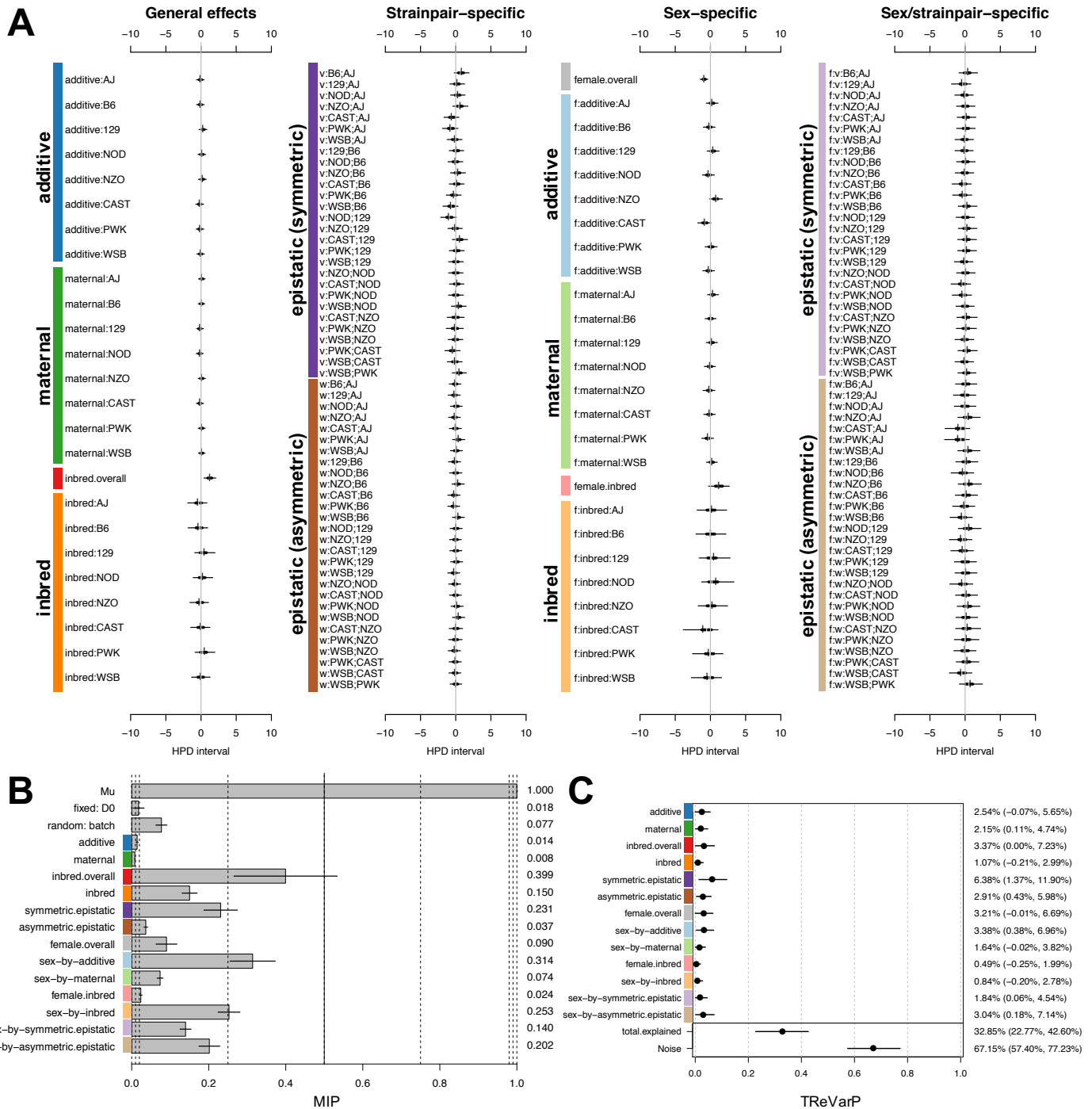
Figure S9 Diallel effects on host infection response (weight change) at D3 post-infection, using multiple imputation matched quartets. Effect estimates for additive, maternal, inbred, and epistatic effects, including sex-specific effects, are presented as highest posterior density intervals (in percent starting weight) in 8-12 week old mice (n=514). Parameters are labeled according to the methods, and intervals are presented as in Figure 4A. Symmetric epistatic, asymmetric epistatic, and sex-specific parameters are indicated by "v:", "w:", and "f:", respectively. The overall treatment effect θ is -5.594% (-6.470%, -4.729%). (B) Model inclusion probabilities (MIPs) are given (posterior mean $\pm$ 1 s.d.) for effect parameter classes. (C) Treatment response variance projections (TReVarPs), a generalization of heritability to the diallel effects classes, are shown for three overall effects, five random effects classes, and five corresponding sex-specific random effects classes (with posterior median and 95% HPDs).

Figure S10 Diallel effects on host infection response (weight change) at D4 post-infection, using multiple imputation matched quartets. Effect estimates for additive, maternal, inbred, and epistatic effects, including sex-specific effects, are presented as highest posterior density intervals (in percent starting weight) in 8-12 week old mice (n=513). Parameters are labeled according to the methods, and intervals are presented as in Figure 4A. Symmetric epistatic, asymmetric epistatic, and sex-specific parameters are indicated by "v:", "w:", and "f:", respectively. The overall treatment effect θ is -8.849% (-9.920%, -7.779%). (B) Model inclusion probabilities (MIPs) are given (posterior mean $\pm$ 1 s.d.) for effect parameter classes. (C) Treatment response variance projections (TReVarPs), a generalization of heritability to the diallel effects classes, are shown for three overall effects, five random effects classes, and five corresponding sex-specific random effects classes (with posterior median and 95% HPDs).
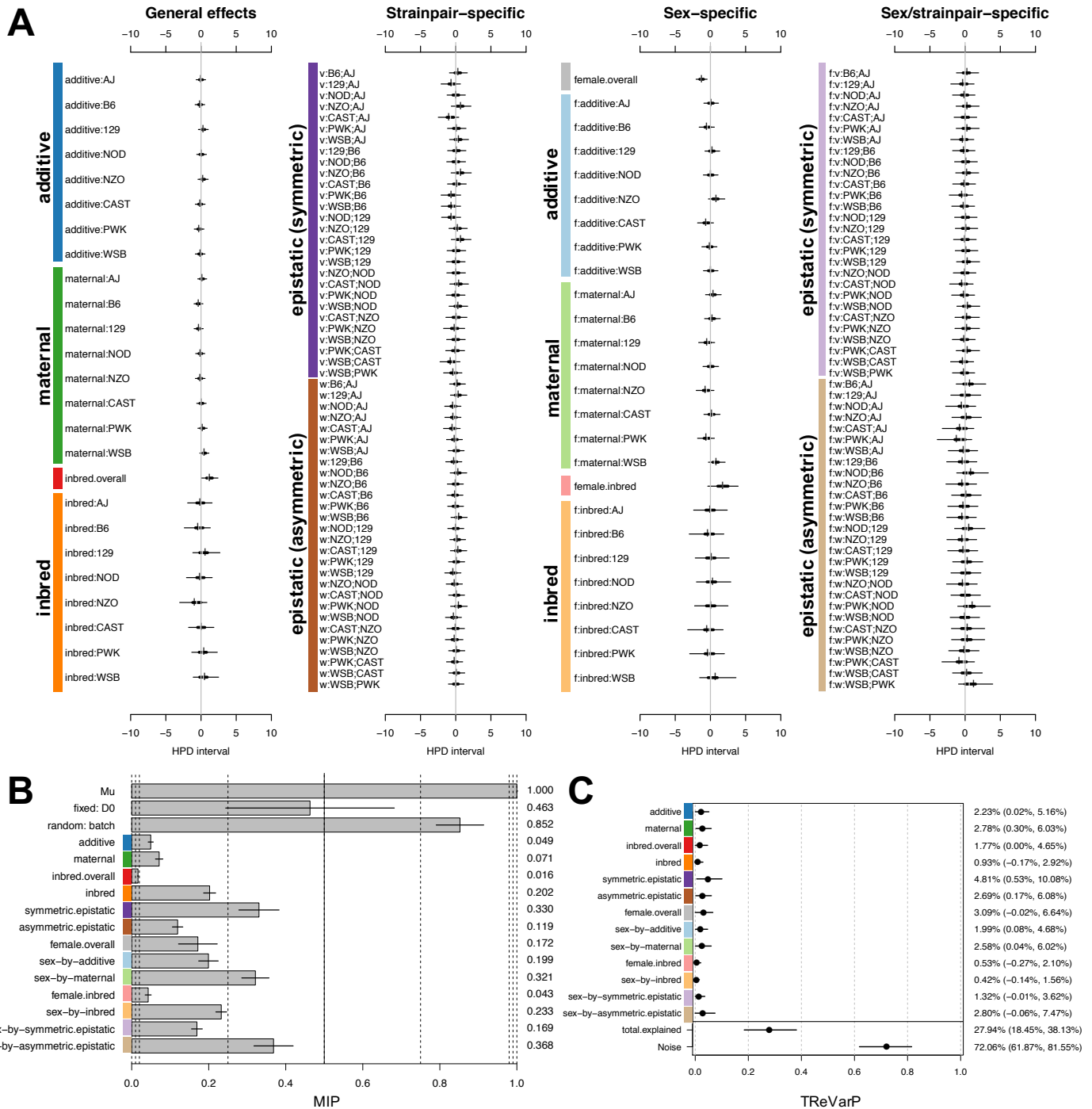
Figure S11 Diallel effects on host infection response (weight change) at D1 post-infection, using multiple imputation matched quartets and accounting for *Mx1*. Effect estimates for additive, maternal, inbred, and epistatic effects, including sex-specific effects, are presented as highest posterior density intervals (in percent starting weight) in 8-12 week old mice (n=1,042) after including random effect $u^{(Mx1 \text{ diplo})}$. Parameters are labeled according to the methods, and intervals are presented as in Figure 4A. Symmetric epistatic, asymmetric epistatic, and sex-specific parameters are indicated by "v:", "w:", and "f:", respectively. The overall treatment effect θ is -0.193% (-1.128%, 0.707%). (B) Model inclusion probabilities (MIPs) are given (posterior mean $\pm$ 1 s.d.) for effect parameter classes. (C) Treatment response variance projections (TReVarPs), a generalization of heritability to the diallel effects classes, are shown for three overall effects, five random effects classes, and five corresponding sex-specific random effects classes (with posterior median and 95% HPDs).
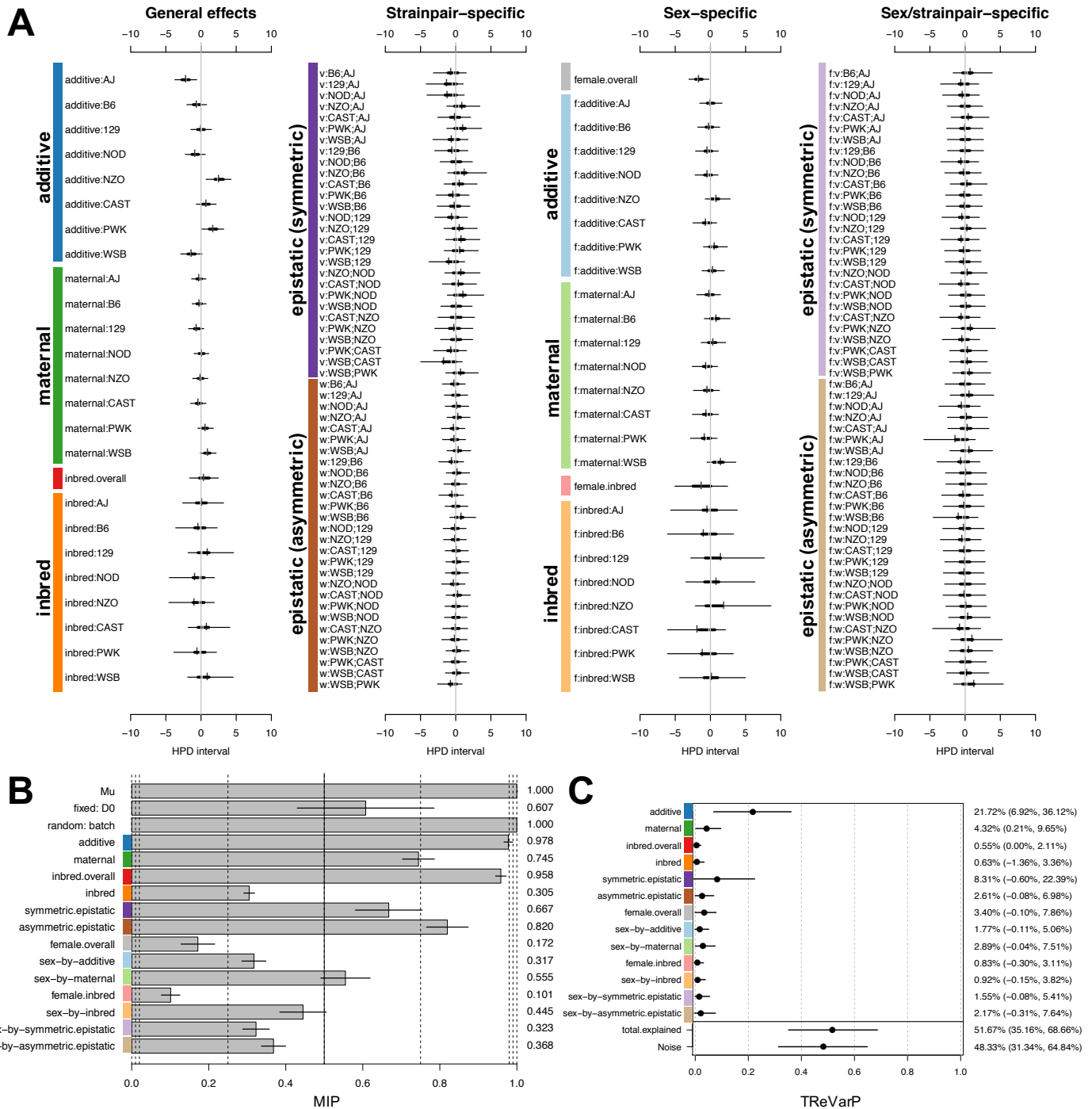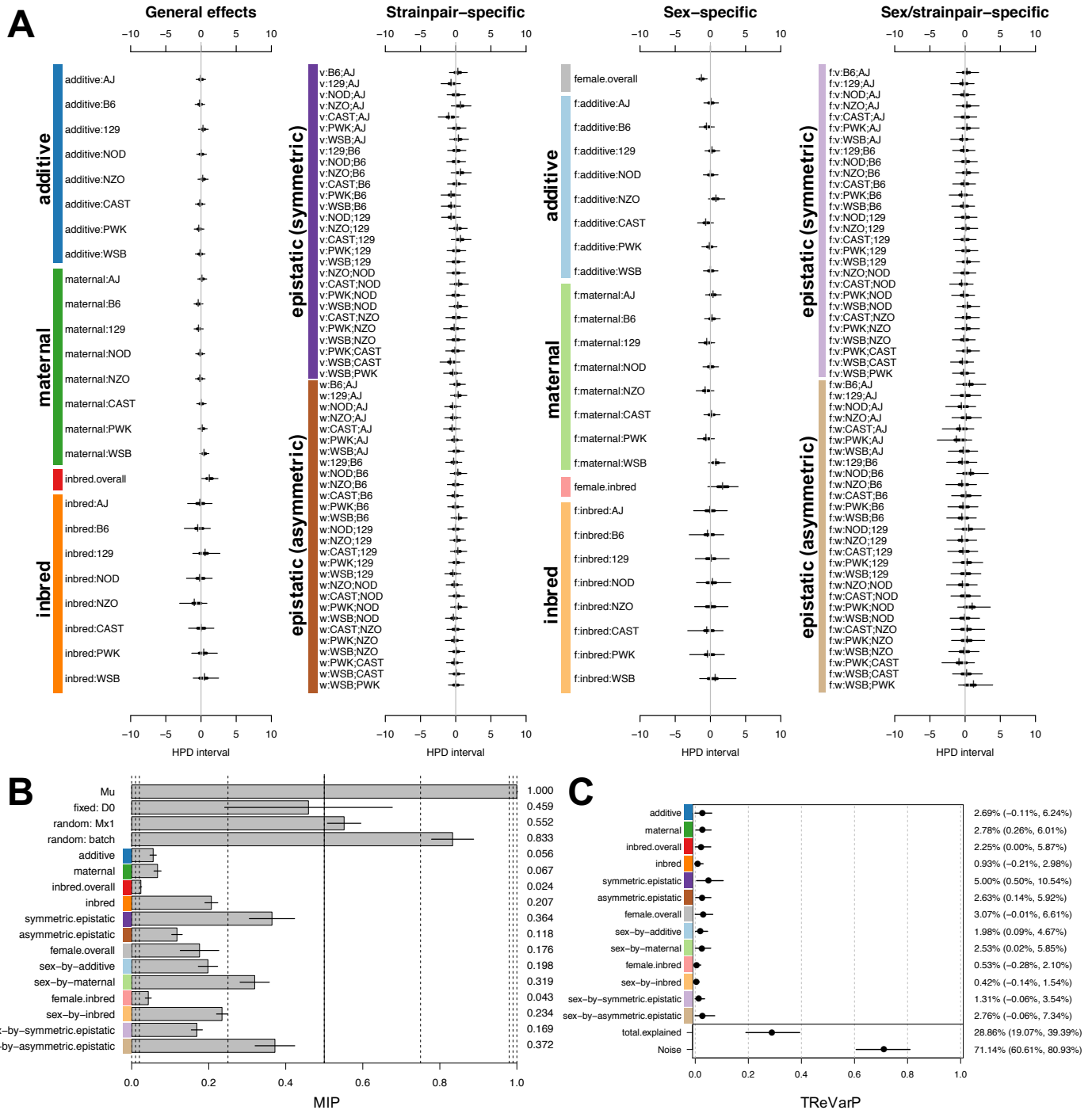
Figure S12 Diallel effects on host infection response (weight change) at D2 post-infection, using multiple imputation matched quartets and accounting for *Mx1*. Effect estimates for additive, maternal, inbred, and epistatic effects, including sex-specific effects, are presented as highest posterior density intervals (in percent starting weight) in 8-12 week old mice (n=1,042) after including random effect $u^{(Mx1\,\text{diplo})}$. Parameters are labeled according to the methods, and intervals are presented as in Figure 4A. Symmetric epistatic, asymmetric epistatic, and sex-specific parameters are indicated by "v:", "w:", and "f:", respectively. The overall treatment effect θ is -0.925% (-1.991%, 0.113%). (B) Model inclusion probabilities (MIPs) are given (posterior mean $\pm$ 1 s.d.) for effect parameter classes. (C) Treatment response variance projections (TReVarPs), a generalization of heritability to the diallel effects classes, are shown for three overall effects, five random effects classes, and five corresponding sex-specific random effects classes (with posterior median and 95% HPDs).
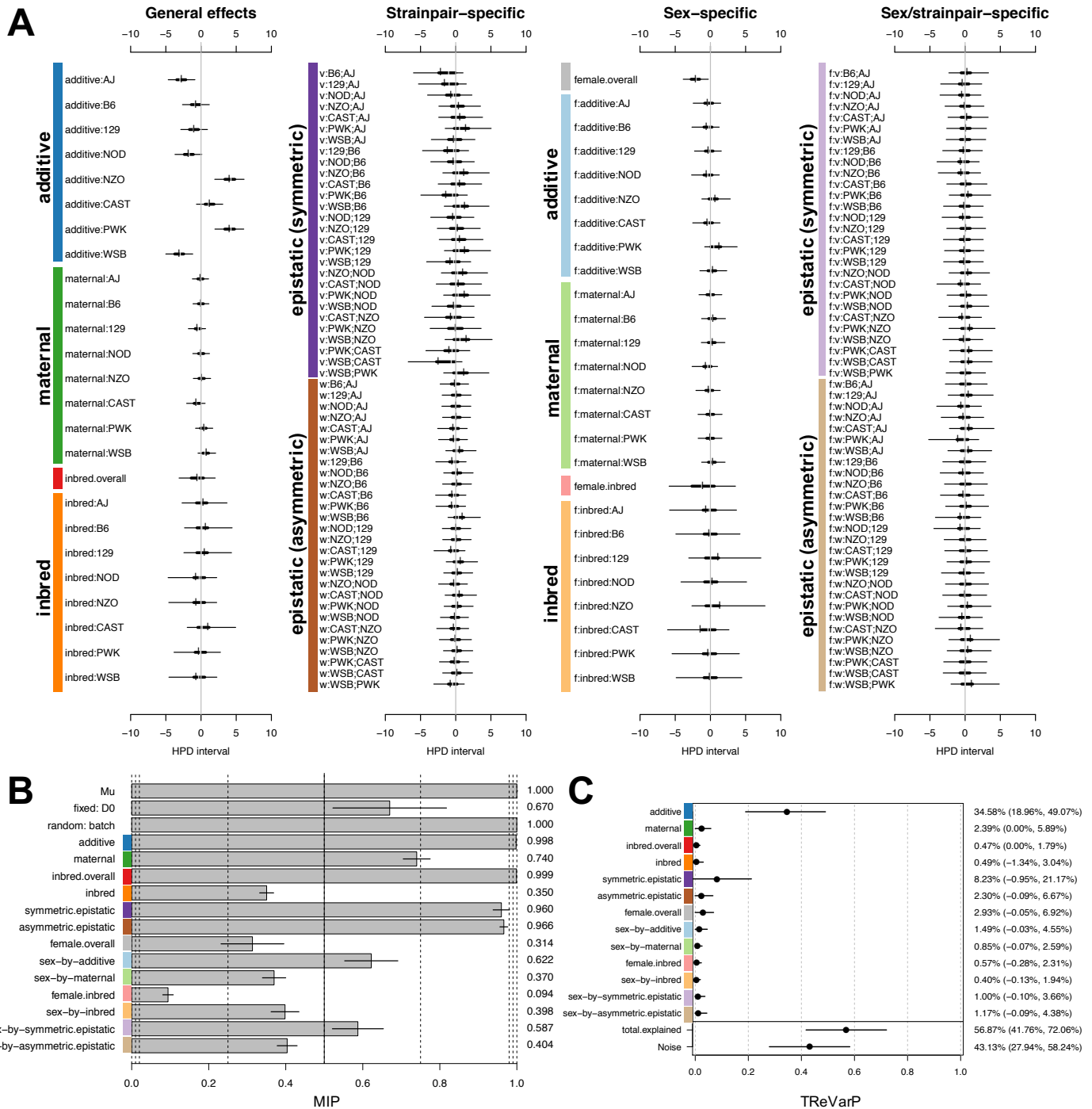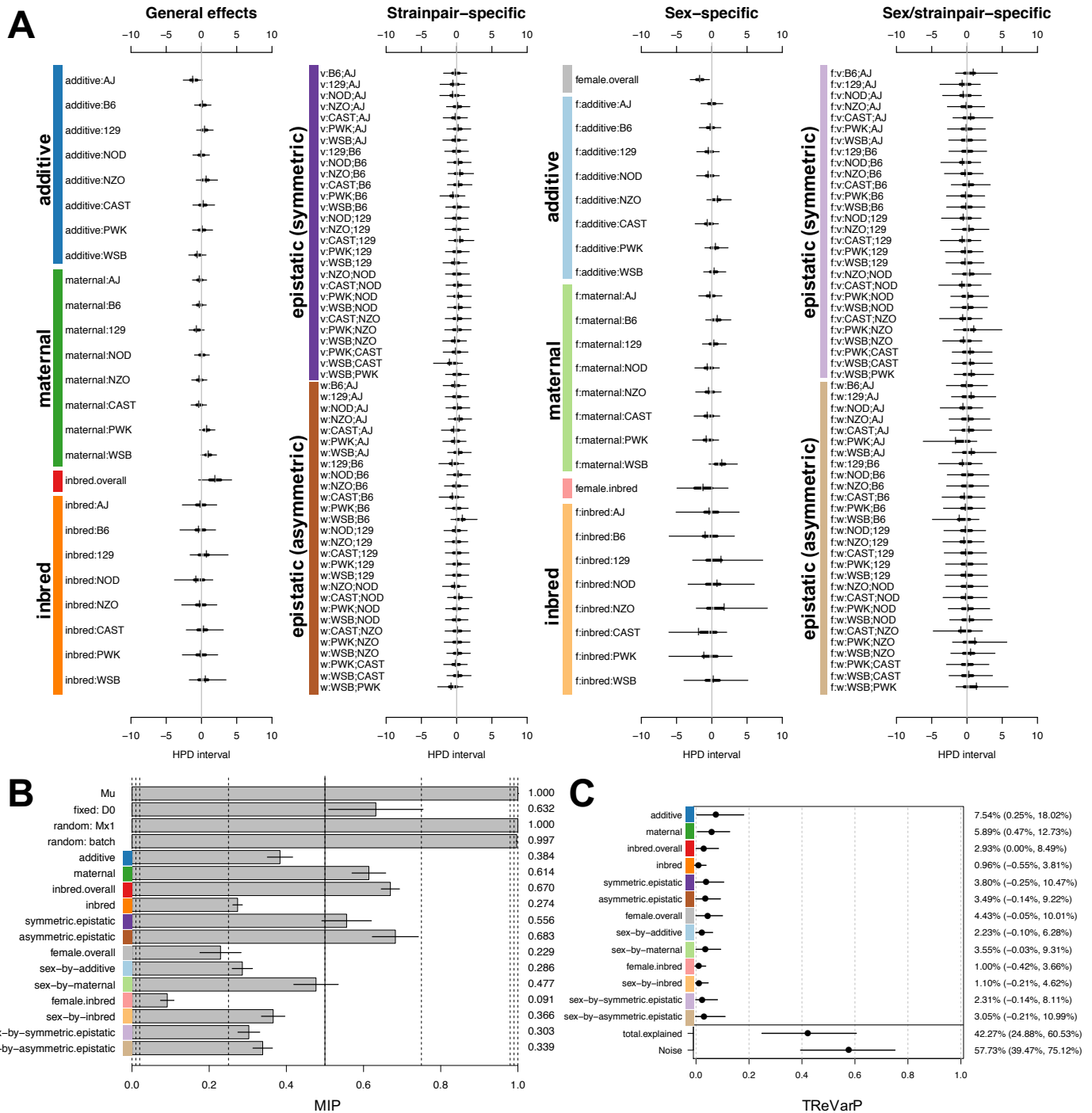
Figure S13 Diallel effects on host infection response (weight change) at D3 post-infection, using multiple imputation matched quartets and accounting for *Mx1*. Effect estimates for additive, maternal, inbred, and epistatic effects, including sex-specific effects, are presented as highest posterior density intervals (in percent starting weight) in 8-12 week old mice (n=514) after including random effect $u^{(Mx1 \, diplo)}$. Parameters are labeled according to the methods, and intervals are presented as in Figure 4A. Symmetric epistatic, asymmetric epistatic, and sex-specific parameters are indicated by "v:", "w:", and "f:", respectively. The overall treatment effect θ is -5.429% (-7.675%, -3.102%). (B) Model inclusion probabilities (MIPs) are given (posterior mean $\pm$ 1 s.d.) for effect parameter classes. (C) Treatment response variance projections (TReVarPs), a generalization of heritability to the diallel effects classes, are shown for three overall effects, five random effects classes, and five corresponding sex-specific random effects classes (with posterior median and 95% HPDs).
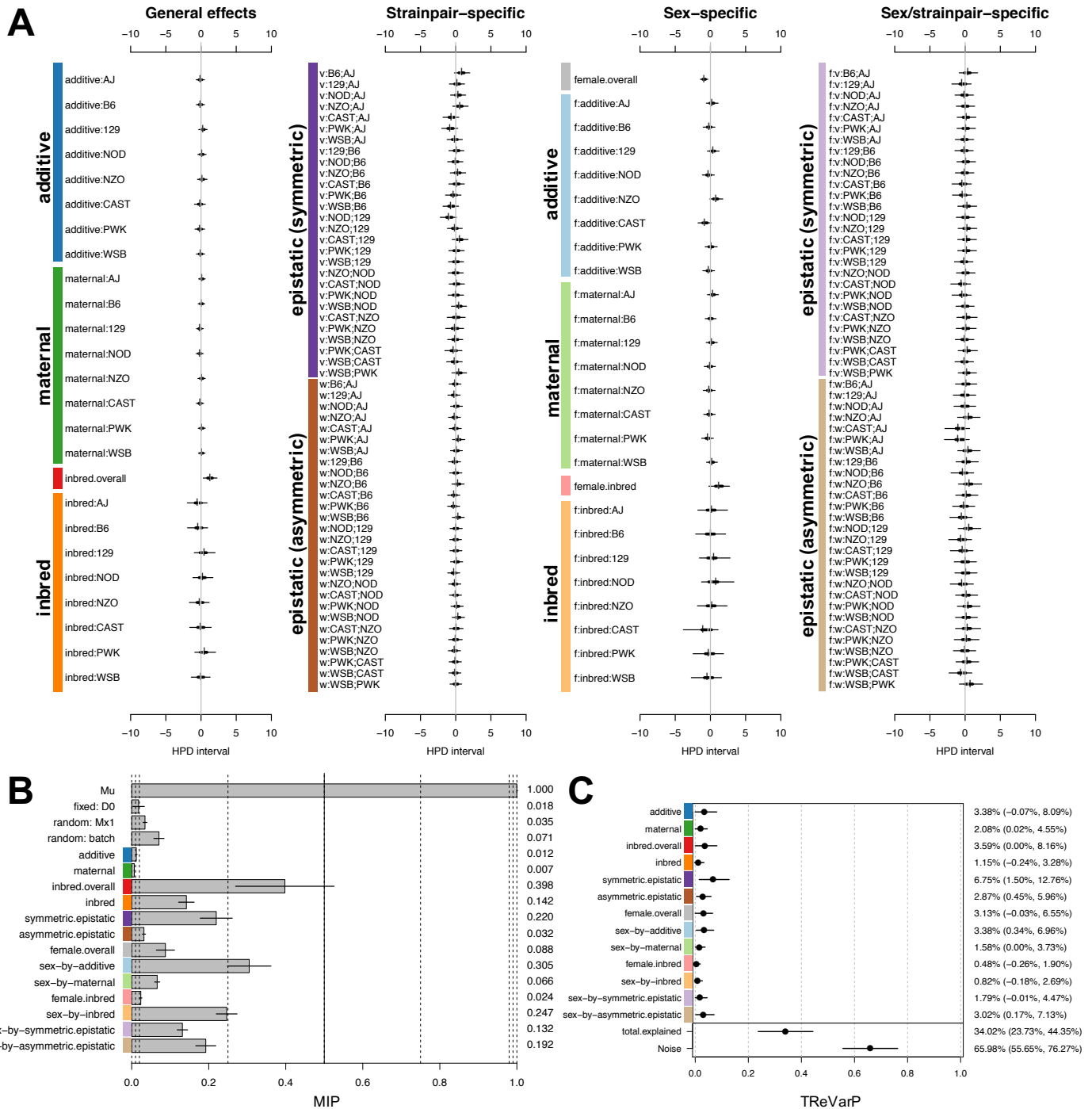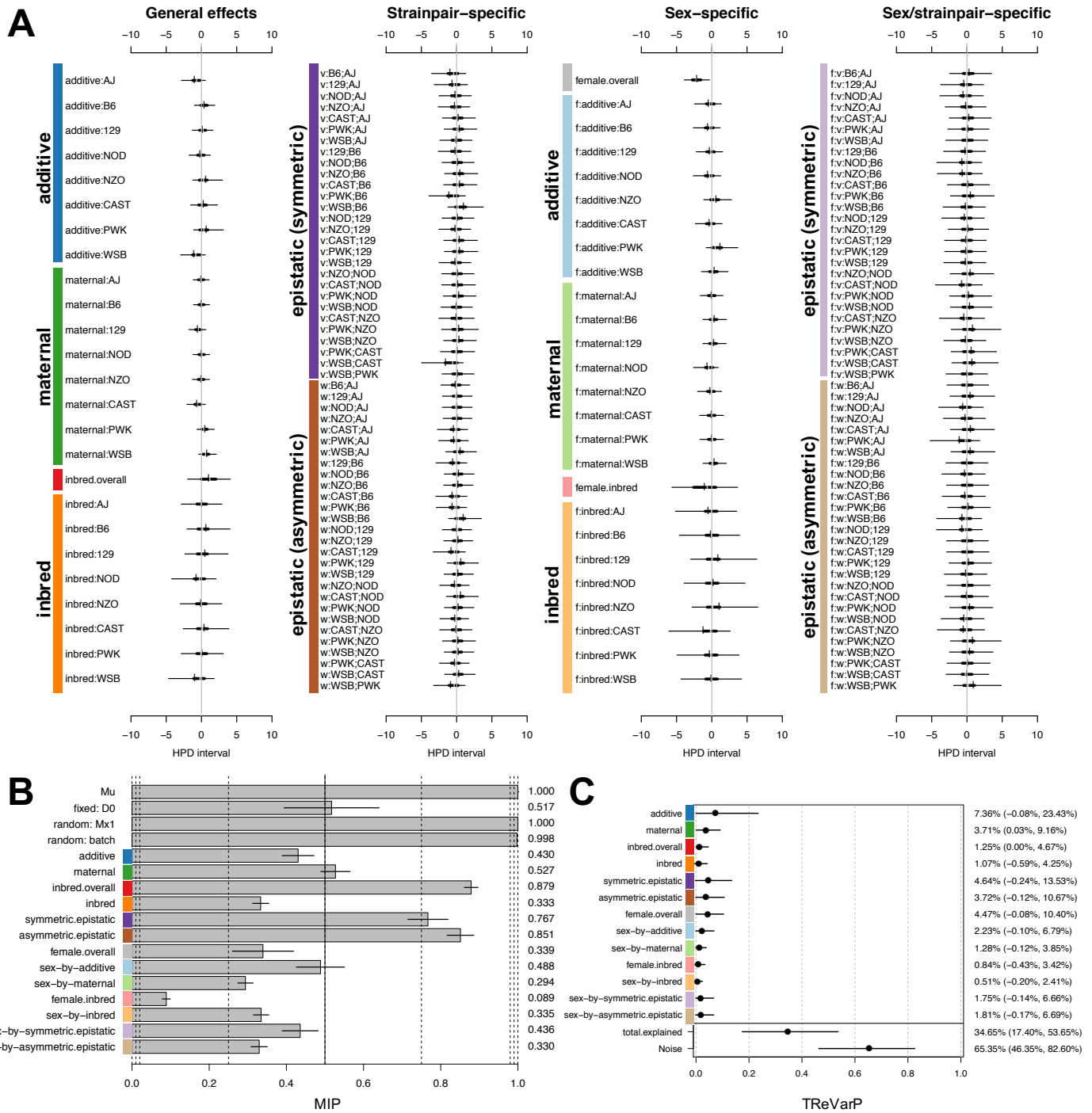
Figure S14 Diallel effects on host infection response (weight change) at D4 post-infection, using multiple imputation matched quartets and accounting for *Mx1*. Effect estimates for additive, maternal, inbred, and epistatic effects, including sex-specific effects, are presented as highest posterior density intervals (in percent starting weight) in 8-12 week old mice (n=513) after including random effect $u^{(Mx1 \text{ diplo})}$. Parameters are labeled according to the methods, and intervals are presented as in Figure 4A. Symmetric epistatic, asymmetric epistatic, and sex-specific parameters are indicated by "v:", "w:", and "f:", respectively. The overall treatment effect θ is -7.986% (-11.202%, -4.147%). (B) Model inclusion probabilities (MIPs) are given (posterior mean $\pm$ 1 s.d.) for effect parameter classes. (C) Treatment response variance projections (TReVarPs), a generalization of heritability to the diallel effects classes, are shown for three overall effects, five random effects classes, and five corresponding sex-specific random effects classes (with posterior median and 95% HPDs).

■ **Table S1 Proportion of variance in IAV-induced weight loss attributable to diallel effect classes across 4 days post-infection.** Part C of **Figure S7** through **Figure S10** show Bayesian confidence interval plots of treatment response variance projection (TReVarP) values presented here.

Effect Class [a]	D1	0.025	0.975	D2	0.025	0.975	D3	0.025	0.975	D4	0.025	0.975
additive	0.0229	-0.0007	0.0565	0.0197	0.0002	0.0516	0.2163	0.0692	0.3612	0.3477	0.1896	0.4907
maternal	0.0192	0.0011	0.0474	0.0253	0.0030	0.0603	0.0381	0.0021	0.0965	0.0196	0.0000	0.0589
inbred (overall)	0.0306	0.0000	0.0723	0.0142	0.0000	0.0465	0.0025	0.0000	0.0211	0.0021	0.0000	0.0179
inbred	0.0082	-0.0021	0.0299	0.0064	-0.0017	0.0292	0.0031	-0.0136	0.0336	0.0023	-0.0134	0.0304
symmetric epistatic	0.0605	0.0137	0.1190	0.0433	0.0053	0.1008	0.0655	-0.0060	0.2239	0.0692	-0.0095	0.2117
asymmetric epistatic	0.0264	0.0043	0.0598	0.0233	0.0017	0.0608	0.0203	-0.0008	0.0698	0.0163	-0.0009	0.0667
female (overall)	0.0296	-0.0001	0.0669	0.0282	-0.0002	0.0664	0.0299	-0.0010	0.0786	0.0256	-0.0005	0.0692
sex-by-additive	0.0309	0.0038	0.0696	0.0169	0.0008	0.0468	0.0131	-0.0011	0.0506	0.0103	-0.0003	0.0455
sex-by-maternal	0.0143	-0.0002	0.0382	0.0224	0.0004	0.0602	0.0230	-0.0004	0.0751	0.0059	-0.0007	0.0259
female inbred (overall)	0.0024	-0.0025	0.0199	0.0027	-0.0027	0.0210	0.0047	-0.0030	0.0311	0.0027	-0.0028	0.0231
sex-by-inbred	0.0054	-0.0020	0.0278	0.0024	-0.0014	0.0156	0.0034	-0.0015	0.0382	0.0012	-0.0013	0.0194
sex-by-symm. epis.	0.0152	0.0006	0.0454	0.0100	-0.0001	0.0362	0.0089	-0.0008	0.0541	0.0052	-0.0010	0.0366
sex-by-asymm. epis.	0.0259	0.0018	0.0714	0.0218	-0.0006	0.0747	0.0119	-0.0031	0.0764	0.0059	-0.0009	0.0438
total explained	0.3276	0.2277	0.4260	0.2775	0.1845	0.3813	0.5164	0.3516	0.6866	0.5705	0.4176	0.7206
noise	0.6724	0.5740	0.7723	0.7225	0.6187	0.8155	0.4836	0.3134	0.6484	0.4295	0.2794	0.5824

[a] To indicate the relative contribution of different diallel effects on host response to IAV, TreVarPs are given for overall effects (female, inbred, female inbred) and strain/strainpair-specific effects (additive, maternal, inbred, symmetric epistatic, asymmetric epistatic) on D1delta through D4delta (median and 95% HPD intervals).

■ **Table S2 Proportion of variance in IAV-induced weight loss attributable to diallel effect classes across 4 days post-infection, after accounting for *Mx1* diplotype.** Part C of **Figure S11** through **Figure S14** show Bayesian confidence interval plots of treatment response variance projection (TReVarP) values presented here.

Effect Class [a]	D1	0.025	0.975	D2	0.025	0.975	D3	0.025	0.975	D4	0.025	0.975
additive	0.0292	-0.0007	0.0809	0.0233	-0.0011	0.0624	0.0631	0.0025	0.1802	0.0496	-0.0008	0.2343
maternal	0.0188	0.0002	0.0455	0.0250	0.0026	0.0601	0.0530	0.0047	0.1273	0.0309	0.0003	0.0916
inbred (overall)	0.0318	0.0000	0.0816	0.0183	0.0000	0.0587	0.0215	0.0000	0.0849	0.0062	0.0000	0.0467
inbred	0.0087	-0.0024	0.0328	0.0064	-0.0021	0.0298	0.0052	-0.0055	0.0381	0.0054	-0.0059	0.0425
symmetric epistatic	0.0639	0.0150	0.1276	0.0450	0.0050	0.1054	0.0286	-0.0025	0.1047	0.0333	-0.0024	0.1353
asymmetric epistatic	0.0260	0.0045	0.0596	0.0227	0.0014	0.0592	0.0272	-0.0014	0.0922	0.0268	-0.0012	0.1067
female (overall)	0.0288	-0.0003	0.0655	0.0280	-0.0001	0.0661	0.0395	-0.0005	0.1001	0.0393	-0.0008	0.1040
sex-by-additive	0.0308	0.0034	0.0696	0.0168	0.0009	0.0467	0.0167	-0.0010	0.0628	0.0152	-0.0010	0.0679
sex-by-maternal	0.0138	0.0000	0.0373	0.0219	0.0002	0.0585	0.0286	-0.0003	0.0931	0.0089	-0.0012	0.0385
female inbred (overall)	0.0023	-0.0026	0.0190	0.0026	-0.0028	0.0210	0.0056	-0.0042	0.0366	0.0040	-0.0043	0.0342
sex-by-inbred	0.0053	-0.0018	0.0269	0.0023	-0.0014	0.0154	0.0041	-0.0021	0.0462	0.0017	-0.0020	0.0241
sex-by-symm. epis.	0.0147	-0.0001	0.0447	0.0100	-0.0006	0.0354	0.0132	-0.0014	0.0811	0.0088	-0.0014	0.0666
sex-by-asymm. epis.	0.0257	0.0017	0.0713	0.0213	-0.0006	0.0734	0.0165	-0.0021	0.1099	0.0091	-0.0017	0.0669
total explained	0.3389	0.2373	0.4435	0.2866	0.1907	0.3939	0.4186	0.2488	0.6053	0.3381	0.1740	0.5365
noise	0.6611	0.5565	0.7627	0.7134	0.6061	0.8093	0.5814	0.3947	0.7512	0.6619	0.4635	0.8260

[a] To indicate the relative contribution of different diallel effects on host response to IAV, TreVarPs are given for overall effects (female, inbred, female inbred) and strain/strainpair-specific effects (additive, maternal, inbred, symmetric epistatic, asymmetric epistatic) on D1delta through D4delta (median and 95% HPD intervals).

■ **Table S3 Model inclusion probabilities for diallel effects classes, (A) before and (B) after accounting for *Mx1* diplotype.** We consider the following levels for strength of evidence for inclusion: positive {(0.05, 0.25] or [0.75, 0.95)}, strong {(0.01, 0.05] or [0.95, 0.99)} and very strong {[0, 0.01] or [0.99, 1]}, as described in the Statistical Methods. Part B of **Figures S7 through S14** show bar plots of posterior MIP values presented here.

(A) Effect Class	D1	D2	D3	D4	(B) Effect Class	D1	D2	D3	D4
theta	1.0000	1.0000	1.0000	1.0000	theta	1.0000	1.0000	1.0000	1.0000
fixed: D0	0.0179	0.4630	0.6074	0.6699	fixed: D0	0.0180	0.4590	0.6319	0.5172
random: batch	0.0772	0.8523	1.0000	0.9999	random: batch	0.0708	0.8332	0.9969	0.9979
					random: *Mx1* diplo	0.0345	0.5515	1.0000	1.0000
additive	0.0141	0.0494	0.9779	0.9980	additive	0.0120	0.0558	0.3835	0.4305
maternal	0.0082	0.0713	0.7446	0.7400	maternal	0.0068	0.0671	0.6138	0.5272
inbred (overall)	0.3995	0.0164	0.9584	0.9992	inbred (overall)	0.3977	0.0238	0.6696	0.8789
inbred	0.1504	0.2024	0.3050	0.3504	inbred	0.1420	0.2068	0.2737	0.3334
symmetric epistatic	0.2309	0.3305	0.6674	0.9598	symmetric epistatic	0.2195	0.3642	0.5561	0.7668
asymmetric epistatic	0.0366	0.1193	0.8197	0.9662	asymmetric epistatic	0.0318	0.1176	0.6825	0.8511
female (overall)	0.0904	0.1718	0.1719	0.3135	female (overall)	0.0876	0.1762	0.2294	0.3394
sex-by-additive	0.3140	0.1993	0.3174	0.6220	sex-by-additive	0.3051	0.1981	0.2859	0.4884
sex-by-maternal	0.0738	0.3212	0.5550	0.3697	sex-by-maternal	0.0662	0.3194	0.4769	0.2939
female inbred (overall)	0.0237	0.0428	0.1012	0.0943	female inbred (overall)	0.0237	0.0432	0.0913	0.0889
sex-by-inbred	0.2527	0.2325	0.4448	0.3981	sex-by-inbred	0.2466	0.2345	0.3658	0.3345
sex-by-symmetric epistatic	0.1399	0.1694	0.3228	0.5873	sex-by-symmetric epistatic	0.1317	0.1692	0.3028	0.4359
sex-by-asymmetric epistatic	0.2016	0.3683	0.3682	0.4037	sex-by-asymmetric epistatic	0.1924	0.3719	0.3387	0.3296
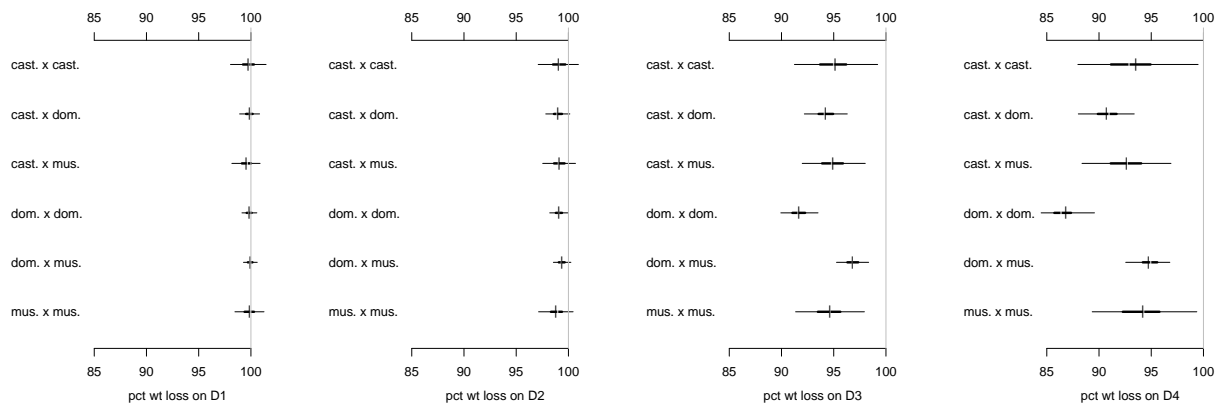
Figure S15 Timecourse of posterior predictive estimates of for *Mx1* diplotype mean effects across four days post-infection. From left to right, predictive estimates of IAV-induced weight change are provided for D1, D2, D3 and D4 p.i.
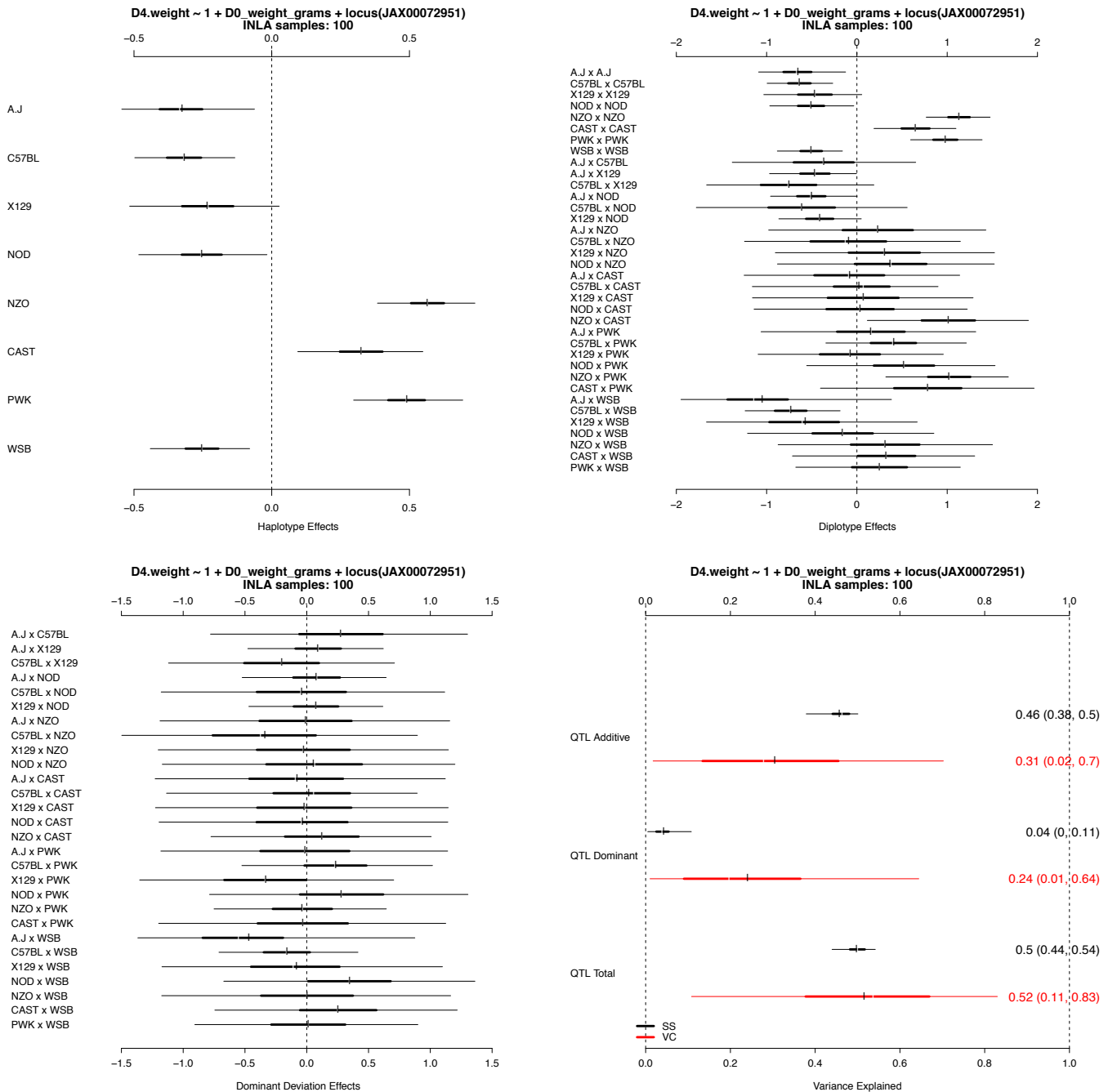
Figure S16 *Mx1* effects and proportion of variance explained on weight loss in the pre-CC. [Top Left] Additive *Mx1* haplotype effects in pre-CC mice (n=155) infected with IAV (PR8) at day 4 post-infection. [Top Right] Bayesian credible intervals of the posterior predictive distribution of mice with *Mx1* diplotype. [Bottom Left] Dominance deviation *Mx1* effects in the pre-CC mice. Wide intervals are indicative of the low levels of heterozygosity observed in the mostly inbred pre-CC mice. [Bottom Right] Bayesian credible intervals of the posterior predictive distribution of the proportion of the phenotypic variance explained by the *Mx1* additive effects, dominant effects and the combination of both effects. Black intervals (VC) are based on the posterior samples of the variance components. Red intervals (SS) are based on the posterior samples of sums of squares estimators. SS estimators are (1) not dependent on variance component estimates, which tend to be disperse, and (2) are based on the observed strains and crosses, rather than all possible strains/crosses, with (1) and (2) resulting in much narrower confidence intervals.
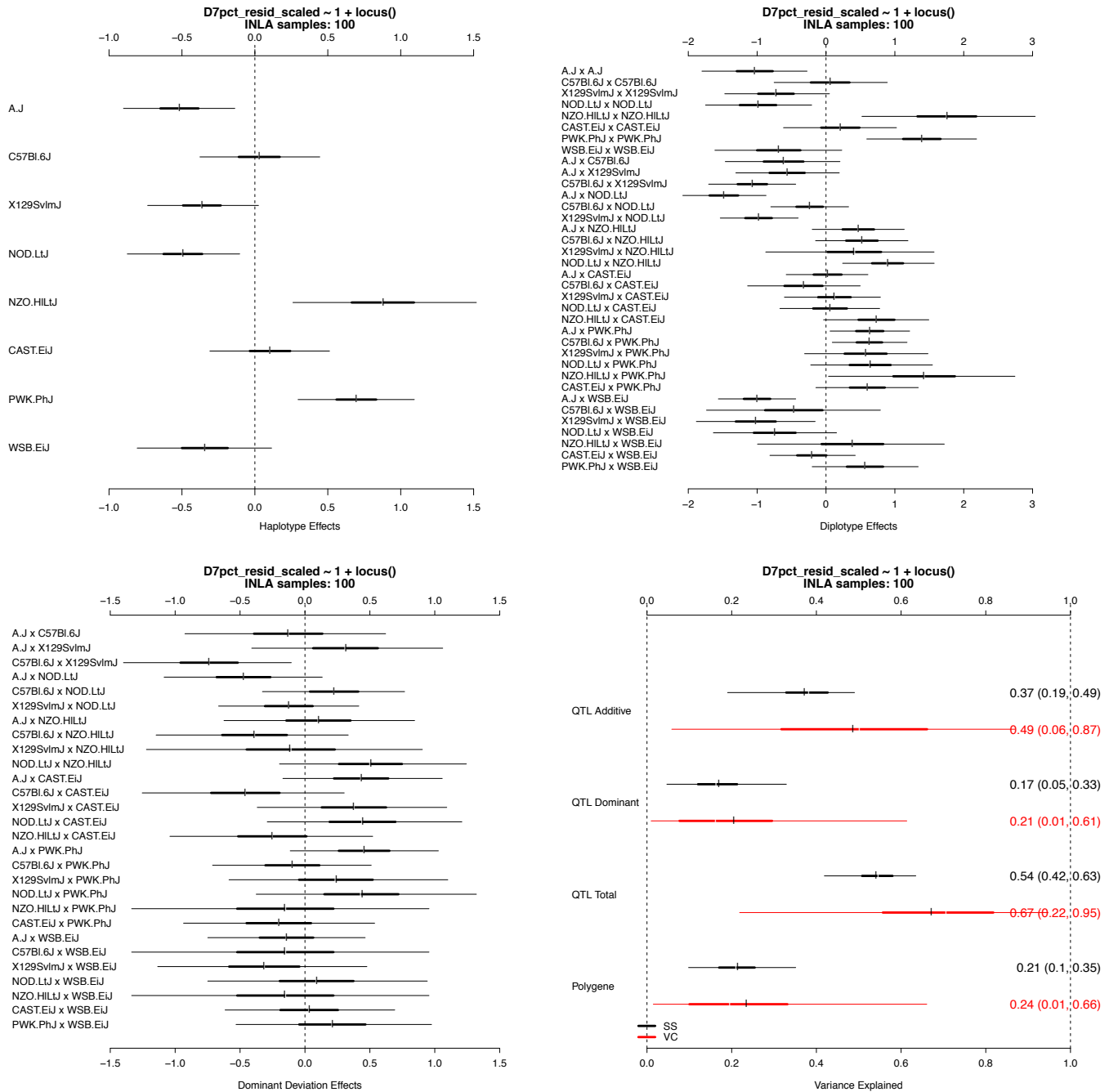
Figure S17 *Mx1* allele effects and proportion of variance explained on weight loss in the CC-RIX. [Top Left] Additive *Mx1* haplotype effects in CC-RIX mice (n=1,402) infected with IAV (CA04) at day 7 post-infection. [Top Right] Bayesian credible intervals of the posterior predictive distribution of mice with *Mx1* diplotype. [Bottom Left] Dominance deviation *Mx1* effects in the CC-RIX mice. Narrower intervals compared to observed in pre-CC is indicative of the high levels of heterozygosity CC-RIX mice. [Bottom Right] Bayesian credible intervals of the posterior predictive distribution of the proportion of the phenotypic variance explained by the *Mx1* additive effects, dominant effects, the combination of both *Mx1* effects, and cumulative effects of other loci captured in the relationship matrix. In the CC-RIX, the relationship matrix models the expected increased phenotypic correlation between CC-RIX mice that share a single CC parent. Black intervals (VC) are based on the posterior samples of the variance components. Red intervals (SS) are based on the posterior samples of sums of squares estimators. SS estimators are (1) not dependent on variance component estimates, which tend to be disperse, and (2) are based on the observed strains and crosses, rather than all possible strains/crosses, with (1) and (2) resulting in much narrower confidence intervals.

■ **Table S4** Details of populations analyzed for additive strain-specific effects in **Figure 7**.

POPULATION	diallel	pre-CC	CC-RIX
Recombinant	no	yes	yes
Inbreds	yes (some)	yes	no
Heterozygotes	yes (most)	no	yes
Sexes	males & females	females	females
IAV used	H1N1 (PR8)	H1N1 (PR8)	H1N1 (CA04)
Post-infection day analyzed	day 4	day 4	day 7
Model	Bayes Diallel	Diploffect	Diploffect

■ **Table S5** Table of CC-RIX lines used in this experiment. A total of 1,402 mice from 105 CC-RIX strains (about 13 mice per strain), originating from a sparse diallel cross of 65 CC lines, were assayed for weight loss on day 7 post-infection.

CC-RIX ID	count	CC-RIX ID	count	CC-RIX ID	count
CC001xCC055	16	CC020xCC008	17	CC042xCC019	13
CC001xCC074	11	CC021xCC023	15	CC042xCC025	5
CC002xCC011	14	CC021xCC032	3	CC043xCC033	21
CC002xCC021	15	CC022xCC024	11	CC043xCC037	27
CC003xCC051	12	CC022xCC044	3	CC044xCC060	18
CC003xCC062	18	CC023xCC025	18	CC045xCC044	11
CC004xCC011	15	CC024xCC023	15	CC046xCC068	21
CC004xCC012	12	CC024xCC052	11	CC049xCC036	8
CC005xCC001	15	CC025xCC028	20	CC051xCC005	14
CC005xCC040	15	CC026xCC034	17	CC051xCC009	14
CC006xCC007	20	CC026xCC042	7	CC052xCC007	3
CC006xCC039	3	CC027xCC036	3	CC052xCC014	15
CC007xCC070	12	CC027xCC045	14	CC055xCC028	21
CC008xCC009	3	CC028xCC024	21	CC056xCC033	20
CC008xCC010	16	CC028xCC030	18	CC057xCC052	16
CC008xCC018	10	CC029xCC027	16	CC058xCC022	17
CC009xCC040	12	CC029xCC071	6	CC059xCC065	4
CC010xCC015	21	CC030xCC023	23	CC060xCC006	15
CC010xCC060	9	CC030xCC061	17	CC061xCC025	16
CC011xCC032	13	CC032xCC013	18	CC061xCC026	16
CC011xCC042	15	CC032xCC017	15	CC061xCC039	15
CC012xCC032	12	CC033xCC046	18	CC062xCC046	3
CC012xCC038	20	CC033xCC068	21	CC062xCC072	3
CC013xCC041	28	CC034xCC016	10	CC063xCC001	3
CC014xCC059	4	CC035xCC071	14	CC063xCC002	7
CC015xCC018	12	CC036xCC051	16	CC065xCC010	10
CC015xCC059	15	CC037xCC046	12	CC065xCC072	1
CC016xCC038	18	CC037xCC057	19	CC068xCC043	9
CC016xCC061	13	CC038xCC013	14	CC070xCC003	15
CC017xCC004	13	CC039xCC020	14	CC071xCC053	12
CC017xCC041	16	CC040xCC003	16	CC072xCC063	4
CC018xCC009	19	CC040xCC015	13	CC072xCC075	9
CC018xCC065	16	CC041xCC012	12	CC074xCC058	7
CC019xCC002	19	CC041xCC016	18	CC075xCC021	3
CC019xCC004	16	CC042xCC017	14	CC075xCC035	14

■ **Table S6** Summary of overall and additive effects from **Figures 4A, S7A, S8A, S9A,** and **S10A**. Posterior median and 95% HPD intervals are provided for D1 through D4 p.i.

Diallel Effect	D1	0.025	0.975	D2	0.025	0.975	D3	0.025	0.975	D4	0.025	0.975
treatment (overall) (θ)	-0.131	-0.484	0.223	-0.833	-1.328	-0.318	-5.594	-6.470	-4.729	-8.849	-9.920	-7.779
inbred (overall)	1.258	0.407	2.100	1.212	-0.002	2.413	0.416	-1.641	2.477	-0.524	-3.122	2.018
female (overall)	-0.895	-1.447	-0.362	-1.245	-2.037	-0.460	-1.655	-3.066	-0.220	-2.108	-3.868	-0.295
female inbred (overall)	1.221	-0.269	2.680	1.771	-0.375	3.940	-1.286	-5.052	2.438	-1.077	-5.872	3.559
fixed: D0 weight	-0.135	-0.285	0.017	-0.306	-0.522	-0.093	-0.450	-0.928	0.025	-0.473	-1.061	0.123
additive: AJ	-0.089	-0.641	0.445	-0.016	-0.689	0.647	-2.167	-3.721	-0.611	-2.767	-4.661	-0.864
additive: B6	-0.086	-0.642	0.450	-0.153	-0.845	0.524	-0.606	-2.010	0.801	-0.730	-2.638	1.181
additive: 129	0.270	-0.283	0.840	0.316	-0.379	1.031	0.002	-1.442	1.462	-0.997	-2.878	0.917
additive: NOD	0.115	-0.440	0.667	0.062	-0.608	0.771	-0.827	-2.249	0.601	-1.764	-3.703	0.116
additive: NZO	0.191	-0.363	0.747	0.276	-0.437	1.021	2.536	0.719	4.269	4.066	1.948	6.121
additive: CAST	-0.184	-0.752	0.362	-0.120	-0.812	0.579	0.731	-0.674	2.157	1.235	-0.649	3.092
additive: PWK	-0.149	-0.699	0.411	-0.258	-0.967	0.425	1.698	0.116	3.228	4.061	1.971	6.076
additive: WSB	-0.067	-0.610	0.471	-0.108	-0.809	0.567	-1.350	-2.889	0.157	-3.088	-5.008	-1.176
σ^2	3.808	2.923	4.786	8.188	6.284	10.182	12.199	6.881	17.899	19.679	12.024	28.777

■ **Table S7** Summary of overall, additive, and *Mx1* effects from **Figures S11A**, **S12A**, **S13A**, and **S14A**. Posterior median and 95% HPD intervals are provided for D1 through D4 p.i.

Diallel Effect	D1	0.025	0.975	D2	0.025	0.975	D3	0.025	0.975	D4	0.025	0.975
treatment (overall) (θ)	-0.193	-1.128	0.707	-0.925	-1.991	0.113	-5.464	-7.675	-3.102	-7.986	-11.202	-4.147
inbred (overall)	1.296	0.313	2.276	1.385	0.017	2.738	1.945	-0.417	4.282	1.046	-1.971	4.101
female (overall)	-0.894	-1.435	-0.356	-1.251	-2.039	-0.468	-1.681	-3.061	-0.333	-2.105	-3.905	-0.339
female inbred (overall)	1.224	-0.231	2.705	1.765	-0.364	3.931	-1.221	-4.945	2.312	-1.018	-5.663	3.654
fixed: D0 weight	-0.137	-0.289	0.012	-0.313	-0.528	-0.099	-0.548	-0.996	-0.096	-0.576	-1.155	-0.016
additive: AJ	-0.094	-0.679	0.489	-0.015	-0.718	0.691	-1.147	-2.589	0.112	-0.854	-2.819	0.549
additive: B6	-0.086	-0.664	0.501	-0.145	-0.867	0.567	0.190	-0.980	1.352	0.401	-1.017	1.891
additive: 129	0.272	-0.327	0.873	0.323	-0.404	1.076	0.457	-0.695	1.663	0.174	-1.299	1.600
additive: NOD	0.113	-0.453	0.722	0.067	-0.639	0.799	-0.046	-1.221	1.130	-0.148	-1.769	1.266
additive: NZO	0.167	-0.510	0.859	0.232	-0.576	1.068	0.635	-0.737	2.279	0.447	-1.221	2.979
additive: CAST	-0.137	-0.935	0.619	-0.048	-0.942	0.831	0.267	-1.225	1.866	0.230	-1.545	2.277
additive: PWK	-0.162	-0.857	0.506	-0.303	-1.146	0.493	0.105	-1.273	1.578	0.523	-1.124	3.116
additive: WSB	-0.072	-0.653	0.501	-0.111	-0.836	0.605	-0.514	-1.811	0.650	-0.909	-2.962	0.533
Mx1: cast × cast	-0.043	-1.555	1.470	-0.016	-1.712	1.652	0.511	-2.990	4.202	1.257	-3.773	6.904
Mx1: cast × dom	0.057	-1.077	1.193	-0.089	-1.397	1.183	-0.311	-3.008	2.256	-1.287	-5.596	2.401
Mx1: cast × mus	-0.238	-1.572	1.028	0.036	-1.409	1.521	0.317	-2.619	3.433	0.451	-3.933	5.062
Mx1: dom × dom	0.028	-1.076	1.217	0.015	-1.253	1.290	-2.831	-5.872	-0.131	-5.274	-9.857	-0.779
Mx1: dom × mus	0.135	-0.897	1.213	0.290	-0.870	1.522	2.198	-0.207	4.743	2.624	-1.118	6.299
Mx1: mus × mus	0.061	-1.251	1.445	-0.234	-1.817	1.213	0.016	-3.171	3.295	1.948	-2.574	7.167
σ^2	3.797	2.913	4.769	8.190	6.328	10.268	11.270	6.644	16.627	19.296	12.210	27.397

■ **Table S8** Summary of dominance index for *Mx1* from *cast* or *mus*, combined with *Mx1* from *dom* in our diallel study. Posterior mode and and 80% HPD intervals are provided from D1 through D4 p.i. The posterior mode is obtained from the value of $\mathcal{D}$ that has the maximum posterior density within the range $[-1, 2]$, via the `density` function from the `stats` package in R.

index	D1	D2	D3	D4
$\mathcal{D}^{(cast;\ dom)}$	0.726 (-1.322, 2.676)	0.708 (-1.476, 2.833)	0.421 (-0.534, 0.907)	0.491 (-0.028, 0.836)
$\mathcal{D}^{(mus;\ dom)}$	0.650 (-1.181, 2.460)	0.832 (-1.410, 3.101)	-0.278 (-2.547, 0.329)	0.068 (-0.568, 0.381)
$\mathcal{D}^{(cast;\ mus)}$	0.468 (-2.060, 3.042)	0.521 (-2.037, 2.966)	0.450 (-1.884, 2.794)	0.526 (-2.197, 3.135)

Algorithm 1: Multiple Imputation Matched Quartets (MIMQ)

Data: Treatment diallel data frame (T)

Result: Posterior effect estimates for phenotypes in P

1   $P \leftarrow$ phenotypes (*e.g.* $\mathrm{pct}^{D1}, \ldots, \mathrm{pct}^{D4}$);

2   $D \leftarrow$ diallel categories ($\{jk, s, h\}$);

3   $R \leftarrow$ total number of replicates ($n = 1000$);

4   $C \leftarrow$ covariates;

5   **for** $p \in P$ **do**

6   **for** $d \in D$ **do**

7   Identify number of individuals to be deleted from this class (0-1); if > 0, add class to set of classes to have deletions (D_{delete})

8   Identify number of individuals to be imputed from this class (0-3); if > 0 add class to set of classes to have imputation (D_{impute})

9   **end**

10   **for** $r \leftarrow 1$ **to** R **do**

11   Make copy of T: $T^{(r)}$

12   **for** $d \in D_{delete}$ **do**

13   Randomly delete row from class d in $T^{(r)}$;

14   **end**

15   **for** $c \in C$ **do**

16   Obtain diallel effect ($\hat{\boldsymbol{\beta}}_c$) and variance ($\hat{\sigma}_c^2$) estimates by fitting covariate data for c with BayesDiallel;

17   **for** $d \in D_{impute}$ **do**

18   Insert row(s) for class d into $T^{(r)}$, imputing c_d according to the following: $\tilde{c}_d^r \sim N(\mathbf{d}\hat{\boldsymbol{\beta}}_c, \hat{\sigma}_c^2)$; based on counts from (8), multiple rows with different c_d values may be inserted;

19   **end**

20   **end**

21   Obtain diallel effect ($\hat{\boldsymbol{\beta}}_p$) and variance ($\hat{\sigma}_p^2$) estimates by fitting phenotype data for p with BayesDiallel, conditional on imputed covariate(s);

22   **for** $d \in D_{impute}$ **do**

23   Impute p_d into phenotype column of respective $T^{(r)}$ row(s) according to the following: $\tilde{p}_d^r | \tilde{c}_d^r \sim N(\mathbf{d}\hat{\boldsymbol{\beta}}_p, \hat{\sigma}_p^2 | \tilde{c}_d^r)$

24   **end**

25   Run BayesDiallel on $T^{(r)}$;

26   **end**

27   Concatenate MCMC results from each of the $T^{(r)}$ runs and summarize;

28   **end**